LAWRENCE TECHNOLOGICAL UNIVERSITY

EVALUATING LONG TERM CAPACITY & DUCTILITY OF CARBON FIBER REINFORCED POLYMER PRESTRESSING AND POST TENSIONING STRANDS SUBJECT TO LONG TERM LOSSES, CREEP, AND ENVIRONMENTAL FACTORS, AND DEVELOPMENT OF CFRP PRESTRESSING SPECIFICATIONS FOR THE DESIGN OF HIGHWAY BRIDGES

Submitted to

MICHIGAN DEPARTMENT OF TRANSPORTATION

Research Administration
Bureau of Field Services
Federal Project Number: OR14-024

By

Nabil F. Grace, PhD, P.E., Project Investigator
Mena Bebawy, PhD, P.E., Co-Project Investigator

Department of Civil Engineering
Lawrence Technological University
Southfield, MI 48075-1058, U.S.A.

Sept. 30th, 2019

TECHNICAL REPORT DOCUMENTATION PAGE

1. Report No. SPR-1690	2. Government Accession No. N/A	3. Recipient's Catalog No.
4. Title and Subtitle Evaluating Long Term Capacity & Ductility of Carbon Fiber Reinforced Polymer Prestressing & Post Tensioning Strands Subject to Long Term Losses, Creep, and Environmental Factors, and Development of CFRP Prestressing Specifications for the Design of Highway Bridges		5. Report Date Sept. 30th, 2019 6. Performing Organization Code N/A
7. Author(s): Nabil Grace, PhD, P.E.; Mena Bebawy, PhD, P.E., Marc kasabasic: Ernest Al-Hassan; Abinash Acharya; Kerolos Abdo; & Mohamed Mohamed		8. Performing Organization Report No. N/A
9. Performing Organization Name and Address Center for Innovative Material Research (CIMR) Lawrence Technological University University Advancement Office 21,000 West Ten Mile Road, Southfield, MI-48075		10. Work Unit No. N/A 11. Contract or Grant No. LTU 2013-0065 Z2
12. Sponsoring Agency Name and Address Michigan Department of Transportation (MDOT) Research Administration 8885 Ricks Road P.O. Box 33049 Lansing, Michigan 48909		13. Type of Report & Period Covered Final Report, 10/1/2013 to 9/30/2019 14. Sponsoring Agency Code N/A
15. Supplementary Notes Conducted in cooperation with the U.S. Department of Transportation, Federal Highway Administration. MDOT Research reports are available at www.michigan.gov/mdotresearch.		

16. Abstract

Comprehensive experimental, analytical, and numerical investigations were executed to establish the main design criteria of bridge beams prestressed with carbon fiber reinforced polymer (CFRP) strands. The investigation evaluated the short and long-term performance of CFRP under various environmental and loading conditions. Main CFRP design parameters such as maximum tensile strength, guaranteed strength, environmental reduction factors, relaxation, creep rupture strength, short and long-term prestress loss, and performance at elevated temperatures have been evaluated and documented. The experimental investigation included testing and evaluating unbonded prestressed CFRP strands as well as half-scale CFRP pretentioned decked bulb T-beams. Various test protocols were adopted and included such as testing and evaluating bonded and unbonded CFRP specimens: (1) at ambient temperature and controlled laboratory conditions, (2) under combined fire/loading events, (3) after exposure to cycles of freezing and thawing, (4) after exposure to outdoor harsh Michigan weather conditions for three years, (5) inside an environmental chamber simulating extremely hot and cold weather conditions, and (6) after exposure to elevated temperatures with and without loading. The results from the experimental investigation were implemented in the development of extensive analytical and numerical investigations that addressed the flexural and shear design of full-scale highway bridge beams. Test results were deployed to establish benchmark design criteria, design guidelines, and recommendations in a format similar to that of AASHTO LRFD to facilitate and promote the design and construction of highway bridges with CFRP components.

17. Key Words CFRP; Prestressed highway bridges; Creep Rupture, Relaxation; Fire; Environmental Conditions; Freeze-Thaw.	18. Distribution Statement No Restrictions. This document is available to the public through the Michigan Department of Transportation (MDOT).		
19. Security Classification (of this report) Unclassified	20. Security Classification (of this page) Unclassified	21. No. of Pages 375	22. Price N/A

ACKNOWLEDGEMENTS AND DISCLAIMER

"This material is based upon work supported by the Federal Highway Administration under SPR-1690. Any opinions, findings and conclusions or recommendations expressed in this publication are those of the author(s) and do not necessarily reflect the views of the Federal Highway Administration."

TABLE OF CONTENT

LIST OF FIGURES

LIST OF TABLES

EXECUTIVE SUMMARY

Successful implementation of carbon fiber reinforced polymer (CFRP) in precast prestressed bridge beam construction requires careful assessment for the short and long-term behavior of the material. Besides, different design parameters need to be evaluated and established before wide range deployment of CFRP in highway bridge design. This report presents the details and results of comprehensive experimental and analytical investigations that were executed with the main objective of establishing the main design criteria of bridge beams prestressed with CFRP strands. The investigations evaluated the short and long-term performance of CFRP under various environmental and loading conditions. The experimental investigation started by evaluating and optimizing the performance of different anchorage devices and selecting a device that was adequate for executing other tasks of the investigation. Second, the mechanical properties of the selected CFRP material such as average tensile strength, maximum strain, elastic modulus, and guaranteed strength were established through testing 49-in. (1244-mm) long CFRP specimens. Third, long-term properties of CFRP strands such as relaxation and creep rupture strength were evaluated by testing multiple sets of similar CFRP specimens exposed to different environmental and loading conditions. Some of the test specimens were loaded and monitored at ambient temperature and controlled laboratory conditions, while other test specimens were loaded and monitored while being exposed to harsh Michigan weather for a period exceeding three years. In addition, multiple sets of test specimens with the same configuration were evaluated for strength and prestress loss under severe exposure conditions. For instance, two sets of test specimens were subjected to elevated temperatures and loads under two different test protocols. Another set was prestressed, exposed to 300 cycles of freezing and thawing in a special environmental chamber, and then loaded to failure in a uni-axial test setup.

Parallel to testing un-bonded CFRP specimens, the experimental investigation also included testing and evaluating half-scale decked bulb T-beams prestressed with bonded CFRP strands. Three sets of CFRP precast prestresssed decked bulb T beams were designed, constructed, and tested to failure. The first set included five identical decked bulb T beams that were constructed on the same day from the same concrete batch. Each beam had a span of 26 ft (7.92 m), a depth of 16 in. (406 mm), a flange width of 18 in. (457 mm) and was prestressed with four CFRP strands with an initial prestressing force of approximately 22.5 kip (100 kN) /strand. The first beam served

as a control beam and was tested to failure under four-point-load setup after 28 days of construction. Two of the remaining four beams were preserved in controlled laboratory conditions and were monitored for prestress loss, while the other two beams were stored outdoors where they were exposed to extreme Michigan weather and they were also monitored for prestress loss. After one year, one indoor beam and one outdoor beam were tested to failure under the same four-point-load setup as that of the control beam. The remaining two beams were tested to failure under the same loading setup after two years of construction. The cracking loads, decompression loads, and ultimate loads of the beams were observed and compared to estimate the prestress loss in each beam and assess the effect of environmental exposure on the performance of CFRP prestressed beams.

The second set of decked bulb T beams consisted of eight beams prestressed with CFRP strands and one beam prestressed with steel strands. All beams were identical in cross section and dimensions and had a span of 16 ft (4.87 m), depth of 16 in. (406 mm), and a top flange width of 18 in. (457 mm). Out of the eight CFRP prestressed beams, one beams was prestressed with an initial prestressing force of 72 kip (320 kN) /beam, six were prestressed with an initial prestressing force of 100 kip (445 kN) /beam, and one was prestressed with an initial prestressing force of 132 kip (587 kN) /beam. The steel prestressed beams served as a control beam and was prestressed with an initial prestressing force of 132 kip (587 kN) /beam. All the beams were subjected to a fire event according to ASTM E119 combined with a service loading applied through a three-point-load setup. The test took place inside a large-scale natural-gas fire chamber, where the air temperature, beam temperature, load, and deflection were monitored during the entire test through a special data acquisition system. The test ended when the test beam failed to support the applied service load. Test results were assembled and analyzed to establish fire resistance criteria for beams prestressed with CFRP strands.

To study the effect of seasonal temperature change and the influence of freezing and thawing cycles on the performance of CFRP prestressed bridge beams, a third set of CFRP prestressed decked bulb T beams was designed, constructed and tested. The set included six identical beams with a span of 16 ft (4.87 m), a depth of 16 in. (406 mm), and a top flange width of 18 in. (457 mm). The beams were built from the same concrete batch and were provided with an initial prestressing force of 132 kip (587 kN) /beam. All beams were tested under three-point-load setup to approximately 67 % of their theoretical load carrying capacity. Two beams served as control beams and were preserved and tested in controlled laboratory conditions. Two beams were tested at hot conditions with air and beam temperatures of 176 °F (80 °C). Then the beams were allowed to cool down and test was repeated at ambient temperature at 68 °F (20 °C). The last two beams were tested at severe cold conditions, where the air/beam temperature was lowered to -40 °F (-40 °C). Then, the beams were allowed to warm up and the test was repeated at ambient conditions. Test results were used to back calculate the effective prestressing force in each beam during the time of the testing and were used to estimate the change of the prestressing force due to seasonal temperature change.

The test also extended to evaluate the performance and residual strength of the beams after exposure to 300 cycles of freezing and thawing according to ASTM C666. The control beams were kept in controlled laboratory conditions, while the remaining four beams were subjected to the freezing and thawing cycles inside a large-scale environmental chamber. After the conclusion of the freeze-thaw cycles, all the beams including the control beams were loaded to failure under three-point-load setup. Parameters such as loss of prestressing force, mode of failure, and residual strength were examined and documented.

Parallel to the experimental investigation, a comprehensive analytical investigation was conducted to examine the test results and develop analytical models for the performance of CFRP materials. The outcome of the analytical investigation was deployed in the development of detailed Mathcad sheets for the design of CFRP precast prestressed highway bridge beams. The Mathcad sheets were calibrated and tested then were used in the design of I-75 bridge beams over Sexton and Kilfoil Drain in Allen Park, MI. In addition, finite element models were generated for a single bridge beam as well as the entire superstructure of the bridge of I-75. The models were analyzed under construction loads, superimposed dead loads, live loads, and also under different seasonal and gradient temperature conditions. Results from finite element analysis were compared with those obtained analytically and were used to further tune the analytical models and the Mathcad sheets.

Test results of the investigation provided valuable information and design parameters that accurately described the short and long-term performances of unbonded and bonded CFRP strands. Those design parameters were deployed to establish benchmark design criteria, design guidelines, and recommendations that were assembled in a format similar to that of AASHTO LRFD to facilitate the design and construction of highway bridges with CFRP components. The design guidelines as well as the Mathcad sheets for CFRP bridge beam design are attached to this report under the Appendix section.

CHAPTER 1: INTRODUCTION

1.1 Overview

Michigan Department of Transportation (MDOT) pioneers in the deployment of innovative materials such as non-corrosive CFRP to enhance the design, construction, and durability of highway bridge beams. This is influenced by the harsh Michigan weather and the overwhelming corrosion and durability issues associated with steel prestressed beam bridges (Grace et al. 2004 and 2002b). Supported by decades of research and analysis (Grace and Abdel-Sayed 200b), the use of CFRP as a prestressing and reinforcement material has started in Michigan in 2001 with the construction of Bridge street bridge in Southfield, MI. Since then, several bridges have been successfully designed and built with CFRP components. For instance, in 2011, a two-span side-by-side precast prestressed box-beam bridge was constructed to carry Pembroke Rd over M-39 in Detroit, MI. The bridge is transversely post-tensioned with twelve 1.57-in. (40-mm) diameter un-bonded carbon fiber composite cable (CFCC) strands. In 2012, a three-span side-by-side box beam bridge carrying M-50 over NSRR railroad in Jackson, MI was also constructed and transversely post-tensioned using twenty un-bonded CFCC strands. In 2013 and 2014, two simply supported 45°-skewed prescast prestressed spread box-beam bridges were constructed to carry the east and west bounds of M-102 over Plum Creek in Southfield, MI. The box-beams are prestressed with 0.6-in. (15.2 -mm) diameter CFCC strands and are provided with CFCC stirrups in the transverse direction. The cast-in-place deck slabs for both bridges are also reinforced with CFCC strands. In 2016, a 102.5-ft (31.2-m) long simply supported bulb T beam bridge was constructed to carry M-86 over Prairie River in Centreville, MI. Each of its seven bridge beams is prestressed with 59 CFCC strands with a diameter of 0.6 in. (15.2 mm). In 2017, the construction of the 137-ft (41.7-m) long I-75 highway bridge over Sexton and Kilfoil Drain in Allen Park, MI marked the construction of the world's longest bridge span prestressed with CFRP strands.

Several other highway bridges with CFCC components are currently in either the design or construction phase. Nevertheless, with the wide deployment of CFRP strands in highway bridge construction, it is crucial to carefully evaluate the short and long-term performance of CFCC material to ensure safety and longevity of the constructed bridges.

1.2 Research Scope

A four-year-old extensive research investigation has recently been completed with the focus on the long-term and durability of CFCC strands in bridge beams. The investigation was executed with the scope of:

1. Reviewing CFRP design guidelines and research reports
2. Develop experimental program to address drawbacks and evaluate long-term performance of CFRP strands
3. Review data collected through field monitoring
4. Perform numerical and analytical investigations as necessary to evaluate and justify experimental results
5. Develop empirical equations, design criteria, and items necessary for developing a guide specification
6. Report results to MDOT along with design examples

1.3 Research Outcome

The outcome of this research can be summarized as:

1. Verifying CFRP design values including creep rupture strength, relaxation, prestress levels, and long-term losses
2. Establishing appropriate levels and strength reduction factors for CFRP strands considering creep rupture strength and long-term losses
3. Experimentally verifying material resistance for: bond fatigue, fire damage, and severe environmental conditions
4. Develop design methodologies, criteria, and empirical equations for inclusion in MDOT Bridge Design Manual (including details for inclusion in MDOT Bridge Design Guide)
5. Develop Mathcad design tools for CFRP prestressed highway bridge beams

6. Develop Design Guide Specifications in LRFD format for the design and construction of highway bridge beams pretensioned with CFRP strands

1.4 Report Outlines

This report documents the details and the results of the research investigation. Through the report, the work is presented in separate chapters that are split based on the objective of the work. Each chapter starts with an introduction and a brief literature review, if needed, followed by details of the research subject under consideration and finally, a summary for the test results, observations, and recommendations. The final chapter of the report summarizes main findings and recommendations of the research investigation. In addition, based on the findings and recommendations of the report, design guidelines and Mathcad sheets for the design and construction of CFRP precast prestressed highway bridge beams were developed. The design guidelines and the Mathcad sheets are attached to the report under the Appendix section. The chapters of the report are arranged as follows:

Chapter Two: Anchorage and tensile strength of CFCC strands

Chapter Three: Creep rupture and relaxation strength of CFCC strands

Chapter Four: Environmental effects

Chapter Five: Freeze-thaw effect

Chapter Six: Fire and heat resistance of CFRP strands

Chapter Seven: Splicing and bond fatigue of CFRP strands

Chapter Eight: Long-term performance of beams with CFRP strands

Chapter Nine: Flexural and shear design of CFCC prestressed beams

Chapter Ten: Summary and conclusions

Appendix I: Design guidelines in LRFD Format

Appendix II: Mathcad sheet for the design of CFCC highway prestressed beams

CHAPTER 2: ANCHORAGE AND TENSILE STRENGTH

2.1 Introduction

An adequate anchorage device is mandatory to establish a successful testing protocol for CFRP materials. Several types of anchorage devices have been recently developed, tested, and implemented in field applications for either post-tensioning or pre-tensioning applications (Grace et al. 2012c, 2011a, 2010a, 2010b, and 2002a). The two most common types of anchorage are sleeve-type anchorage and wedge-type anchorage. Through the investigation provided in this chapter, both types of anchorages were evaluated and tested. A series of 49-in. (1245-mm) long test specimens loaded in a uni-axial test setup to failure using either sleeve or wedge anchorage devices. Test results showed no significant difference in the average tensile strength of the test specimens with regard to the anchorage device. Nevertheless, sleeve-type anchorage appeared to be efficient and adequate for the expedited and consistent construction of the test specimens for the rest of the research investigation and therefore it was selected as the standard anchorage device for the research investigation.

2.2 Test Specimens

The strand specimens used in anchorage testing were 47-in. (1194 mm) long 7-wire CFCC strands, manufactured by Tokyo Rope Mfg. Co., Ltd., Japan, with a diameter of 0.6 in. (15.2 mm), cross sectional area of 0.179 in.^{2} (115.6 mm^2), and mechanical properties per lot, reported by the manufacturer, as shown in Table 2.2-1. After installing the anchorage devices at both ends, a uni-axial tensile test was conducted in accordance with ASTM Standard D7205/7205M-06 “Standard Test Method for Tensile Properties of Fiber Reinforced Polymer Matrix Composite Bars.”

The CFCC strands were delivered in spools as shown in Figure 2.2-1 and the test specimens were cut to the required length using power grinder. The cut specimens followed the curvature of the spool and to straighten them, the specimens were stretched in a wooden frame and subjected to a moderate heating at a temperature of 140 ºF (60 ºC) for at least 15 hours as shown in Figure 2.2-2.

Table 2.2-1 Mechanical properties of CFCC as provided by manufacturer, Tokyo Rope

Strand configuration & Lot No.	1 x 7, G34	1 x 7, G82
Date of testing	8/22/2011	2/23/2012
Diameter, in. (mm)	0.6 (15.40)	0.6 (15.33)
Guaranteed breaking load, kip (kN)	60.7 (270)	60.7 (270)
Effective cross-sectional area, in.^{2} (mm^2)	0.179 (115.6)	0.179 (115.6)
Average breaking load, kip (kN)	76.2 (339)	64.3 (286)
Max. breaking load, kip (kN)	78.7 (350)	64.5 (287)
Min. breaking load, kip (kN)	72.8 (324)	63.8 (284)
No. of test specimens	5	5
Average tensile strength, ksi (GPa)	425 (2.93)	358 (2.47)
Average tensile modulus, ksi (GPa)	21,610 (149)	20,885 (144)
Elongation, %	2.0	1.7

Figure 2.2-1 Spool of CFCC strands with a diameter of 0.6 in. (15.2 mm)

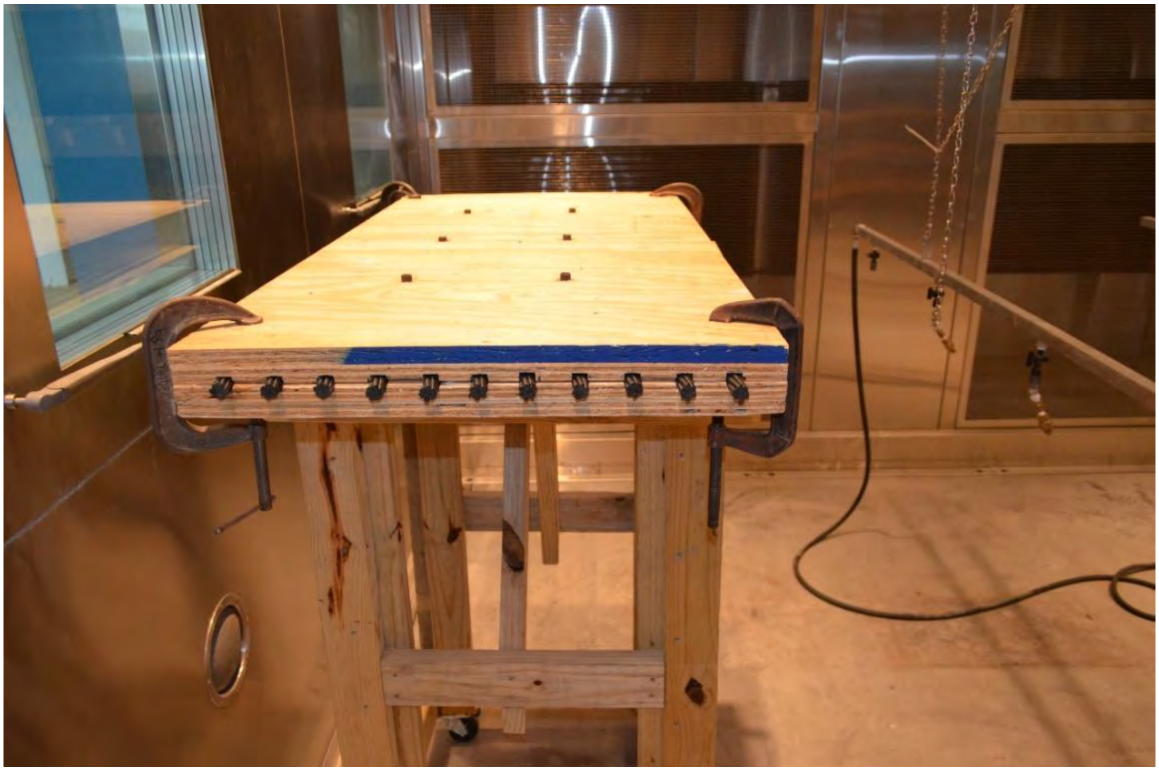

Figure 2.2-2 Heat treatment at 140 °F (60 °C) for 15 hours to straighten CFCC strands

2.3 Steel Wedge Anchorage

The steel wedge anchorage device is composed of four high-strength steel wedges that fit snuggly around the CFCC strand inside a high-strength steel barrel. As the strand is pulled the wedges slide into the steel barrel and confines the movement of the CFCC strand. To avoid damaging the surface of the strand, a buffer system is used between the wedges and the strand. The buffer system consists of a fine steel mesh confined by a braided steel netting. The process of applying the components of the buffer system is illustrated in Figure 2.3-1 and the installation of the wedge-anchorage device is shown in Figure 2.3-2. In addition, the test extended to address newly developed composite buffer material as a replacement for the steel mesh wrap as shown in Figure 2.3-3 and Figure 2.3-4.

(a) Steel mesh as a buffer material

(b) Wrapping steel mesh around CFCC

(c) Securing steel mesh in place with tape

(d) Additional braided steel wire netting

(e) Securing steel wire netting with tape

(f) Preparing four steel wedges

Figure 2.3-1 Applying components of buffer layer around CFCC strands

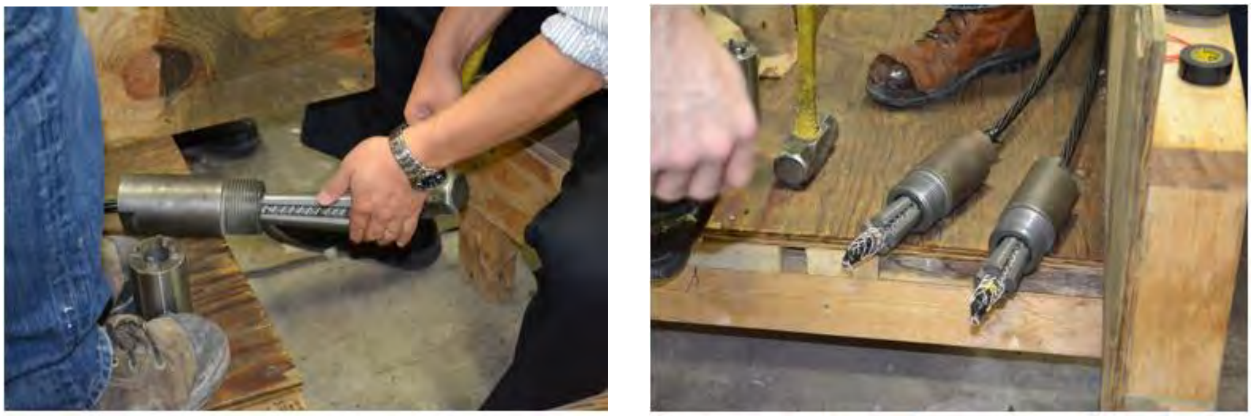

(a) Sliding steel wedges into barrel (b) Completed anchorage device

Figure 2.3-2 Installing steel-wedge anchorage device on CFCC strand with buffer layer

(a) New composite buffer material (b) Confinement with steel wire netting

(c) Steel wedge system (d) Sliding steel wedges using hand pump

Figure 2.3-3 New composite buffer material as a replacement for steel mesh wrap

Figure 2.3-4 Test specimens prepared using composite buffer layer and wedge anchorage

2.4 Sleeve Anchorage

As illustrated in Figure 2.4-1, a sleeve-type anchorage was prepared at Lawrence Technological University (LTU) in collaboration with Tokyo Rope. The anchorage device consisted of an externally threaded socket made of a high-strength steel pipe and a high-strength steel nut. The anchorage device was attached to the CFCC strands using cementitious-based, highly expansive material (HEM). The HEM is a special grout mix that exhibits a high degree of expansion with proper curing and produces a confining pressure of approximately 5800 psi (40 MPa). The mechanical properties of the high-strength steel anchors are given in Table 2.4-1.

Table 2.4-1 Mechanical properties of steel pipes used in anchorage preparation

Type	A53 Grade B
Outer diameter, in. (mm)	1.5 (38)
Inner diameter, in. (mm)	0.875 (22)
Wall thickness in. (mm)	0.3125 (8)
Tensile strength, ksi (MPa)	110 (758)
Yield strength, ksi (MPa)	101 (696)

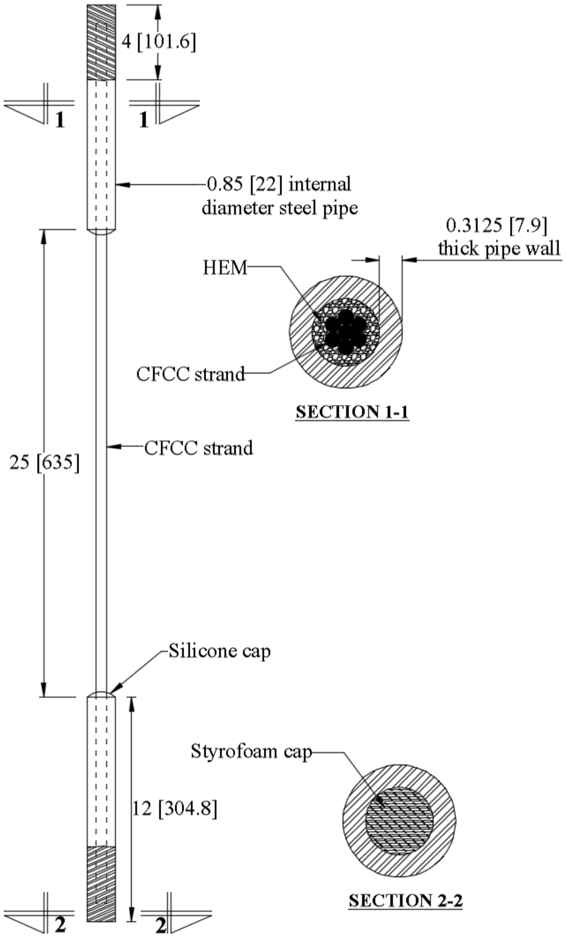

Figure 2.4-1 Sleeve-type anchorage for CFCC strands

The sockets had a length of 12 in. (305 mm) and were externally threaded for a length of 4.0 in. (100 mm) from their ends. After cutting and threading, the sockets were cleaned with compressed air and acetone to remove debris and oil from the cutting and threading process. The strands were centered inside the sockets and were held in place using end caps made of extruded poly polystyrene foam (Styrofoam) that also prevented the HEM from leaking out of the socket (Figure 2.4-2). The CFCC specimen with steel socket attached on one side were positioned and fastened by plastic ties on an in-house wooden jig as shown in Figure 2.4-3

(a) Threading and cutting steel socket (b) Preparing end caps from Styrofoam

(c) Cleaning the socket (d) Center depression for CFCC strand

Figure 2.4-2 Manufacturing of anchorage device at LTU

HEM was mixed with distilled water with a mix ratio of 4:1 by weight until a uniform slurry was obtained. Then, the HEM mix was poured into the anchorage sockets with CFCC strands inside them as shown in Figure 2.4-4. A mechanical vibrator was used to tap the sockets from the outside and ensure proper compaction for the HEM mix inside the sockets. After all sockets were filled, the specimens were allowed to cure at ambient temperature (68 °F or 20 °C) for five hours and at a temperature of 140 ºF (60 ºC) in an environmental chamber for at least 15 hours. After heat curing, the specimens were allowed to gradually cool down and the specimens were released from the wooden frame. The process was repeated for the other end by rotating the specimens and attaching the anchorage devices through the same process. Figure 2.4-5 shows the CFCC specimens with sleeve anchorage devices after proper curing.


(a) Capping the ends of the steel sockets


(b) Placing specimen in wooden stand


(c) CFCC specimens in wooden stand

Figure 2.4-3 Preparing the CFCC specimens for sleeve anchorage devices

A 220-kip (1000-kN) Material Test Systems (MTS®) loading actuator supported by a four-post steel frame was used in the testing and evaluation of different anchorage devices (Figure 2.4-6). Two custom-made steel heads were manufactured to accommodate different CFCC anchorage devices. The steel heads were designed to eliminate any possible eccentricity. Tensile force was applied in a force control mode at a rate of 6.5 kip/min. (29 kN/min) to failure. Tests were conducted in accordance with ASTM Standard D7205/7205M-06: "Standard Test Method for Tensile Properties of Fiber Reinforced Polymer Matrix Composite Bars."

To evaluate the elastic modulus of CFCC, a set of ten test specimens was loaded in the same uni-axial test setup but the load was stopped at a load level of 60 kip (267 kN). An extensometer was attached to the CFCC strand at the mid-height of the specimen as shown in Figure 2.4-6. The load vs. strain was plotted for each test specimen from a load level of 10 kip (44.5 kN) to 60 kip (267 kN) and the elastic modulus was calculated using the slope of the curve.

(a) Measuring the HEM powder (b) Adding water and mixing HEM

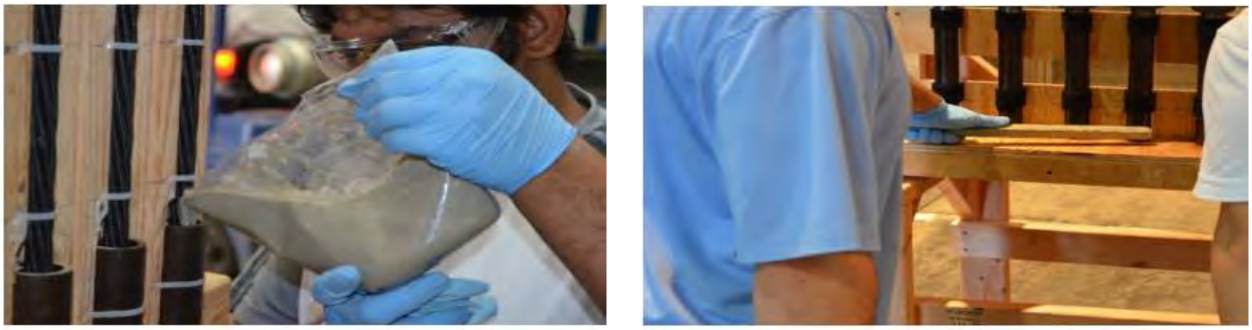

(c) Pouring HEM to the socket (d) Vibrating the HEM in the sockets

Figure 2.4-4 Mixing and placing the HEM inside the steel sockets

Figure 2.4-5 CFCC specimens with sleeve anchorage device after curing

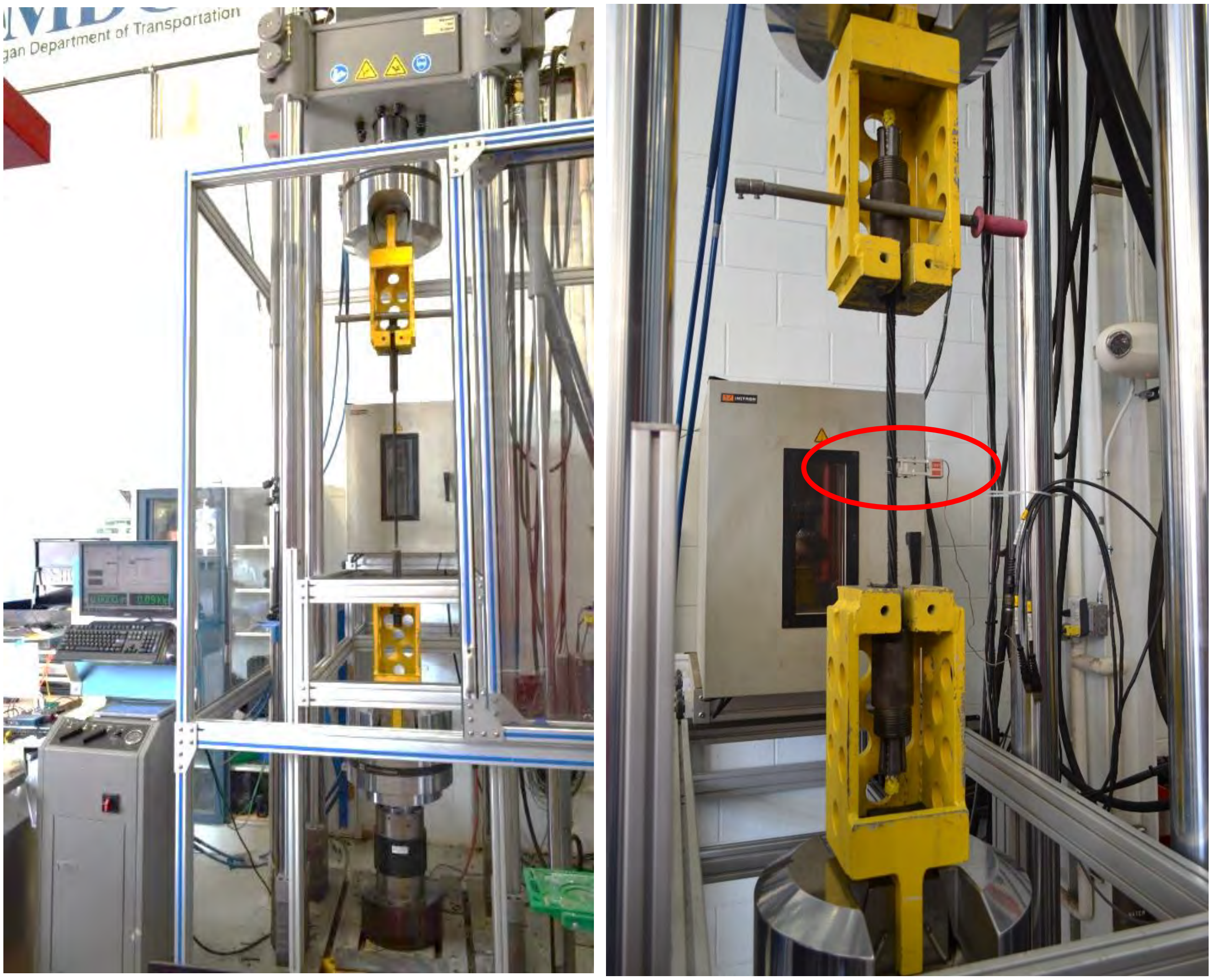

Figure 2.4-6 Left: A CFCC specimen in uni-axial test setup. Right, evaluating strain and elastic modulus of CFCC specimen using extensometer (circled)

2.5 Results

Results of testing CFCC specimens with sleeve anchorage are presented in Table 2.5-1. A total of 11 batches were prepared and tested. Batch 1 was prepared specifically for anchorage evaluation. Batches 2 through 11 of test specimens were prepared for other tests included in the experimental investigation such as relaxation, creep rupture strength, and freeze-thaw tests. Before conducting any of those tests, at least two test specimens were tested under a uni-axial test setup to evaluate the tensile strength of the material and the maximum strength of the anchorage device. As shown in the Table, out of a total of 31 test specimens, slippage of the anchorage occurred in six specimens, while the rest of the specimens failed by rupture of CFCC strands. Anchorage slippage was typically accompanied by a sudden loss in the load while the CFCC strand remained intact. On the other hand, rupture of CFCC strand was an explosive failure that resulted in shattering part or all of the CFCC strand as shown in Figure 2.5-1. It should be noted that post failure inspection showed that some test specimens experienced both slippage and rupture of the CFCC strand nearly at the same time, or at least one type of failure triggered the other type. In addition, nearly all test specimens with strand rupture exhibited the rupture of CFCC strand near the anchorage device. This can be attributed to the effect of the confinement pressure from the anchorage device.

After excluding test specimens with evident anchorage slippage, the average tensile strength of CFCC specimens with sleeve anchorage is approximately 70 kip (311 kN) with a maximum breaking load of 80.2 kip (357 kN), and a minimum breaking load of 66.6 kip (296 kN).

Figure 2.5-1 Typical failure mode of CFCC specimens with sleeve type anchorage

Table 2.5-1 Uni-axial test results of sleeve-type anchorage

Test Group	Failure Load kip (kN)	Failure Mode
Batch 1	67.6 (301)	Strand rupture
	66.6 (296)	Strand rupture
	64.6 (288)	Slippage
	62.4 (278)	Slippage
	66.6 (296)	Strand rupture
	68.2 (303)	Strand rupture
	68.2 (303)	Strand rupture
	71.3 (317)	Strand rupture
	67.8 (302)	Strand rupture
Batch 2	70.7 (314)	Strand rupture
	71.5 (318)	Strand rupture
Batch 3	75.4 (335)	Strand rupture
	80.3 (357)	Strand rupture
Batch 4	68.6 (305)	Strand rupture
	71.1 (316)	Strand rupture
Batch 5	64.1 (285)	Slippage
	67.2 (299)	Strand rupture
Batch 6	64.4 (287)	Slippage
	68.4 (304)	Strand rupture
Batch 7	75.3 (335)	Strand rupture
	60.7 (270)	Slippage
	67 (298)	Strand rupture
	73.9 (329)	Strand rupture
Batch 8	68.6 (305)	Strand rupture
	68.6 (305)	Strand rupture
Batch 9	63.2 (281)	Slippage
	68.3 (304)	Strand rupture
Batch 10	71.8 (320)	Strand rupture
	73.8 (325)	Strand rupture
Batch 11	66.9 (297)	Strand rupture
	66.9 (297)	Strand rupture

Test results of wedge anchorage are shown in Table 2.5-2. Strand rupture was the common mode of failure in all test specimens regardless of the buffer system. The average tensile strength of CFCC specimens with wedge anchorage is approximately 70.1 kip (311 kN) with a maximum tensile strength of 76.4 kip (340 kN) and minimum strength of 65.9 kip (293 kN). Typical test setup and failure of the test specimens with wedge anchorage devices is shown in Figure 2.5-2 and Figure 2.5-3. The average tensile strength from the combined test results of sleeve and wedge anchorage test specimens is approximately 70 kip (311 kN).

Figure 2.5-4 shows the load vs. strain for test specimens loaded to 60 kip (267 kN) and then released. Based on the test results, the average elastic modulus for CFCC strand was calculated approximately as 22,828 ksi (157.4 GPa). It should be noted that the wide range of strain values shown on the Figure was due to the initial stretching of the CFCC specimen when it was first loaded. By correcting the initial reading in all test specimens, the difference in strain diminishes.

Table 2.5-2 Uni-axial test results of wedge anchorage

Test Group	Failure Load kip (kN)	Failure Mode
Steel buffer	69.2 (308)	Strand rupture
	68.4 (304)	Strand rupture
	71.3 (317)	Strand rupture
	72.1 (321)	Strand rupture
	70.5 (314)	Strand rupture
Composite buffer	75.5 (336)	Strand rupture
	72.3 (322)	Strand rupture
	66.8 (297)	Strand rupture
	76.4 (340)	Strand rupture
	65.9 (293)	Strand rupture
	73.3 (326)	Strand rupture
	67.6 (301)	Strand rupture
	66.1 (294)	Strand rupture
	69.4 (309)	Strand rupture
	67 (298)	Strand rupture

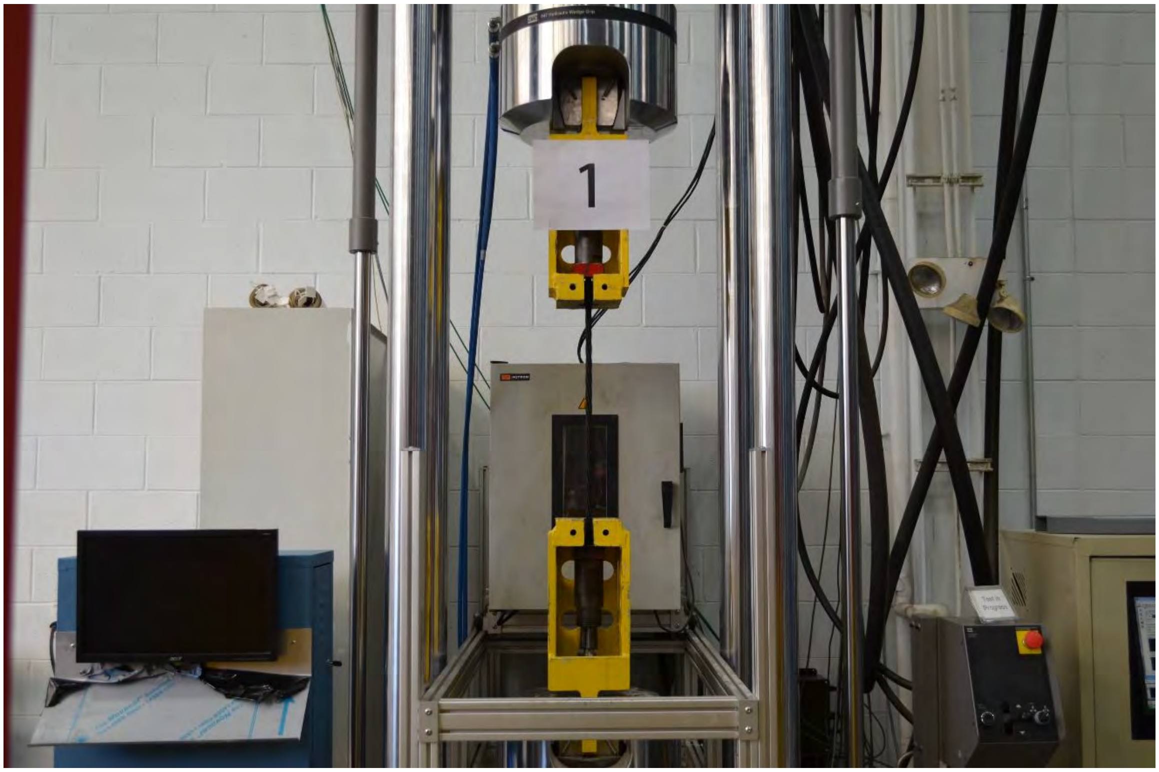

Figure 2.5-2 Uni-axial test setup for test specimens with wedge anchorage devices

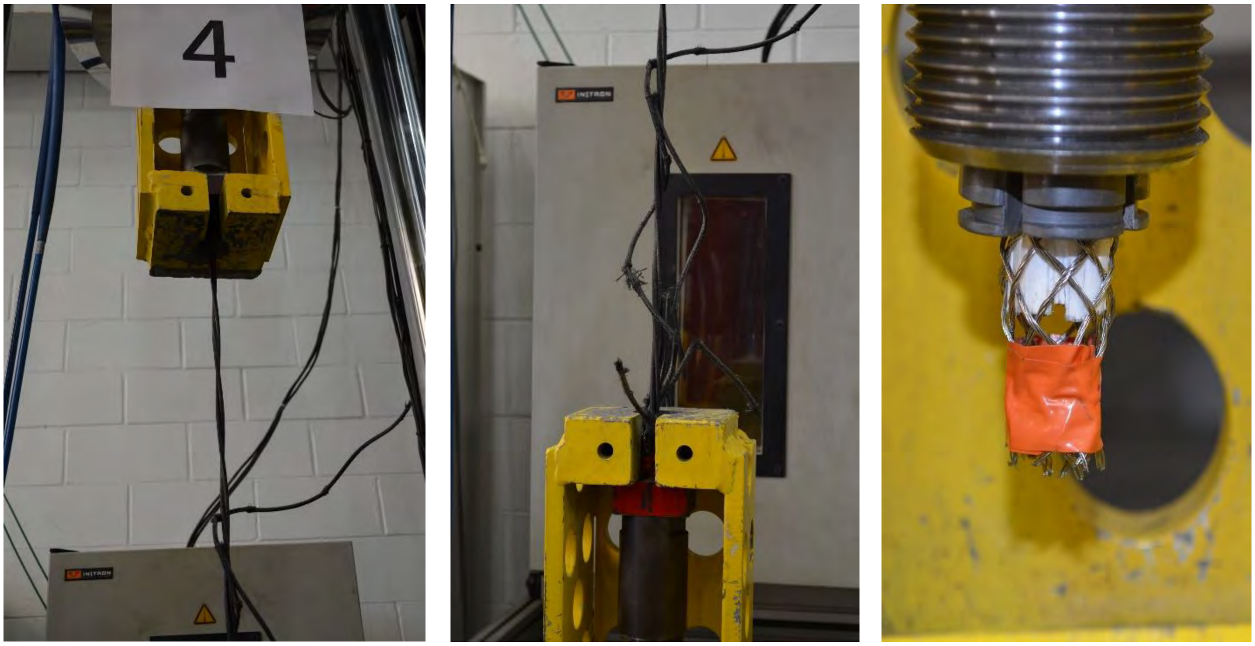

Figure 2.5-3 Failure of test specimens with wedge anchorage devices

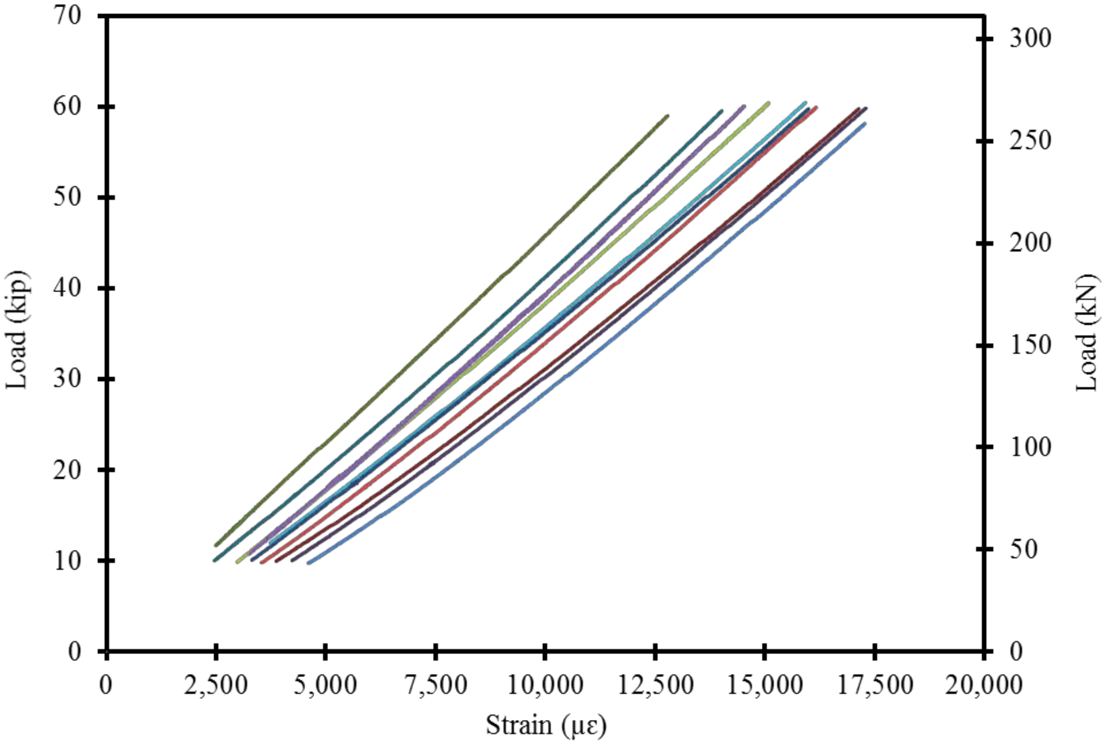

Figure 2.5-4 Establishing elastic modulus of CFCC based on uni-axial test results

2.6 Discussion of Test Results

Through the experimental investigation, sleeve and wedge anchorage devices were prepared and tested on CFCC strands with a diameter of 0.6 in. (15.2 mm). Test results showed an average CFCC tensile strength of 70 kip (311 kN), which is approximately 15 % higher than the guaranteed tensile strength recommended by the manufacturer (60.7 kip or 270 kN).

Few of the CFCC sleeve anchorages exhibited failure by anchorage slippage. Nevertheless, none of the test specimens including those with anchorage slippage failed at a load less than the guaranteed tensile strength of the CFCC strand. In addition, failure of the CFCC specimens at the maximum load initiated near the anchorage because of the lateral confinement pressure induced by the anchorage system on the strand. Therefore, test standards and guidelines shall be updated to acknowledge the failure near the anchorage points as an acceptable mode of CFRP strand failure.

CFRP tensile strength test results are highly dependent on the quality control of assembling the anchorage devices. This can be an issue when establishing the guaranteed strength of a CFRP material. For instance, the guaranteed strength is calculated as the average tensile strength minus three times the standard deviation of the test results. Inadequate anchorage handling and assembling can result in dispersed test results and a larger standard deviation, which can impact the calculations of the guaranteed tensile strength. Therefore, when anchorage malfunction is suspected in a certain test result, it may be eliminated from the pool of the test results.

CHAPTER 3: CREEP RUPTURE & RELAXATION OF CFRP

3.1 Introduction

Creep rupture, relaxation, and long-term prestress loss of CFRP strands due to exposure to various environmental conditions are key parameters in the design and construction of CFRP prestressed concrete highway bridge beams.

Relaxation is the loss of stress in a strand or tendon under constant strain (Hollaway 1993) and is affected by factors such as initial imposed stress level, type of fiber, durability factors (Gerritse and Den Uijl 1995), and creep coefficient which is defined as the ratio of creep strain to the initial elastic strain at a particular time. The stress relaxation of FRP composite materials remains a controversial issue within the engineering community because loss of prestressing force overtime in concrete structures reduces camber and could lead to low serviceability cracking loads.

Relaxation of fibers, resin matrix and straightening of fibers are the three main sources of relaxation losses in FRP materials (Oskoue and Taleie 2010). The viscoelastic property of FRP resins causes it to relax when it is stressed and thus lose a portion of its contribution to the load carrying capacity of the fiber. The straightening of incompletely parallel fibers through the resin matrix during loading also results in stress losses. Furthermore, exposure to environmental conditions such as alkaline environment, chloride ions, ultraviolet radiation, moisture and water, and elevated temperatures has a ripple effect on the relaxation characteristics of FRP composite materials. However, each type of FRP responds differently to these exposures. As a result, many design guidelines specify FRP strength reduction factors to account for long-term relaxation losses under severe environments (Ali et al. 2018).

ACI 440.4R-04 (ACI 2004) and Intelligent Sensing for Innovative Structures (ISIS) assumes a general loss in prestressing force of FRPs due to relaxation of 0.6 to 1.2 % and 1 to 2 % for polymer relaxation and fiber straightening, respectively. ACI 440.4R-04 reports that CFRP has almost zero fiber relaxation, which is contradicted by the 1.8 % over a 100-year period reported by ISIS. CAN/CSA S6-06 (2006) provides no provision for the evaluation of losses due to relaxation of FRP in prestressed concrete structures.

(Patrick and Zou (2003) suggest that Carbon FRP exhibits negligible losses due to relaxation when the initial applied stress is equal to or below 50 % of the ultimate tensile strength. This is due partly to the low creep coefficient under such applied stress. Balazs and Borosnyoi (2001) estimated relaxation of 1.8 to 2 % for CFRP tendons and 5 to 8 % for AFRP over a 1000-hour period. Extrapolated to 50 years, relaxation of GFRP, CFRP and AFRP tendons were estimated as 4 to 14 %, 2 to 10.5 %, and 11 to 25 % respectively, depending on the applied initial stress. Experimental works conducted by Ando et al. (1997) on 0.5-in. (12.5-mm) diameter CFRP and 0.6-in. (15-mm) diameter AFRP at 20 ºC, 40 ºC and 60 ºC for time periods of 3000 hours indicated that higher temperatures facilitate greater relaxation rate and this effect was pronounced in AFRP bars.

This chapter presents test setups and test results of a comprehensive study that was conducted to establish those design parameters. Multiple sets of 4-ft (1.2-m) long CFRP specimens were prepared, provided with sleeve anchorages, and loaded in special steel frames or in a four-post loading frame with a closed-loop MTS® hydraulic actuator. Multiple sets of specimens were tested to establish the creep rupture strength. One set was loaded in a steel frame to establish the one-million-hour relaxation rate of CFRP. Four sets of test specimens were loaded with high initial force levels in steel frames and were subjected to harsh Michigan weather for a period of three years, while similar sets of specimens were kept in a controlled laboratory conditions for the same period.

Test results of this investigation showed that the one-million-hour creep rupture strength of CFCC strands is at least 86 % of their average tensile strength. In addition, the one-million-hour relaxation rate of CFCC was found to be less than 2 %. Furthermore, it appears that various environmental conditions such as moisture, rain, freezing rain, and harsh change in daily and seasonal temperature do not have a significant influence on the strength of CFCC strands and do not lead to accelerated deterioration in the material or significant loss in the prestressing force.

3.2 Creep Rupture

Currently ACI 440.4R-04 limits the jacking strength in CFRP strands to 65 % of their guaranteed strength because of concerns associated with creep rupture failure. Meanwhile, ACI 440.1R-06 acknowledges that higher creep rupture capacities, as high as 85 % of the guaranteed strength, have been documented and reported by CFRP manufacturers and researchers. While a higher creep rupture capacity of CFRP strands will promote a higher jacking strength and a more efficient prestressed member, it is essential that a clear understanding of the creep rupture phenomenon be established for every CFRP material before it is deployed in highway bridge construction. Besides, limits of prestressing force and jacking strength shall be established based directly on the creep rupture strength, not based on the guaranteed strength because high guaranteed strength does not directly imply excellent creep rupture performance or higher creep rupture strength.

3.2.1 Test setup

A total of thirty CFCC specimens were constructed and tested to determine the one-million-hour creep rupture strength of CFCC strands. The tests were conducted in accordance with JSCE-E 533-1995, “Test Method for Creep Failure of Continuous Fiber Reinforcing Materials”. The CFCC specimens were prepared using sleeve anchorages bonded to the CFCC strands using HEM. The construction process of the specimens followed the same procedures described earlier in Chapter 2.

Two test setups were used in creep rupture evaluation. The first test setup used two custom-made steel frames that accommodated five specimens per frame. The steel frames were fabricated from ASTM A500 Grade B HSS rectangular sections, 13.5 in. (343 mm) × 2 in. (50.8 mm) ASTM A36 plates, and 1.0-in. (25.4-mm) diameter ASTM A193 Grade B7 threaded rods. To avoid excessive prestress loss and maintain a constant level of prestressing force through the duration of the test, high strength steel springs with an outside diameter of 12.5 in. (318 mm) and a linear stiffness of 10 kip/in. (1.75 kN/mm) were attached to the specimens as shown in Figure 3.2-1. The test specimens in the first frame was loaded to approximately 48 kip (213 kN)/strand, while the test specimens in the second frame were loaded to approximately 55 kip (245 kN)/strand. Those load levels represent approximately 70 and 80 % of the average tensile strength of CFCC or 79 and 91 % of the manufacturer’s guaranteed tensile strength. In-line load cells and vibrating wire displacement transducer were attached to each of pre-tensioned CFCC specimen to monitor the prestressing force and the strain, respectively. Load cells were manufactured by OMEGA® with a maximum capacity of 50 kip (222 kN), whereas displacement transducers were Geokon Model 4410 Strand-meter with a range of +3 mm (tension only). All the attached sensors were connected to a data acquisition system the continuously monitor and record the prestressing force and strain in loaded strands. Figure 3.2-2 through Figure 3.2-6 show the steel frames and the instrumentation of the test specimens.

Figure 3.2-1 Test setup for evaluating creep rupture strength of CFRP with high strength steel springs to maintain the load level

Figure 3.2-2 Stressing creep rupture specimens to 70 % of the average tensile strength of CFCC

Figure 3.2-3 Creep rupture specimens after stressing showing the compressed steel springs

Figure 3.2-4 Inline load cells to monitor the force of creep rupture specimens

Figure 3.2-5 Two sets of creep rupture specimens prestressed to 70 % and 80 % of average tensile strength of CFCC

Figure 3.2-6 Strand-meter for strain evaluation in creep rupture specimens

Due to safety concerns, the second test setup used a hydraulic actuator supported by four-post loading frame to apply and maintain load levels higher than 90 % of the CFCC average tensile strength and higher than the manufacturer's guaranteed strength. In this test setup, each CFCC specimen was loaded to the assigned load level and the load was maintained using a closed-loop hydraulic system until the failure of the specimen or 1000 hours, whichever came first. The prestressing force was applied through a hydraulic jacking system at a rate of 6 kip/min (26.7 kN/min). The load was monitored using a load cell attached to the loading actuator, while the strain was monitored in select test specimens using an extensometer attached to the CFCC strand at the mid-height of the specimen. Figure 3.2-7 and Figure 3.2-8 show the test setup for creep rupture testing of CFCC specimens with a load level higher than 90 % of the average CFCC tensile strength.

Figure 3.2-7 Creep rupture test setup for stress levels higher than 90 % of the CFCC average tensile strength

Figure 3.2-8 Creep-rupture test setup for stress level of 94 % of average CFCC tensile strength

3.2.2 Test results

Test specimens with 70 % of tensile stress (79 % of the guaranteed strength) were loaded and monitored continuously for 90 days (2160 hours). Figure 3.2-9 shows the load-time history for this set of test specimens. A slight load loss was observed in the first 7 days. Therefore, the specimens were reloaded again to increase the stress ratio back to 48 kip (213 kN). After 90 days, there was no failure in any of the specimens. Therefore, the decision was made to release this set of specimens, while continue monitoring the force in the second set with initial prestressing force of 55 kip (245 kN)/strand. Monitoring of the other set has been going on for over 1200 days as shown in Figure 3.2-10 and Figure 3.2-11 that show the change in force and strain in the specimens with time. As shown in the figures, there was a slight decrease in the load over time but since the decrease in the load was minimal, it was decided not to disturb the specimens as long as the load does not go below 50 kip (222 kN)/strand

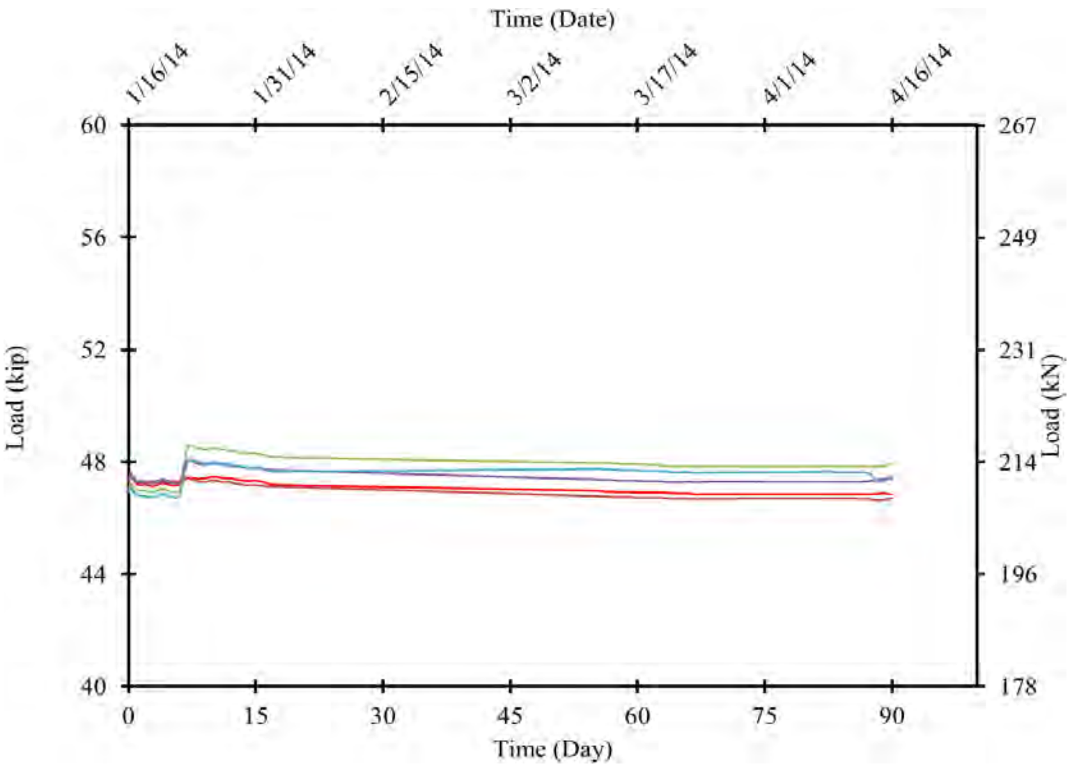

Figure 3.2-9 Force monitoring of CFCC specimens with a load of 48 kip (213 kN) per strand

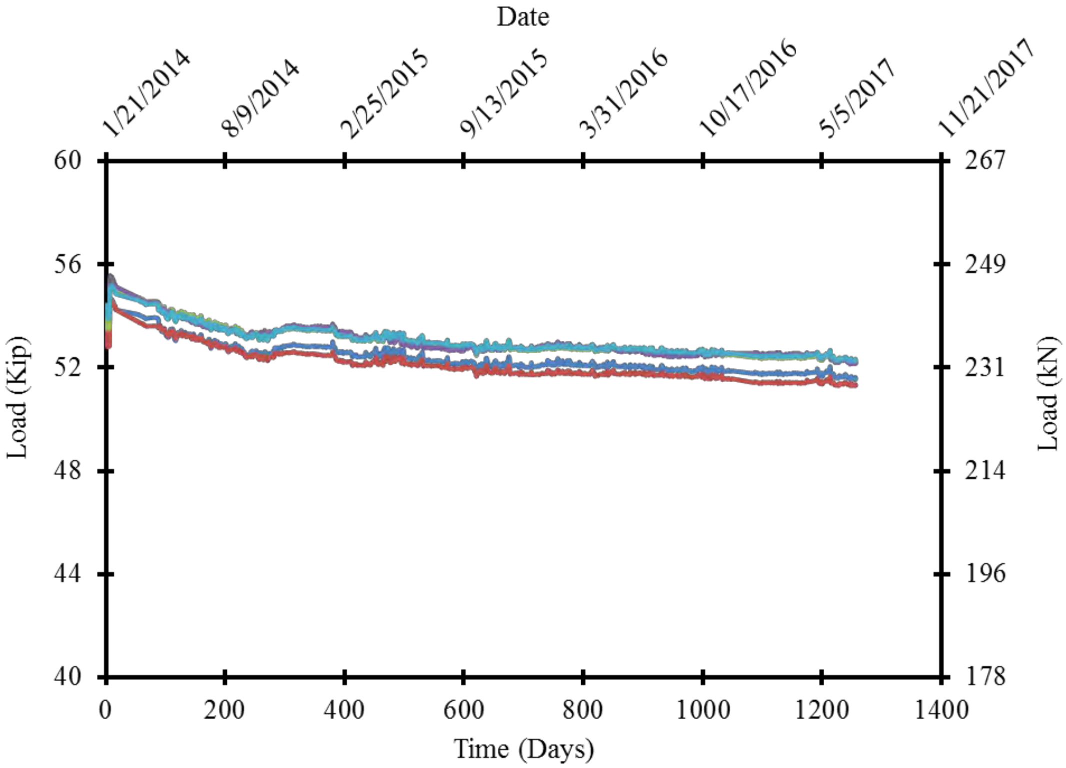

Figure 3.2-10 Force monitoring of CFCC specimens with a load of 55 kip (245 kN) per strand

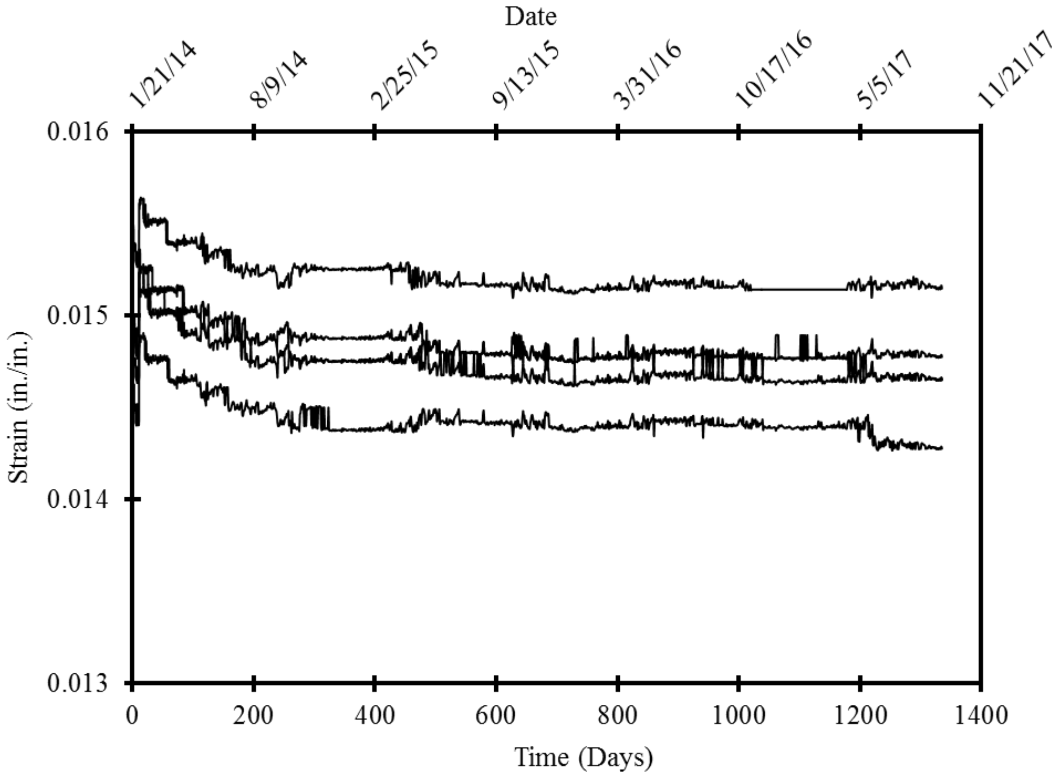

Figure 3.2-11 Strain monitoring of creep rupture CFCC specimens

Test results of the second test setup that was performed in the MTS-four-post loading actuator are summarized in Table 3.2-1. As shown in the Table, test specimens with a load level as high as 94.6 % of the average CFCC tensile strength sustained the applied load for 1000 hours without failure. In addition, it appears that the test specimen either sustained the load or experienced failure within the first 100 hours of loading. It should be also noted that one load level resulted in several outcomes and the results did not seem to follow a certain trend. For instance, Specimen #18 with a load level of 63.71 kip (283 kN) sustained the load for approximately 57 hours before it failed. Specimen # 19, on the other hand, sustained the same load level for 1000 hours, after which it was released. The difference in performance can be attributed to different factors such as preparation and handling of the specimens or curing of the HEM for the anchorage. But overall, it was evident that very high load levels are needed to cause rupture of the CFCC strand and it appears that the rupture was less likely due to a typical creep phenomenon but rather due to the load being very close to the tensile strength of the specimen.

Table 3.2-1 Results of creep rupture test performed on CFCC strand specimens with a diameter of 0.6 in. (15.2 mm)

Test #	Average tensile strength	Sustained load	Load ratio	Duration	Mode
	Kip (kN)	Kip (kN)	%	Hours	
1	≈ 70 (311)	66.84 (297)	95.6	0.073	Failure
2		66.84 (297)	95.6	0.013	Failure
3		66.84 (297)	95.6	5.951	Failure
4		66.80 (297)	95.6	0.000	Failure
5		66.84 (297)	95.6	16.922	Failure
6		66.84 (297)	95.6	0.621	Failure
7		66.13 (294)	94.6	1000	Suspended
8		65.08 (289)	93.1	0.052	Failure
9		65.08 (289)	93.1	38.658	Failure
10		65.08 (289)	93.1	0.026	Failure
11		65.08 (289)	93.1	34.306	Failure
12		65.08 (289)	93.1	0.088	Failure
13		64.39 (286)	92.1	0.011	Failure
14		64.39 (286)	92.1	0.194	Failure
15		64.39 (286)	92.1	0.799	Failure
16		64.39 (286)	92.1	0.005	Failure
17		64.39 (286)	92.1	0.023	Failure
18		63.71 (283)	91.1	57.183	Failure
19		63.71 (283)	91.1	1000	Suspended
20		61.65 (274)	88.2	1000	Suspended

3.3 Relaxation of CFCC Strands

3.3.1 Test setup

After releasing the creep test specimens with a load level of 48 kip (213 kN) per strand, the steel frame was used to conduct the relaxation test, where five CFCC specimens were prestressed and monitored for stress loss. The specimens were pretensioned to a force level of 47.5 kip (211 kN), which represented approximately 67 % of the average tensile strength of CFCC. The relaxation test was conducted in accordance with JSCE 534-1995: "Test Method for Long-Term Relaxation of Continuous Fiber Reinforcing Materials". It should be noted that this load level was higher than the jacking strength recommended by ACI-440-4R-04 (39.5 kip or 175 kN).

As shown in Figure 3.3-1 through Figure 3.3-4, CFCC specimens were connected to load cells and threaded rods at one end (dead end) and fastened at the other end (live end) by a nut and washer. Prestressing force was applied in predetermined sequence at the live end through a hydraulic jack at a rate of 6 kip/min (26.7 kN/min) and monitored through the installed load cells. Strains were monitored using Geokon strand-meters attached to the CFCC strands. The load cells and the strand-meters are attached to data acquisition system and the readings have been recorded for the last three years.

Figure 3.3-1 Relaxation test setup

Figure 3.3-2 Inline load cells for force monitoring of relaxation specimens

Figure 3.3-3 Stressing relaxation specimens to an initial load level of 47.5 kip (211 kN)

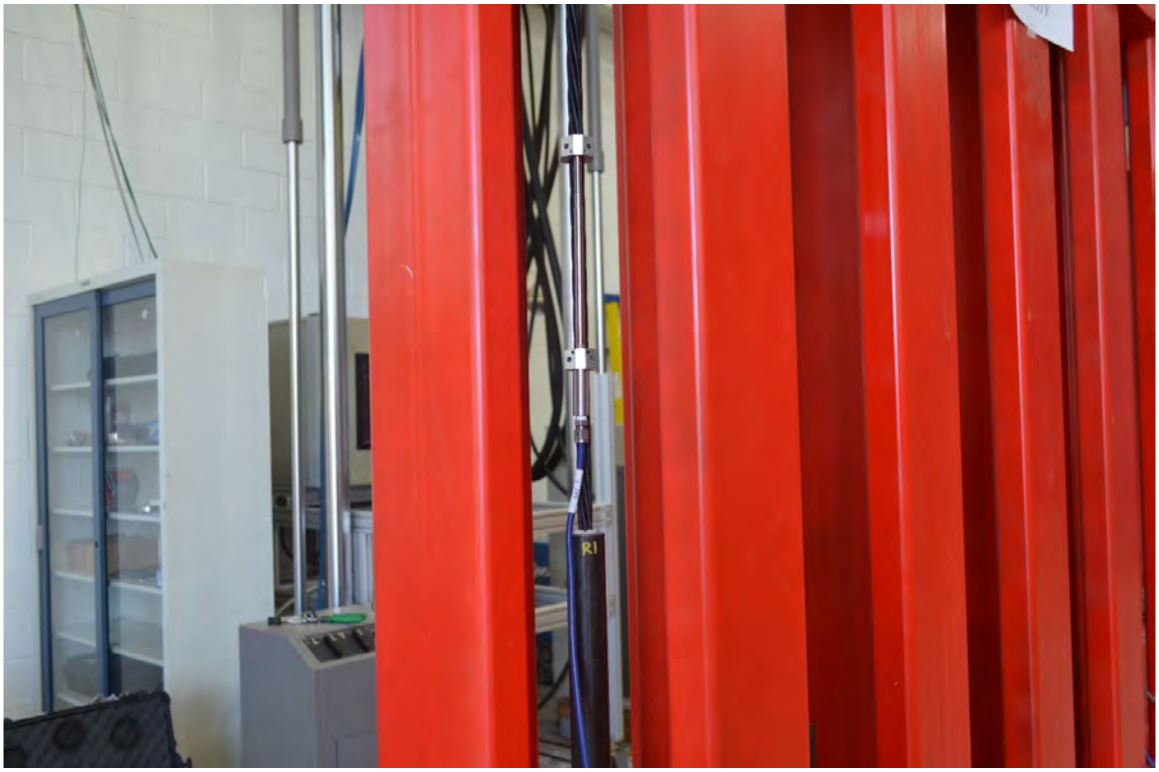

Figure 3.3-4 Strand-meters to evaluate the strain in CFCC relaxation specimens

3.3.2 Test results

Figure 3.3-5 shows the load vs. time curve for the five CFCC specimens. All specimens displayed a bi-linear pattern of load loss with approximate force loss of 4.5 % in the first 4 months (120 days) and additional force loss of 3 % and occurred between 4 and 36 months. The average total loss at the time of writing this report seem to be approximately 7.5 %.

When looking at the strain readings vs. time, shown in Figure 3.3-6, it appears that the loss of the prestressing force was accompanied by a reduction in the strain readings over time. In an ideal situation, where the loss in prestressing force occurs because of strand relaxation only, the strain readings shall be increasing with time, not decreasing. That is because relaxation of the strand leads to strand elongation between the anchor points, which causes the prestress loss. Therefore, the recorded reduction in the strain readings indicated that the loss in the prestressing force was due to a combination between strand relaxation and anchorage relaxation. When anchorage devices relax, they tend to induce a reduction in the strain readings in the CFCC specimens because the strands retract back as the anchorage devices give away finite displacements.

The loss in prestressing force due to strand relaxation and due to anchor relaxation can be mathematically separated by analyzing the strain readings vs. the corresponding load cell reading. If strand relaxation loss is denoted (X) and anchor relaxation loss is denoted (Y), then the attached load cells in the setup measured total relaxation losses (X+Y) from the anchor and the strand. The strand-meter on the strands however measured the net loss due to anchor relaxation and strand relaxation (Y-X). By converting the strain reading to equivalent loss in prestressing force and solving the two equations simultaneously, the loss due to strand relaxation (X) and due to anchorage relaxation (Y) can be determined.

As shown in Figure 3.3-7, the total loss of the prestressing force was approximately 3.6 kip (16 kN) as shown in Figure 3.3-8. The loss due to anchorage relaxation was calculated as 3.1 kip (14 kN), while the loss due to strand relaxation was approximately 0.5 kip (2 kN) as shown in Figure 3.3-9. This loss accounts to approximately 1 % of initial prestressing force as shown in Figure 3.3-10. When plotted on a logarithmic scale, the estimated one-million-hour relaxation loss (relaxation rate) is approximately 1.91 % as shown in Figure 3.3-11.

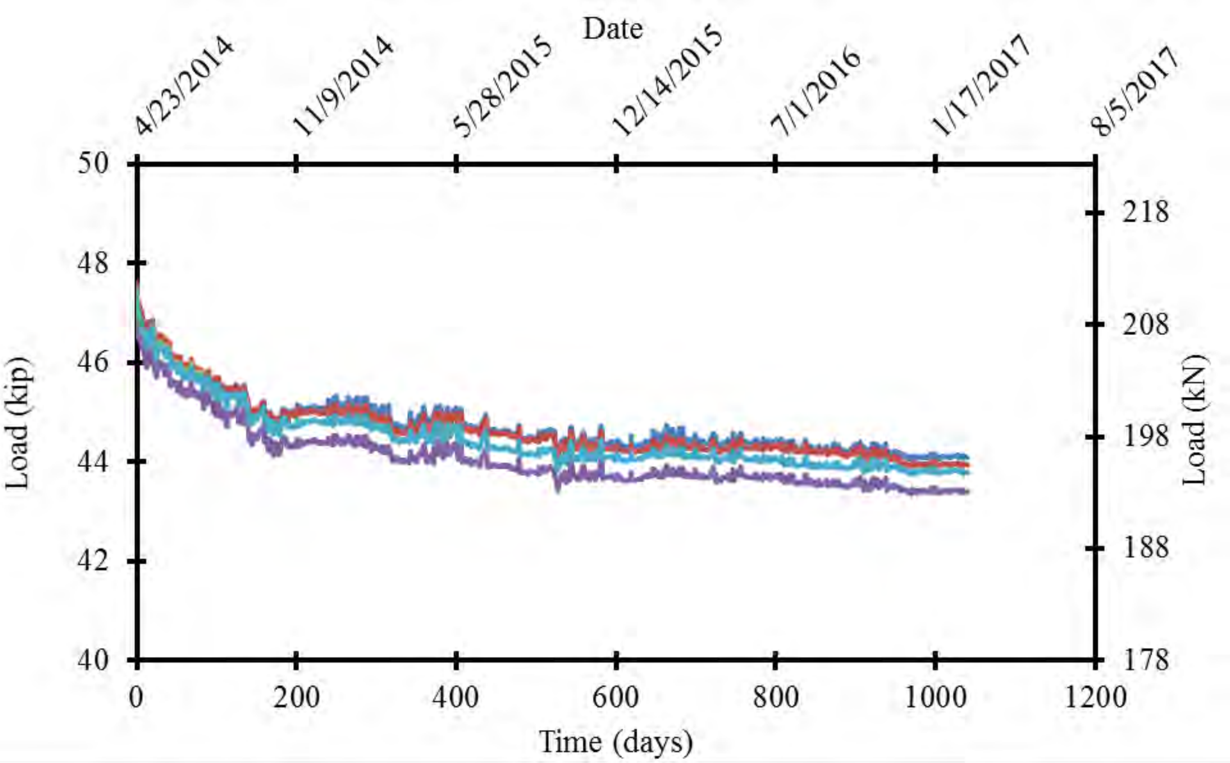

Figure 3.3-5 Force monitoring in relaxation CFCC specimens

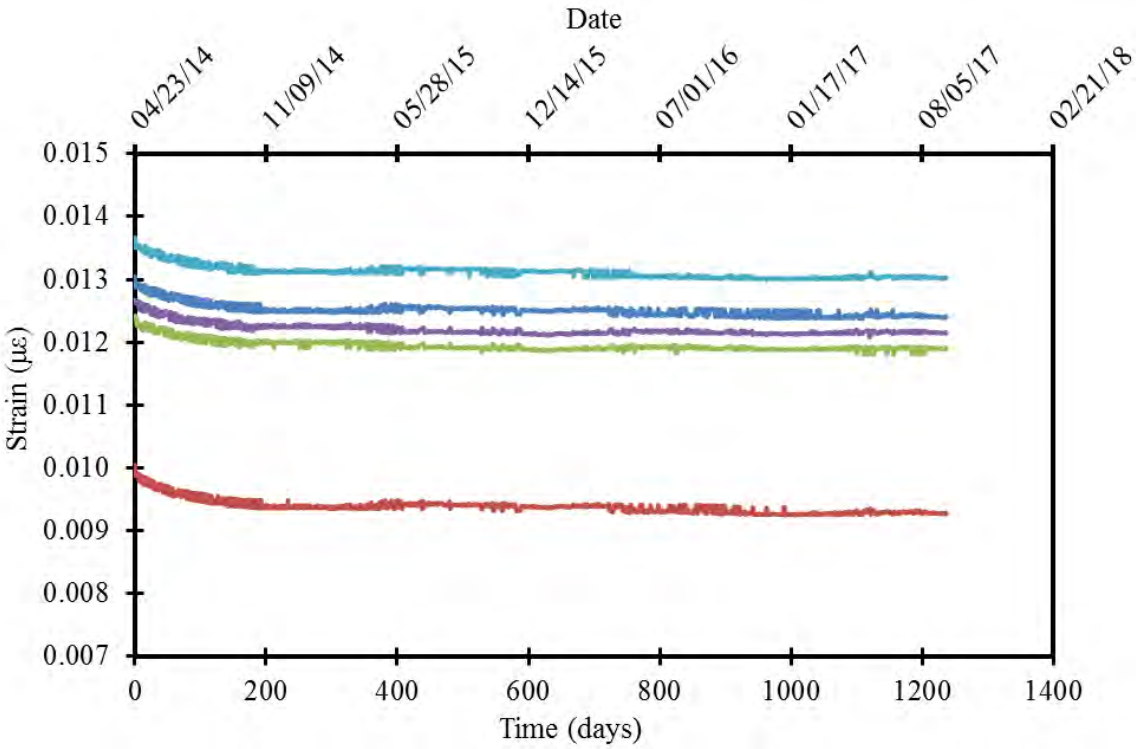

Figure 3.3-6 Strain monitoring of relaxation CFCC specimens

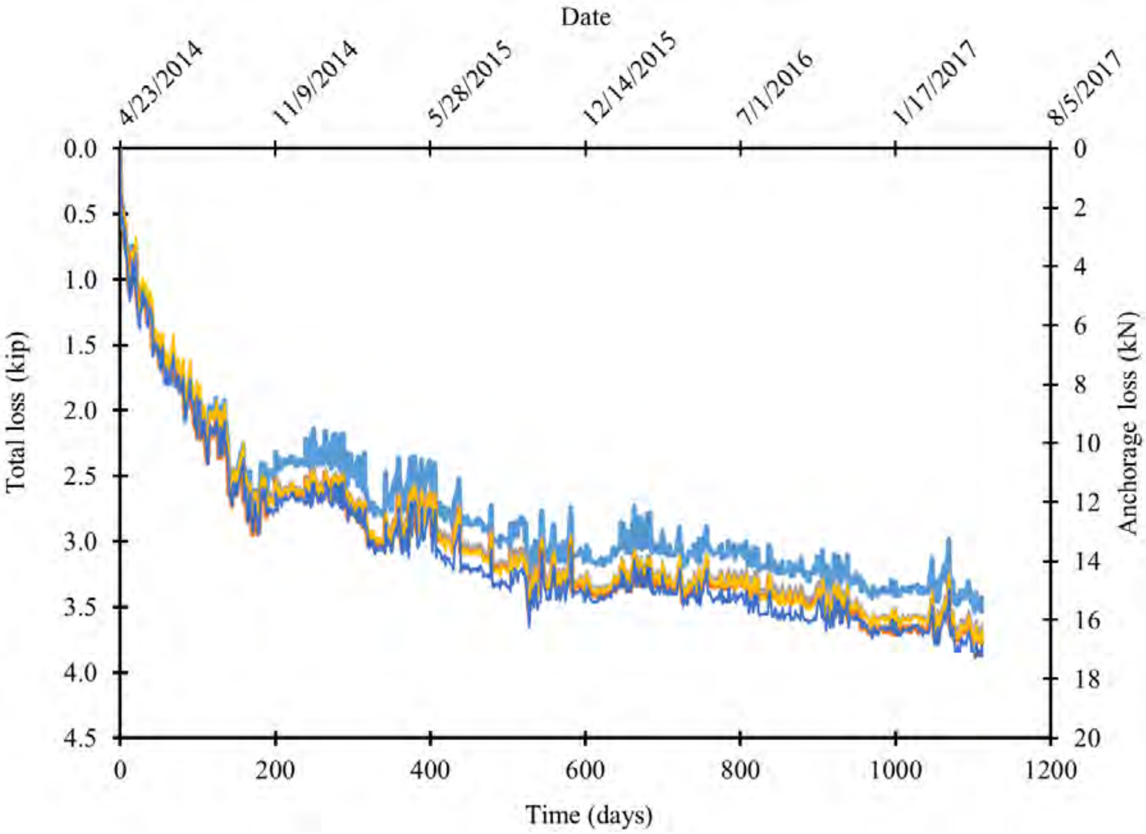

Figure 3.3-7 Total loss of the force in CFCC specimens due to anchorage and CFCC relaxation

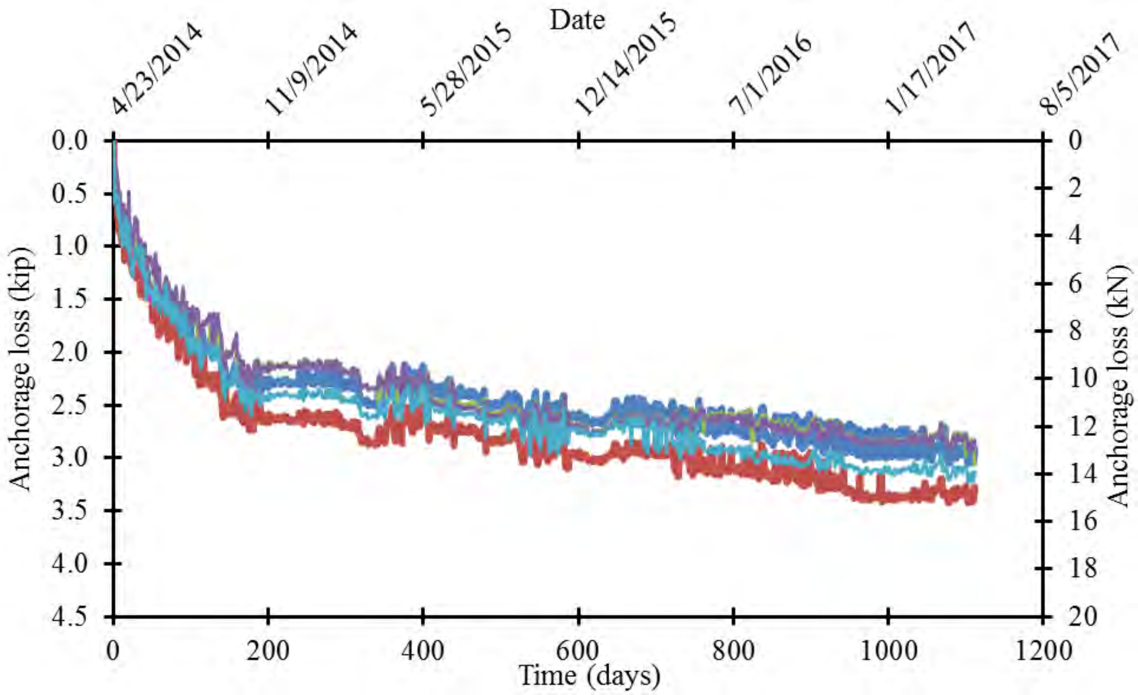

Figure 3.3-8 Loss of the force in CFCC specimens due to anchorage relaxation

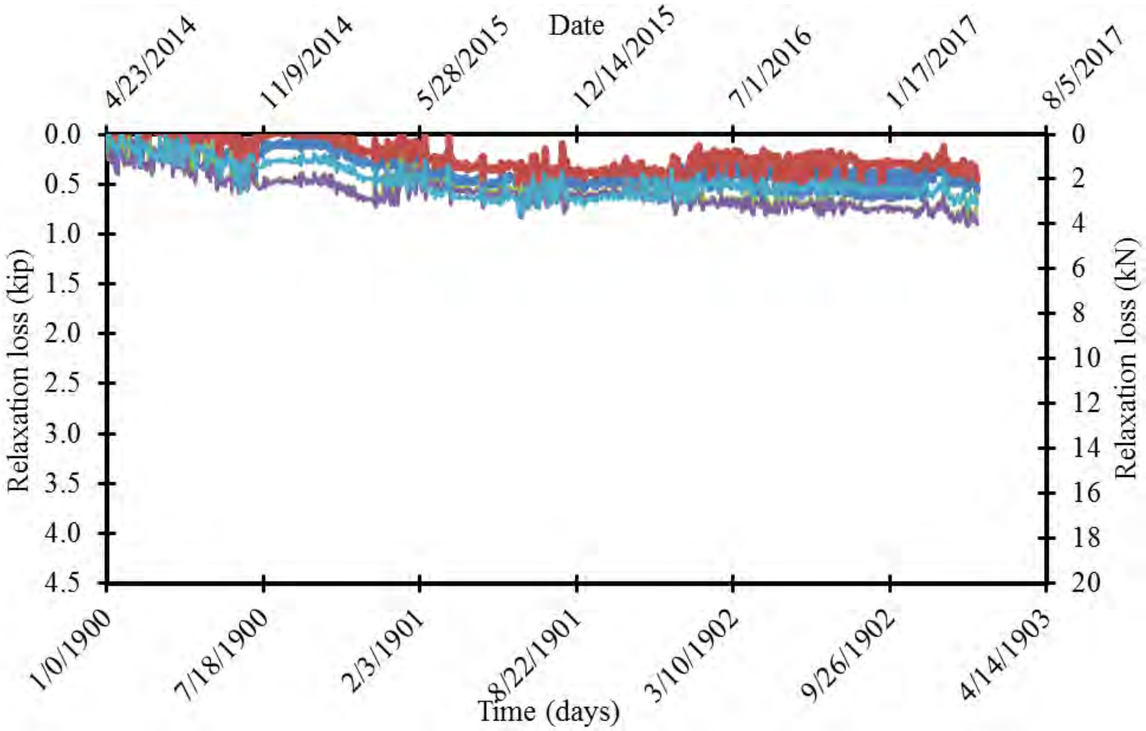

Figure 3.3-9 Loss of force in CFCC specimens due to relaxation of CFCC

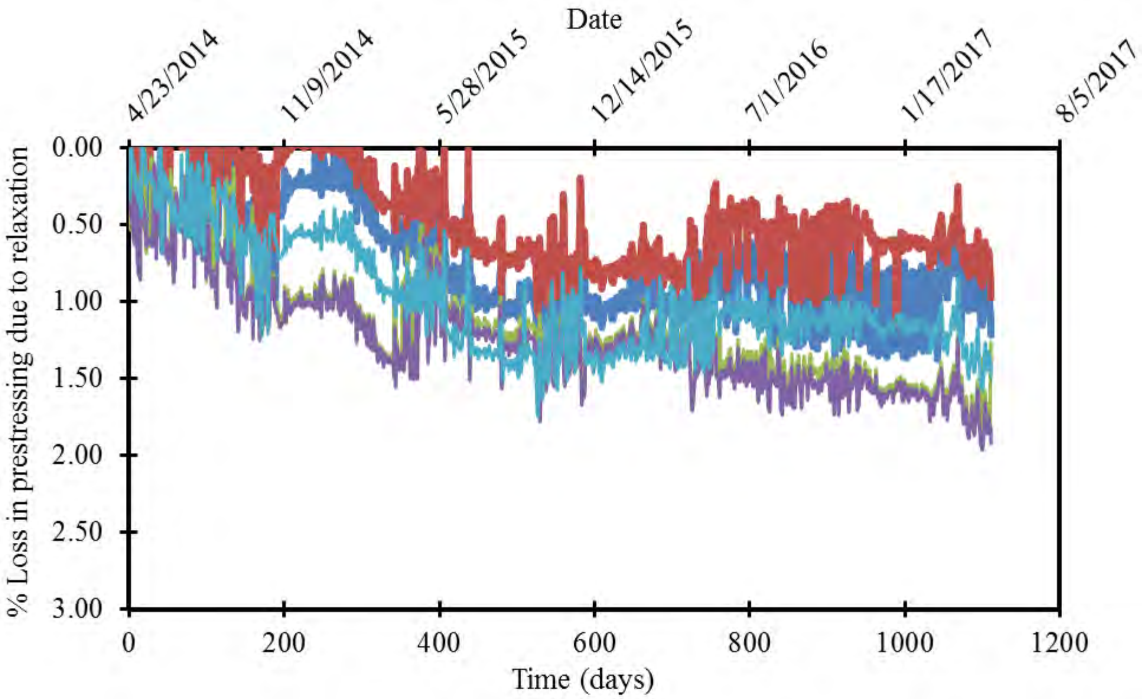

Figure 3.3-10 Percentage loss of force in CFCC specimens due to CFCC relaxation only

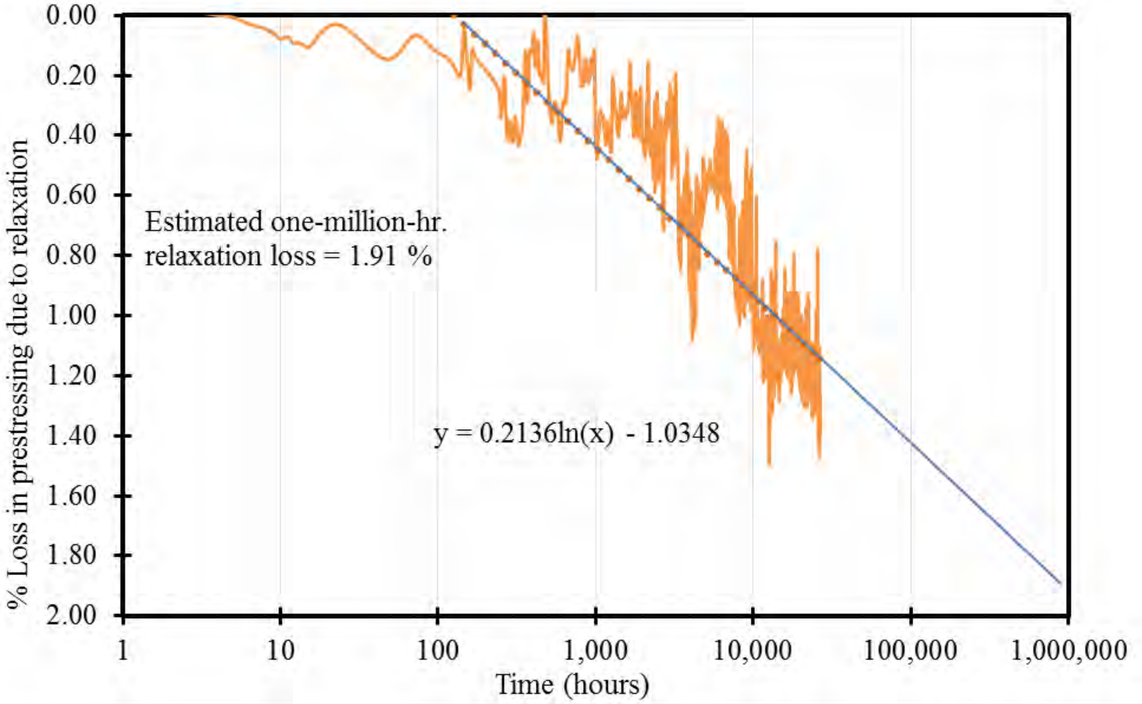

Figure 3.3-11 Estimated one-million-hour relaxation rate in CFCC specimens

3.4 Long-Term Monitoring of CFCC Specimens

In addition to the creep rupture test and the relaxation test, multiple sets of CFCC specimens were prepared and prestressed in steel frames as shown in Figure 3.4-1. Five test specimens prestressed to an initial force level of 50.1 kip (223 kN) and ten specimens prestressed to a force level of 56.5 kip (251 kN) were stored indoors in a controlled laboratory environment as shown in Figure 3.4-2. On the other hand, ten test specimens pretressed to a force level of 56.5 kip (251 kN) and ten specimens prestressed to a force level of 50.1 kip (223 kN) were stored outdoors where they have been subjected to severe Michigan weather as shown in Figure 3.4-3. The force in the all test specimens (indoors and outdoors) have been monitored and recorded for the last three years (Figure 3.4-4 and Figure 3.4-5).

Monitoring charts of all CFCC specimens are presented in Figure 3.4-6 through Figure 3.4-8. As seen on the charts, the loss of the prestressing force in indoor specimens was similar to that exhibited in relaxation testing. The outdoor specimens exhibited a fluctuation in the prestressing force associated with the seasonal change in temperature due to the difference in thermal expansion between steel frames and the CFCC strands. However, when corrected for temperature change, the monitoring charts were similar to those obtained for indoors specimens.

Based on the test results available at the time or writing this report, it can be assumed that outdoor specimens did not experience any significant deterioration during the three years of stressing and monitoring. Or at least, it can be assumed that environmental exposure did not cause the strength of the CFCC strand to deteriorate below the level of the highest prestressing force of 56.5 kip (251 kN) otherwise, a strand failure would have occurred. The level of 56.5 kip (251 kN) represents approximately 80 % of the average tensile strength of CFCC. Another remarkable observation is that, current prestressing levels in the indoor and outdoor specimens establishes a benchmark for the minimum creep rupture strength of CFCC strands as discussed in the following section.

Figure 3.4-1 Stressing CFCC specimens for evaluation of long-term properties

Figure 3.4-2 Long-term monitoring of CFCC specimens in a controlled laboratory environment

Figure 3.4-3 Long-term monitoring of prestressed CFCC specimens stored outdoors and exposed to Michigan weather

Figure 3.4-4 Monitoring the level of prestressing force through inline load cells attached to the CFCC specimens

Figure 3.4-5 CFCC specimens stored outdoors after three years of continuous monitoring

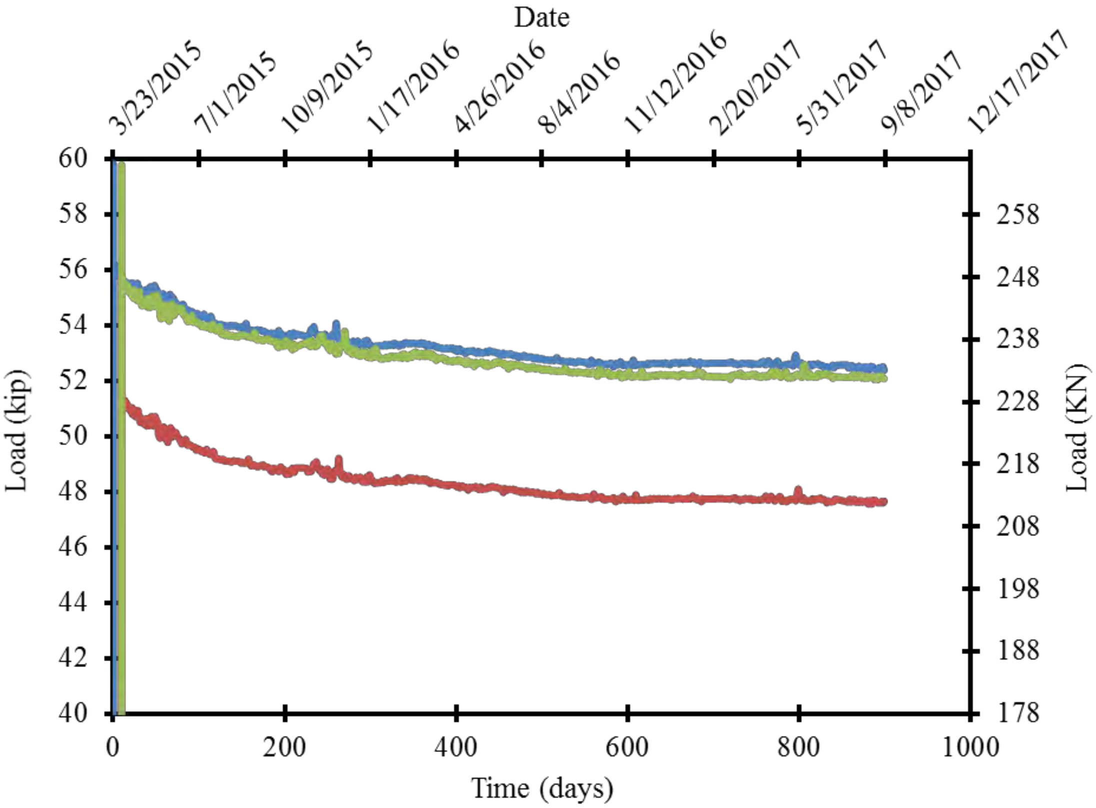

Figure 3.4-6 Long-term monitoring of CFCC specimens loaded in controlled laboratory environment (indoors)

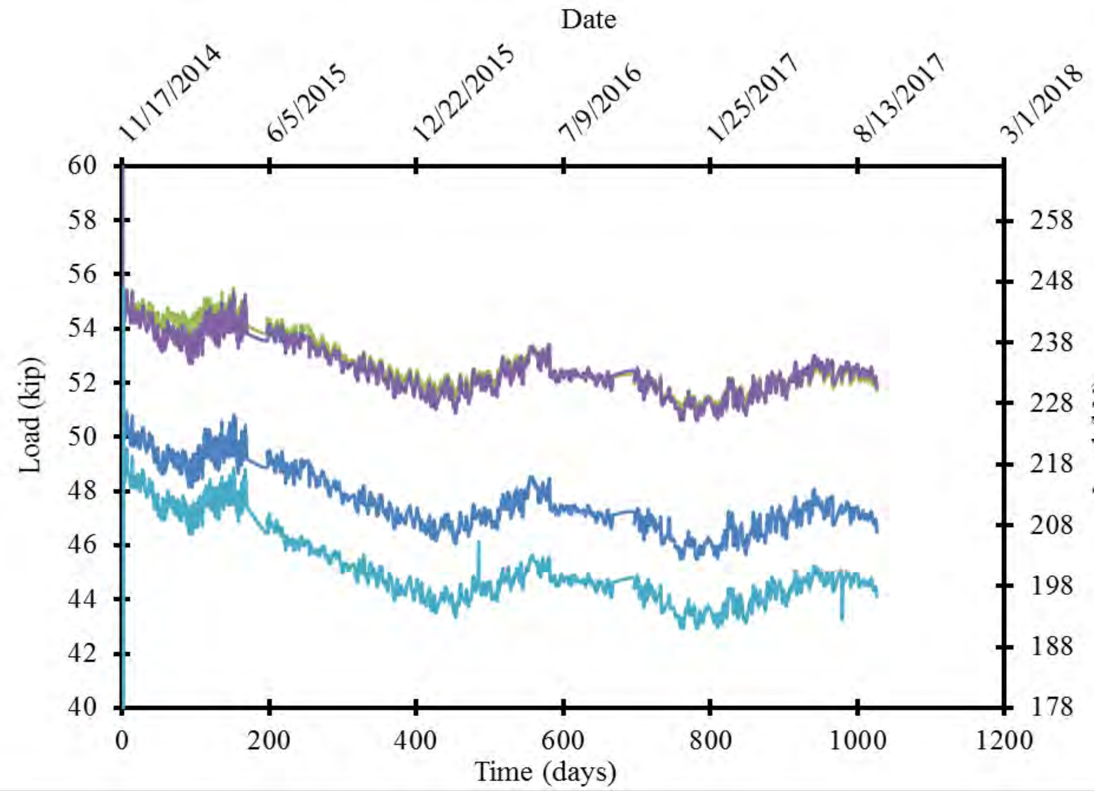

Figure 3.4-7 Long-term monitoring of CFCC specimens stored outdoors

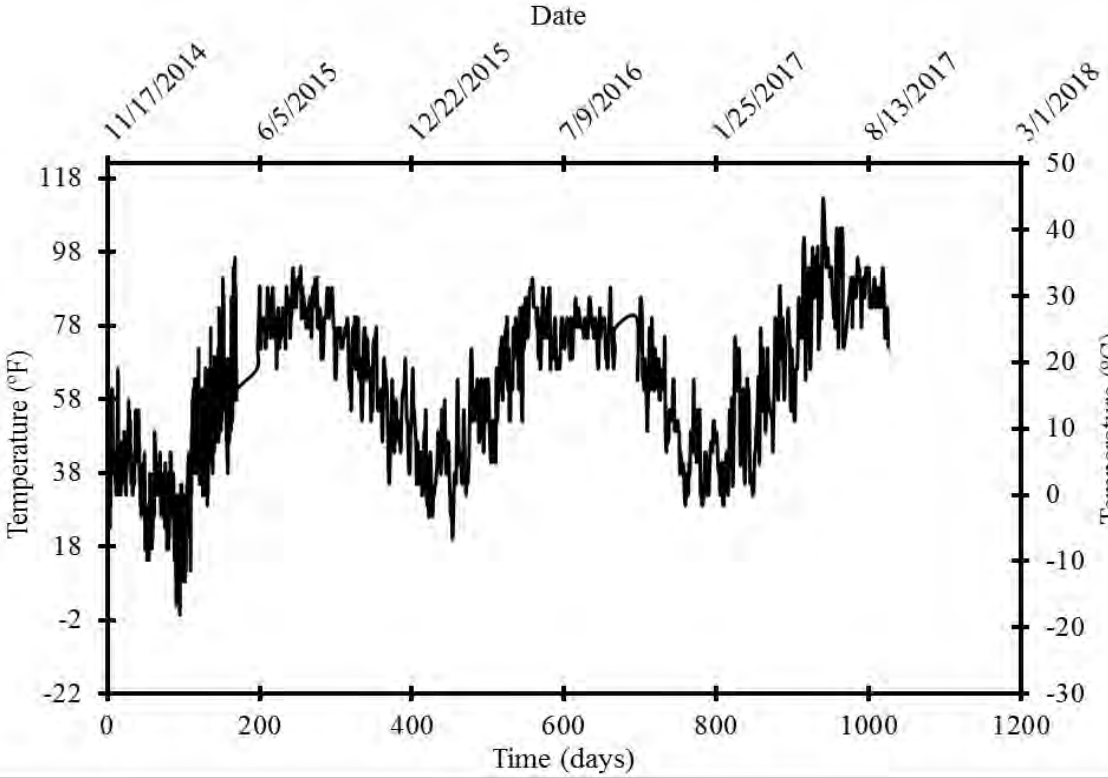

Figure 3.4-8 Temperature change in outdoor CFCC specimens

3.5 Discussion of Test Results

Table 3.5-1 shows a summary for the test specimens that have been loaded or currently under continuous monitoring. The pool of specimens includes creep, relaxation, indoor monitoring, and outdoor monitoring test specimens. It should be noted that other than creep specimens, all test specimens were released prior to the end of the project and were loaded to failure under a uni-axial test setup to evaluate the residual strength after exposure to different environmental and loading conditions. Test results of the residual strength are presented at the end of this chapter. The creep specimens were not released with other specimens and at the time of writing this report, the research team were monitoring and recording the load in them. In addition, Table 3.5-2 shows the test results of a creep-rupture test that was performed on CFCC strands with a diameter of 0.5 in. (12.5 mm) by the manufacturer, Tokyo Rope. Furthermore, Table 3.5-3 show the results of a pilot creep-rupture test that was conducted by the research team on CFCC strands with a diameter of 0.7 in. (18 mm).

An extended segment of the project included loading and monitoring additional five 0.6 in. (15.2 mm) CFCC test specimens a load level of 65 kip (289 kN), which represents approximately 92 % of the average tensile strength or 107 % of the strand guaranteed strength. Furthermore, five CFCC test specimens with a diameter of 0.7 in. (18 mm) were loaded to a load level of 95 kip (422 kN), which represented approximately 84 % of the average tensile strength (113.9 kip or 506 kN) or 110 % of the strand guaranteed strength (86.5 kip or 385 kN). Both sets of specimens were loaded in a custom-made closed-loop hydraulic system that maintains a constant level of load in all specimens. At the time of writing this report, the 0.7-in. (18-mm) CFCC specimens were maintaining the assigned load for 18,360 hours, while 0.6-in. (15.2-mm) CFCC specimens were maintaining the assigned load for 11,000 hours.

By plotting the test results for different diameters of CFCC strands as shown on Figure 3.5-3, a one million-hour creep-rupture strength can be estimated by drawing a line separating the failed specimens from those still sustaining the applied load and under continuous monitoring (Table 3.5-1) or those that sustained the load for a period of time and then were released. The failed specimens from different diameters go above the line, while other specimens can go either above or below the line. In other words, this line separates the unsafe stress zone above the line from the safe stress zone below the line. By extending the line to the end of the graph, an estimate for the one-million-hour creep-rupture strength can be drawn.

Based on available test results at the time of writing this report, the minimum one-million-hour creep-rupture strength for CFCC strands cannot be less than 86 % of the average tensile strength. For instance, for CFCC strands with a diameter of 0.6 in. (15.2 mm) with average tensile strength of (70 kip or 311 kN), the one-million-hour creep rupture strength is approximately 60.2 kip (268 kN). In other words, CFCC strands with a diameter of 0.6 in. (15.2 mm) can be safely loaded to its guaranteed strength of 60.7 kip (270 kN) for 114 years (one-million hour) without experiencing creep rupture. The same can be held true for other CFCC diameters except for the ratio to guaranteed strength since CFCC strands with different diameters have different ratios between the guaranteed and average tensile strengths. Finally, as monitoring for CFCC specimens continues, the points under the line on the figure will continue to shift to the right, while pushing the line upward, which means a higher estimate for the one-million-hour creep-rupture strength.

Figure 3.5-1. Closed-loop hydraulic system to maintain a constant force in creep test specimen

Figure 3.5-2 CFCC specimens under constant load to evaluate creep rupture strength

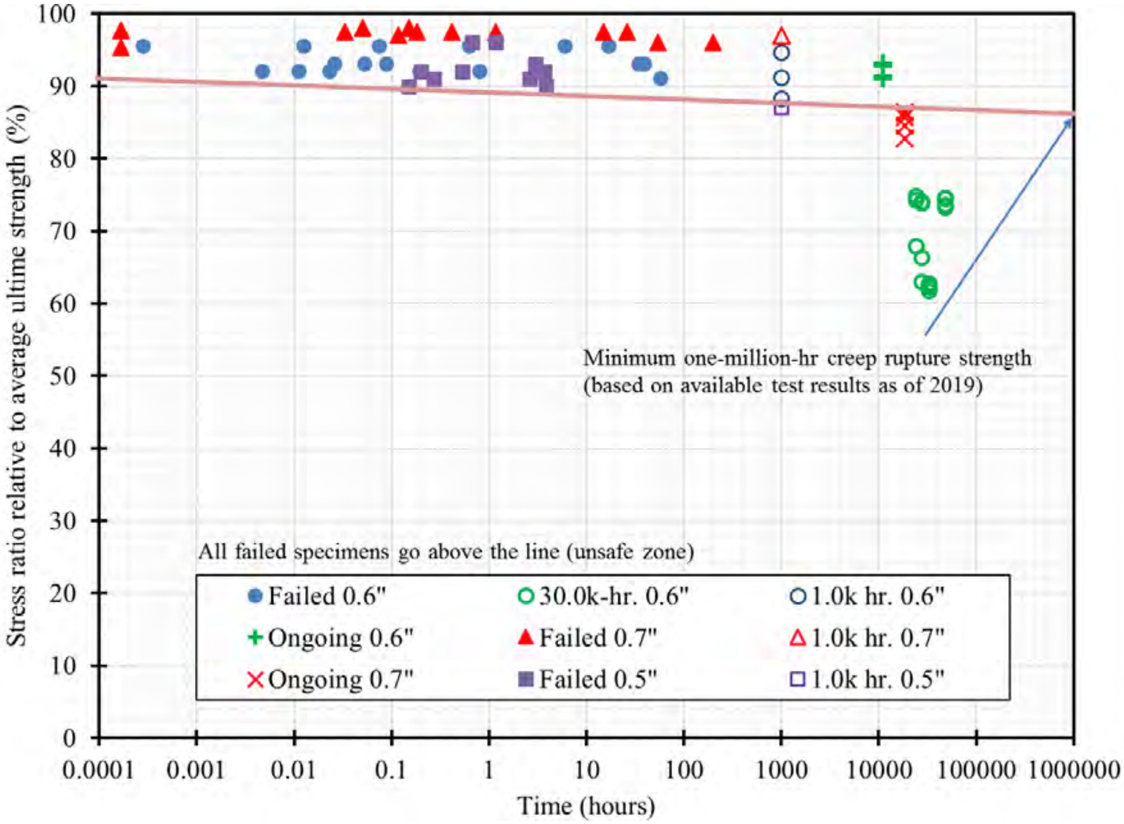

Figure 3.5-3. Lowest estimate for one-million-hour creep-rupture strength based on available test results including long-term monitoring CFCC specimens

Table 3.5-1 Summary of CFCC specimens (diameter of 0.6 in. (15.2 mm)) under monitoring

Test program	Initial load	last load reading	Last load ratio to 70 kip (311 kN)	Time
	Kip (kN)	Kip (kN)	%	hours
Creep (Ongoing)	55 (245)	51.5 (229)	73.6	47,424*
	55 (245)	51.3 (228)	73.3	47,424*
	55 (245)	52.2 (232)	74.5	47,424*
	55 (245)	52.2 (232)	74.5	47,424*
	55 (245)	52.3 (232)	74.7	47,424*
Indoor monitoring	56.5 (251)	52.4(233)	74.8	24,408
	56.5 (251)	52.0 (231)	74.3	23,880
	50.1 (251)	47.6 (212)	68.0	23,856
Outdoor monitoring	56.5 (251)	51.8 (230)	74.0	27,456
	56.5 (251)	51.7 (230)	73.8	27,480
	56.5 (251)	51.9 (231)	74.1	27,480
	50.1 (223)	46.5 (207)	66.4	27,552
	50.1 (223)	44.1 (196)	63.0	27,552
Relaxation	47.5 (211)	43.9 (195)	62.8	32,424
	47.5 (211)	43.8 (195)	62.6	32,424
	47.5 (211)	43.7 194)	62.4	32,424
	47.5 (211)	43.2 (192)	61.8	32,424
	47.5 (211)	43.6 (194)	62.3	32,424

Table 3.5-2 Test results of creep-rupture strength performed by Tokyo Rope using CFCC strands with a diameter of 0.5 in. (12 mm)

Lot #	Test #	Average tensile strength	Sustained load	Load ratio	Time	Mode
		Kip (kN)	Kip (kN)	(%)	(hours)	
0423	1	36.9 (164)	34.4 (153)	93.3	3.00	Failure
	2		33.3 (148)	90.2	0.15	Failure
	3		35.3 (157)	95.7	1.17	Failure
	4		35.3 (157)	95.7	0.67	Failure
	5		32.1 (143)	87.2	1000.00	Suspend
	6		34.4 (153)	93.3	44.00	Suspend
0424	7	34.6 (154)	31.9 (142)	92.2	0.53	Failure
	8		31.9 (142)	92.2	0.20	Failure
	9		31.9 (142)	92.2	3.66	Failure
	10		31.3 (139)	90.3	3.87	Failure
	11		31.5 (140)	90.9	2.61	Failure
	12		31.5 (140)	90.9	0.27	Failure
	13		30.8(137)	89.0	27.00	Suspend
	14		30.8 (137)	89.0	63.50	Suspend

Table 3.5-3 Results of creep-rupture testing on CFCC strands with a diameter of 0.7 in. (18 mm)

Test #	Average tensile strength	Sustained load	Load ratio	Time	Mode
	kip (kN)	Kip (kN)	%	hours	
1	113.93 (507)	111.64 (497)	98.0	0.15	Failure
2		111.68 (497)	98.0	0.05	Failure
3		111.31 (495)	97.7	0.000167	Failure
4		111.04 (494)	97.5	1.166667	Failure
5		111.05 (494)	97.5	0.033333	Failure
6		111.05 (494)	97.5	26	Failure
7		111.05 (494)	97.5	0.416667	Failure
8		111.05 (494)	97.5	15	Failure
9		111.05 (494)	97.5	0.183333	Failure
11		110.53 (492)	97.0	0.116667	Failure
		110.54 (492)	97.0	1000	Suspended
12		109.37 (486)	96.0	54	Failure
13		109.37 (486)	96.0	200	Failure
14		108.63 (483)	95.3	0.000167	Failure

3.6 Release and Uni-axial Tensile Test

After completion of the monitoring project, the indoor, outdoor, and relaxation test specimens were released and were loaded under a uniaxial test setup to failure. Test results of the uni-axial testing are given in Table 3.6-1 through Table 3.6-5 for all test specimens. In addition, test results of unstressed test specimens that were constructed at the same time with other test specimens but were kept in controlled laboratory conditions are presented in Table 3.6-6. All test specimens were loaded in a force-control module with a loading rate of 6.5 kip/minute (29 kN/minute).

As shown in the test results, all test groups achieved a higher tensile strength with an average exceeding 80 kip (356 kN). This was a remarkable increase in the tensile capacity from the stated average tensile capacity of 70 kip (311 kN) that was achieved by testing the fresh specimens after construction. The environmental conditions did not seem to have any detrimental effect on the residual tensile capacity of the CFCC strands. Both indoor and outdoor specimens achieved roughly the same average tensile strength. Besides, the stress level in the CFCC strands during monitoring did not seem to affect the residual tensile strength either. Specimen group with the highest average tensile strength was the indoor group with an initial force of 50.1 kip (223 kN), while the test group with the lowest average tensile strength was also the indoor group with a initial force of 47.5 kip (211 kN) per strand.

Since the unstressed specimens that were kept in laboratory conditions achieved roughly the same tensile capacity, it appears that the increase in the strength is more related to the extended curing of either the epoxy matrix of CFCC strands or the anchorage grout material, or both. However, it can be safely stated that CFCC strands did not experience any loss in strength due to sustained loading of nearly 93 % of the guaranteed strength or due to exposure to severe weather conditions for a period of three years. Therefore, a strength reduction factor that accounts for the durability of CFCC under different environmental conditions may not be necessary in design.

Table 3.6-1 Uni-axial test results of indoor specimens with initial load of 47.5 kip (211 kN)

Specimen	Duration of monitoring (days)	Tensile strength	Strain at failure %
1	1351	83.8 (373)	1.87
2	1351	81.2 (361)	1.80
3	1351	74.8 (333)	1.83
4	1351	80.8 (359)	1.98
5	1351	79.8 (355)	1.61
Average		80.1 (356)	1.82

Table 3.6-2 Uni-axial test results of indoor specimens with initial load of 50.1 kip (223 kN)

Specimen	Duration of monitoring (days)	Tensile strength	Strain at failure %
1	994	82.9 (369)	1.92
2	994	84.5 (376)	1.88
3	994	83.9 (373)	1.94
4	994	83.3 (371)	2.05
5	994	80.4 (358)	1.93
Average		83.0 (369)	1.94

Table 3.6-3 Uni-axial test results of indoor specimens with initial load of 56.5 kip (251 kN)

Specimen	Duration of monitoring (days)	Tensile strength	Strain at failure %
1	1001	82.5 (367)	1.97
2	1001	84.0 (374)	1.96
3	1002	83.6 (372)	2.20
4	1002	83.1 (370)	1.98
5	1002	83.7 (372)	1.95
6	995	85.5 (380)	1.88
7	995	84.0 (374)	1.85
8	995	75.3 (335)	1.50
9	995	84.2 (375)	1.90
10	995	61.9 (275)	1.40
Average		80.8 (359)	1.86

Table 3.6-4 Uni-axial test results of outdoor specimens with initial load of 56.5 kip (251 kN)

Specimen	Duration of monitoring (days)	Tensile strength	Strain at failure %
1	1144	84.5 (375)	1.88
2	1144	82.2 (366)	2.12
3	1144	85.0 (378)	2.25
4	1145	75.3 (335)	1.84
5	1145	74.9 (333)	1.73
6	1145	84.7 (377)	2.03
7	1145	79.9 (355)	1.66
8	1145	79.1 (352)	1.73
9	1145	84.5 (376)	2.11
10	1145	78.5 (349)	1.76
Average		80.9 (360)	1.91

Table 3.6-5 Uni-axial test results of outdoor specimens with initial load of 50.1 kip (223 kN)

Specimen	Duration of monitoring (days)	Tensile strength	Strain at failure %
1	1148	84.1 (374)	1.93
2	1148	77.0 (343)	1.58
3	1148	72.0 (320)	1.66
4	1148	83.8 (373)	1.83
5	1148	84.1 (374)	1.74
6	1148	81.9 (364)	1.82
7	1148	82.0 (365)	1.97
8	1148	84.3 (375)	1.98
9	1148	84.6 (376)	1.83
10	1148	82.9 (369)	1.87
Average		81.7 (363)	1.82

Table 3.6-6 Summary of uni-axial test results of unstressed specimens stored for three years

Specimen	Duration of monitoring, days	Tensile strength, kip (kN)	Strain at failure, %
1	-	80.7 (359)	1.95
2	-	80.4 (357)	1.92
3	-	80.9 (360)	1.96
4	-	79.6 (354)	1.69
5	-	81.48 (362)	1.73
Average		80.6 (359)	1.85

CHAPTER 4: ENVIRONMENTAL EFFECTS

4.1 Introduction

Exposure to fluctuation in temperature is inevitable when CFRP strands are used in highway bridge construction. Starting at the time of construction, CFRP strands are exposed to change in temperature after they are prestressed and before pouring the concrete. While CFRP strands have a negligible coefficient of thermal expansion, the steel strands coupled to them and the steel formwork do not. The difference in the coefficient of thermal expansion between CFCC and surrounding materials leads to a change in the prestressing force that must be calculated and included while establishing the jacking force. In addition, after pouring the concrete and during curing, the temperature of the concrete increases significantly. This increase in temperature could affect the level of the prestressing force in the CFCC strands by producing an additional heat-related relaxation. Furthermore, the daily and seasonal change in temperature, while a CFRP prestressed beam is in service, also affects the level of the prestressing force in the CFRP strands due to the difference in the coefficient of thermal expansion between the CFRP and the surrounding concrete. It should be noted that Laboratory Test Report No. R-5.10_TOK-JP_FDOT933.4 by University of Miami Structures and Materials Laboratory averages the glass transition temperature of CFCC samples at 245 °F (118 °C). Test was conducted according to ASTM E1640-13 “Standard Test Method for Assignment of the Glass Transition Temperature by Dynamic Mechanical Analysis”.

Limited experimental data on relaxation of CFRP cables at elevated temperatures are available but are insufficient to suggest certain relaxation loss at different temperatures. Saadatmanest and Tannous (1999) performed a preliminary study on the relaxation of Leadline tendons and CFCC cables at room and elevated temperatures. Twelve CFCC tendons of 16 in. (400 mm) length were tested for relaxation losses in air at temperatures of -30, 25 and 60 °C for a period of 3000 hour, at stress ratios of 0.4 and 0.6. The authors concluded that the percentage loss in the tensile force increased with the increase of the initial stress level and the temperature of the environments. The extrapolated relaxation loss of CFCC were limited to 10 % over a 50-year period.

Enomoto et al. (2009) showed that relaxation and logarithm of passing time can be represented by a linear relationship at room temperature similar to the steel tendons. They reported a one-million-hour relaxation rate of approximately 2 % of CFRP cables when stressed to 70 % of the guaranteed standard load (average failure load minus three times the standard deviation) at room temperature. In their effort to the study the effect of steam curing of precast members, they carried out relaxation tests of CFRP cables according to JSCE-E 534 (1995) at temperatures of 60, 80 and 100 °C. They found that the relaxation values at 20-80 °C was within the range of 2 %. Whereas, above 80 °C, the estimated relaxation rose sharply due to the softening of the epoxy resin. They also stated the necessity of conducting relaxation tests with temperature as a variable parameter.

Sasaki et al. (2012), in his effort to address the lack of demonstrative data (actual long-term field exposure as opposed to the standard 1000-hour laboratory relaxation test), retrieved and evaluated several properties including relaxation of 17 years old FRP specimens exposed to direct sunlight radiation and salt splash. They concluded that CFRP exhibited a negative response to direct sunlight for relaxation losses unlike AFRP which showed no susceptibility and confirmed the use of the semi-logarithmic plot in a laboratory 1000-hour relaxation test. Apparent relaxation after one-million hours were found to have increased from 10 % for CFRP specimens (prestressed to 70 % of ultimate tensile capacity) not exposed to direct sunlight to between 16 to19 % for specimens exposed to direct sunlight. The increased relaxation rate was attributed significantly to thermal fatigue resulting from stress induced by sunlight. Possibility of the stress increase resulting from matrix degradation to UV exposure was also not discounted even though earlier tests indicated otherwise.

This chapter addresses the issue of temperature fluctuation and presents detailed results obtained from testing unbonded CFCC strands and CFCC prestressed bulb T beams exposed to a change in temperature. The results showed that unbonded prestressed CFCC strands exhibit a prestress loss with by the increase in temperature. However, recurrent temperature increase, to a certain temperature, does not seem to cause any further loss in the prestressing force. In addition, test results of decked bulb T beams prestressed with CFCC strands showed that seasonal change in temperature leads to a change in the level of prestressing force. However, this change in force is found to be temporary and is reversed once the temperature changes back. Details of test setups and main test results are discussed in the following sections.

4.2 Unbonded CFRP Strands

4.2.1 Test setup

The main objective of the test was to evaluate the change in the effective prestressing force, as well as the mechanical properties of CFCC at and after exposure high temperatures. To achieve this objective, five CFCC test specimens with prestressing level of 33 kip (147 kN) were monitored for load loss while being subjected to different elevated temperatures. The nomenclatures of the test specimens are: TH-S1, TH-S2, TH-S3, TH-S4, and TH-S5. The thermal test program was executed through three phases; Phase I, II, and III. The temperature matrices and details Phases I and II are discussed in subsequent sections, while Phase III included testing the specimens to failure through uniaxial tensile test to evaluate the residual tensile capacity and elastic modulus of CFCC. The thermal test specimens, shown in Figure 4.2-1 and Figure 4.2-2, consisted of 49 in. (1.2 m) long CFCC strands with two sleeve anchors. Details on CFCC materials and anchorage preparation are presented earlier in this report.

The thermal test of CFCC specimens was performed in an MTS® electrically heated environmental chamber as shown in Figure 4.2-1. The internal dimensions of the chamber are 12 in. × 12 in. × 12 in. (305 mm × 305 mm × 305 mm). The chamber is designed to reach temperatures up to 400 ºF (204 ºC) in less than 15 minutes and is provided with a temperature controller that displays a set point and current temperature. Heating is achieved using electrical heating elements and a circulation fan that ensures uniform temperatures throughout the chamber while also shielding the specimen from direct exposure to radiant heat. Cooling of the chamber is accomplished with liquid nitrogen but was not used in the current study. The chamber is designed to accommodate small scale specimens with two access holes at the top and bottom of the chamber for gripping purposes. Those holes were blocked with thermal blanks during the test to maintain uniform temperature and eliminate any temperature increase of the anchorage devices at the ends of the specimens.

The loading frame used to apply prestressing force to CFCC specimens was manufactured by MTS®. This 2-post loading frame shown in Figure 4.2-1 consists of a crosshead that can move along two columns using a crosshead hydraulic actuator with a standard stroke of 6 in. (152 mm). The mounting height of the crossheads varies from 7 in. (178 mm) to 62.5 in. (1586 mm) with a constant width between the columns of 25 in. (635 mm). The loading frame includes a force transducer (load cell) to measure the axial force applied to the specimen and an LVDT to measure the displacement of the actuator. The tensile load capacity of the loading frame is 55 kip (245 kN). The specimens were only loaded to 33 kip (147 kN).

An MTS FlexTest™ GT Station Manager controls a hydraulic actuator that applies the prestressing load to the test specimens in the loading frame. For this test, the prestressing force was applied to CFCC specimens in a force-control mode with rate of 6.5 kip/min (29 kN/min) until the load reached 33 kip (147 kN). Then, the MTS software automatically switched the mode to displacement-control mode and locked the actuator heads in place.

In Phase I thermal testing, CFCC test specimens were prestressed to 33 kip (147 kN) and were subjected to different elevated temperatures, while the loss in the prestressing force due to the increased temperature was monitored at each temperature range. Specimen TH-S1 served as a control specimen and was loaded to a force level of 33 kip (147 kN) at a room temperature of 76 °F (24 °C) for four hours and then the load was removed without activating the environmental chamber. The loss in the load due to strand and anchorage relaxation was monitored and captured.

The second test specimen (TH-S2) was loaded to a force level of 33 kip (147 kN) at a room temperature. Two hours after loading the specimen, the environmental chamber was activated and the temperature of the heated length of the CFRP specimen increased to 150 °F (65 °C). The temperature was maintained at 150 °F (65 °C) for two hours, then the heat chamber was turned off and specimen was allowed to naturally cool down to room temperature. After one hour, the load was removed. The heating and cooling rates were approximately 20 °F (10 °C) per minute.

The third test specimen (TH-S3) was loaded to 33 kip (147 kN) at room temperature. After two hours, the temperature of the heated length increased to 150 °F (65 °C). After two hours, the temperature increased again to 235 °F (112 °C). After two more hours, the environmental chamber was allowed to cool down to room temperature. An hour later, the load was removed.

The fourth test specimen (TH-S4) was loaded at room temperature for two hours. Then, the temperature increased to 150 °F (65 °C) for two hours, to 235 °F (112 °C) for two hours, and to 316 °F (158 °C) for two hours. After that, the specimen was allowed to cool down and the load was removed an hour later.

The fifth test specimen was loaded to 33 kip (147 kN) at room temperature for two hours. Then, the temperature increased to 150 °F (65 °C) for two hours, to 235 °F (112 °C) for two hours, to 316 °F (158 °C) for two hours, and to 400 °F (204 °C) for two hours. Finally, the specimen was allowed to cool down for an hour, after which the load was removed.

Phase II of the test started after concluding Phase I. In Phase II, the specimens were heated through a single-step heating to their maximum reached temperature in Phase I as shown in Figure 4.2-4 . For instance, fifth specimen (TH-S5) was loaded to 33 kip (147 kN) at room temperature and after two hours, the temperature increased and was maintained at 400 °F (204 °C) for two hours. Then the specimen was allowed to cool down to room temperature and the load was removed after two hours, with total a test duration of 6 hours.

In Phase III. CFCC specimens were placed in a 270-kip (1200-kN) MTS Axial Load Frame for a uniaxial tensile test. Tensile force was applied in a force-control mode at a rate of 2 kip/min (9 kN/min) to failure. The tensile test was conducted in accordance with ASTM Standard D7205/7205M-06: "Standard Test Method for Tensile Properties of Fiber Reinforced Polymer Matrix Composite Bars".

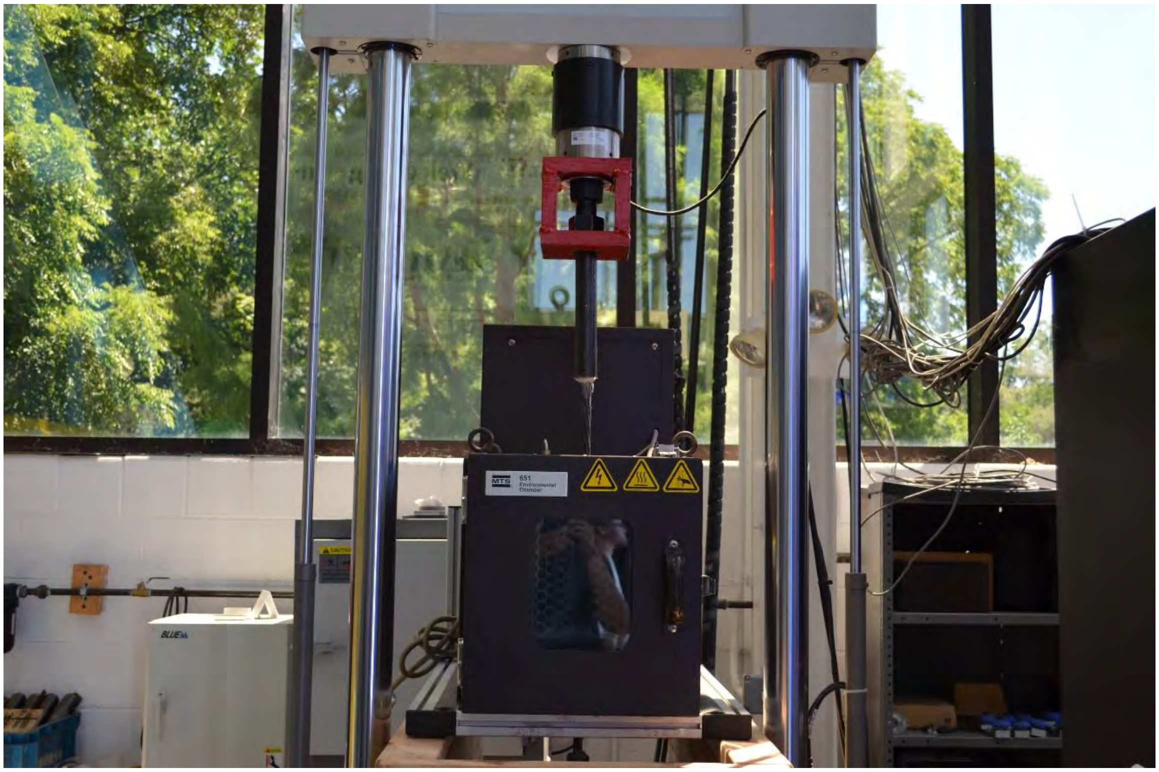

Figure 4.2-1 Evaluating prestress loss in CFCC specimens due to temperature increase

Figure 4.2-2 Heated length of CFCC strand inside the heat chamber

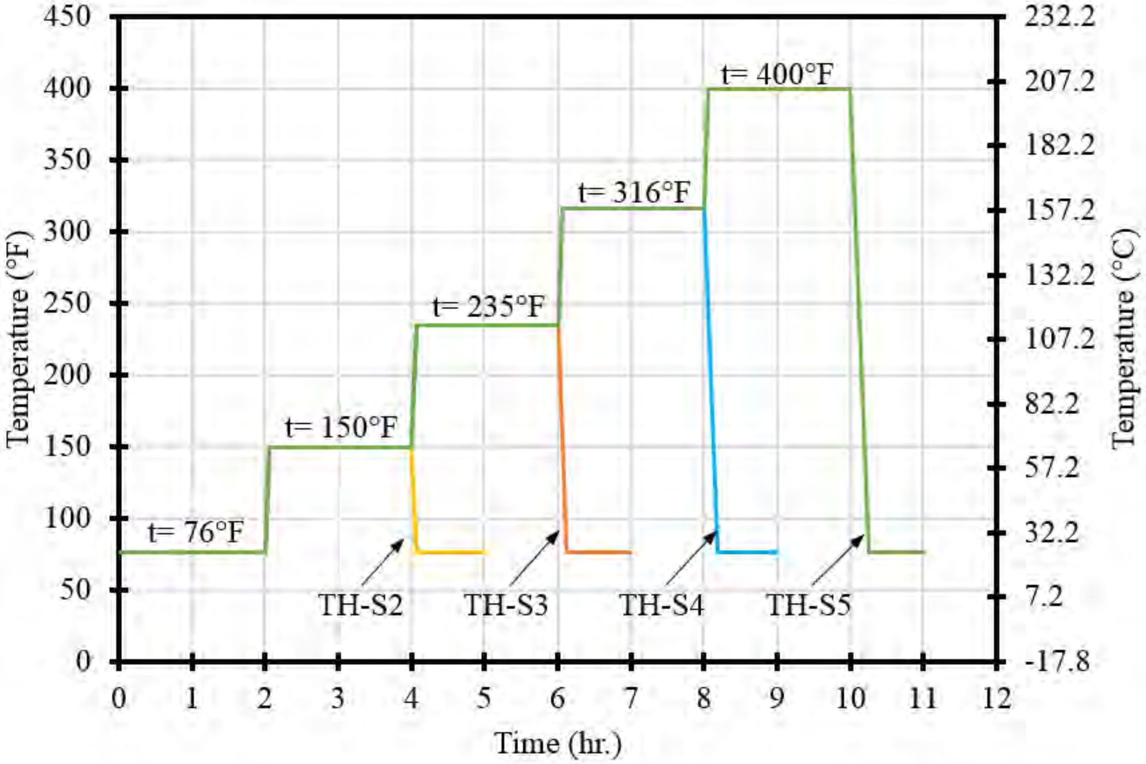

Figure 4.2-3 Time-temperature curves for thermal test specimens in Phase I

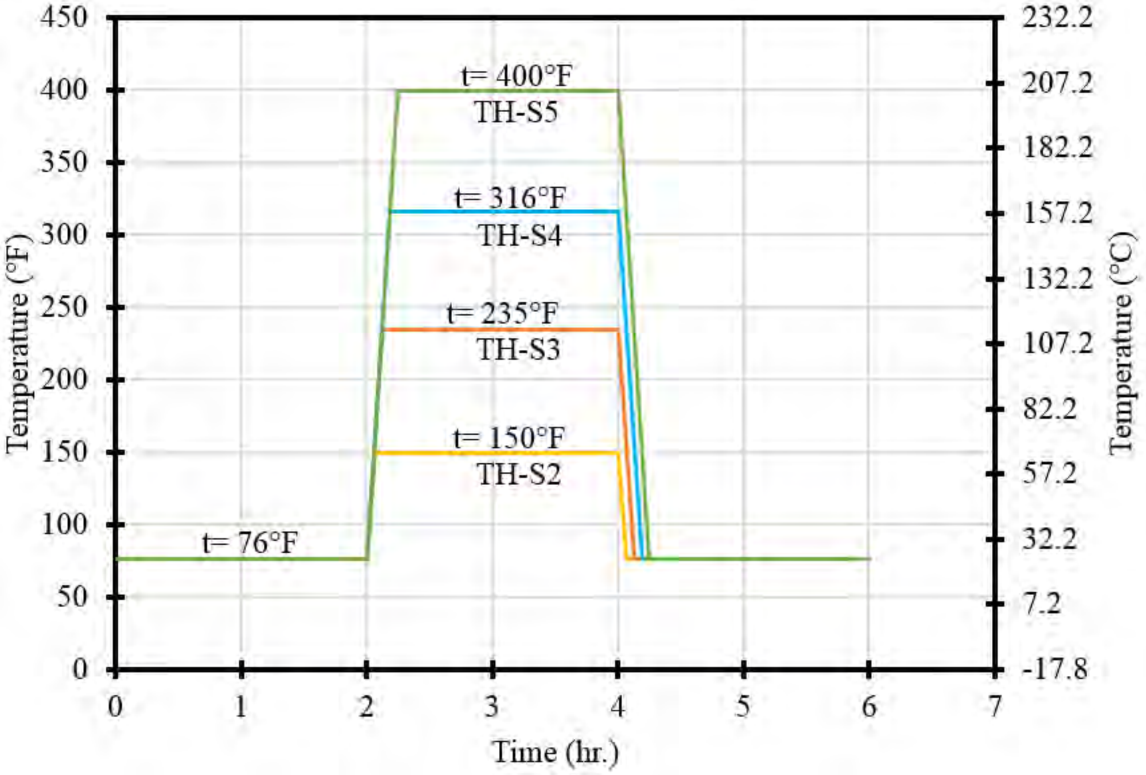

Figure 4.2-4 Temperature profiles for thermal test specimens in Phase II

4.2.2 Test results

The load vs. time curves for all test specimens in Phase I are presented in Figure 4.2-5 through Figure 4.2-9. TH-S1 experienced a typical relaxation loss that was discussed earlier in the report. The prestressing force decreased with the time with a load loss of approximately 0.76 kip (3.4 kN) and 0.84 kip (3.7 kN) after 2 and 4 hrs., respectively with a total prestress loss of 2.5 %.

Specimen TH-S2 displayed the same pattern with a load loss of 0.72 kip (3.2 kN) in the first 2 hrs. (ambient temperature). When the temperature of the specimen was raised to 150 °F (66 °C), there was a step decrease in the load. In order to precisely estimate the load loss that occurred in the specimen due to the thermal change, the slope of the unheated segment was estimated and extended as a linear function between the load and the time. The thermal load loss was determined as the difference between the linear slope and the actual load-time curve. The load loss due to temperature increase was estimated as 0.33 kip (1.5 kN).

TH-S3 was exposed to two temperature increases. With each temperature increase, the specimen exhibited a loss in the load. That is in addition to the initial loss of the load during the first two hours of heating with no increase in temperature. A load loss of 0.67 kip (3kN) was observed in the first 2 hrs with no heat. As shown in Table 4.2-1, a load loss of 0.36 kip (1.6 kN) was associated with the increase in temperature from ambient to 150 °F (66 °C), while a load loss of 0.78 kip (3.5 kN) was associated with the increase in temperature from 150 °F (66 °C) to 235 °F (112 °C).

In addition to the loss in load of 0.73 kip (3.2 kN) before heating, Specimen TH-S4 exhibited a 3-stage loss in load associated with increase in temperature. The recorded losses were, 0.32 kip (1.4 kN), 0.75 kip (3.3 kN), and 0.3 kip (1.3 kN) with the increase in temperatures from ambient to 150 °F (66 °C), to 235 °F (112 °C), and to 316 °F (158 °C), respectively.

Specimen TH-S5 displayed a similar load loss pattern with load losses of 0.67 kip (3 kN) before heating, then a loss of 0.39 kip (1.7 kN), 0.73 kip (3.2 kN), 0.33 kip (1.5 kN), and 0.18 kip (0.8 kN), that corresponded to the temperature increase in the specimen from ambient to 150 °F (66 °C), to 235 °F (112 °C), to 316 °F (158 °C), and to 400 °F (204 °C), respectively.

Load loss in Phase II was significantly less than that observed in Phase I even though the specimens were heated to the same temperature in Phase I. The load vs. time curves for all the specimens during Phase II is presented in Figure 4.2-10 through Figure 4.2-13. In all the specimens, the increase in the temperature did not results in any significant loss of the load and the drop of the load was almost gradual and similar to a typical load loss that could be observed at ambient temperature. It appears that initial heating of a CFCC specimen to a certain temperature level caused the epoxy matrix to relax and expand. Since the specimen was loaded during the heating period, this expansion/relaxation of the epoxy matrix was converted into a loss in the load. After the specimen was allowed to cool down, the epoxy matrix solidified in its standing shape, which explains the inability of the specimens to regain the lost load when they were allowed to cool down. When the CFCC specimens were heated for the second time in Phase II, the epoxy matrix did not experience any further relaxation since the temperature in the second heating cycle did not exceed that of the first cycle and that explains the minimal loss in the load in Phase II. . It should be noted that when the specimens were allowed to cool down at the end of Phase I, the lost load was not recovered, which indicated that the loss in the load was not related to the thermal expansion of the specimens and that the heat relaxation was non-recoverable. This was also confirmed in Phase II since loss of the load due to thermal expansion of the specimens would have been evident during the heating segment in Phase II.

The loss in the load due to the increase in temperature of the test specimens in Phase I was used to calculate the heat relaxation loss and estimate the loss in prestressing force during construction when the concrete is placed around the pretensioned CFRP strands and the heat is generated by concrete hydration. Several studies (Swenson and French 2015; Barr et al. 2005) place the maximum concrete temperature during hydration at 150 °F (65 °C), which is corresponding to a relaxation loss in the heated segment of approximately 287 $\mu\varepsilon$ or a prestress loss of approximately 6.75 ksi (46.5 MPa). The calculations of the heat relaxation loss follow the basics of mechanics of materials. For instance, the heated segment of the CFCC specimen was 12 in. (305 mm) and since both heads of actuator were locked in position, the heat relaxation of the heated segment caused the loss in the load. When heating the specimens from ambient to 150 °F (66 °C), the average load loss among all specimens was 0.35 kip (1.56 kN). This loss of the load happened over the entire length of the specimen. In other words, between the two fixed heads of the actuator. The heat relaxation strain in the heated segment of the specimen that caused this loss in the load can be back calculated based on load loss as follows:

$$\Delta\varepsilon = \frac{\Delta L}{L_h} \tag{4.2-1}$$

$$\Delta L = \frac{\Delta P L_T}{EA} \tag{4.2-2}$$

where:

$\Delta\varepsilon$ = heat relaxation strain of the specimen (relative to the heated segment only)

ΔL = change in length of heat segment due to added heat relaxation, in. (mm)

L_T = length of the specimen between the fixed actuator heads

L_h = heated length of the specimen = 12 in. (305 mm)

A = cross sectional area of the specimen = 0.179 in.^{2} (115.4 mm^2)

E = elastic modulus of CFCC, ksi (GPa)

ΔP = change in the force due to increase in temperature, kip (kN)

The length of the specimen between the fixed actuator heads (L_T) can be challenging to estimate. The total length of the specimen was 49 in. (1244 mm) including two 12-in. (305-mm) long anchorage devices. With a gripping length of 2.5 in. (64 mm) on each end, the specimen length between the fixed heads, from grip to grip, was 44 in. (1118 mm) However, this length had a free strand length of 25 in. (635 mm) and an embedded length inside the anchorage devices of 19 in. (483 mm). Bond mechanism and force transfer in the embedded length complicates the calculations of the elongation in the embedded region.

To avoid the unnecessary difficulty in estimating L_T along with the need for estimating the elastic modulus of CFCC, Eqn. 4.2-1 can be rewritten using the load-elongation curve of the specimen (from zero loading to 33 kip (147 kN)). The displacement of the actuator was recorded during the loading of the specimen. Therefore, the relationship between the elastic modulus and the length of the specimen can be written as:

$$\frac{L_T}{EA} = \frac{\Delta L_L}{\Delta P_L} \tag{4.2-3}$$

where:

ΔP_L = change in the load during the loading of the specimen
ΔL_L = corresponding elongation of the specimen estimated using actuator displacement

From the loading-elongation curves of the five specimens, the average (L_T/EA) was 0.00983 in./kip (0.056 mm/kN), calculated based on an observed change in displacement of 0.1081 in. (2.75 mm) over a change in the load from 22 to 33 kip (98 to 147 kN). Therefore, the heat relaxation strain in the CFCC specimen can be calculated as:

$$\Delta L = \Delta P \frac{L_T}{EA} = 0.35 \times 0.00983 = 0.00344\ in. \tag{4.2-4}$$

$$\Delta \varepsilon = \frac{\Delta L}{L_h} = \frac{0.00344}{12} = 287 \times 10^{-6} = 287\ \mu\varepsilon \tag{4.2-5}$$

It should be noted that these calculations are based on a conservative estimate for the heated length of 12 in. (305 mm), which represents the interior height of the heat chamber. The actual heated length of the CFCC strand specimens was slightly longer than 12 in. (305 mm) since the heat radiated beyond the interior cavity of the heat chamber through the top and bottom holes (holes were block with thermal blanket to minimize heat escape). Temperature on the exterior top surface of the heat chamber was approximately 94.5 °F (34.7 °C) when the temperature inside the chamber was 150 °F (65 °C), while the temperature at the bottom exterior surface did not exceed the ambient (76 °F or 24 °C) during the entire test. Therefore, it can be assumed that the temperature dropped linearly from 150 °F (65 °C) to 94.5 °F (34.7 °C) through the 2-in. (50.1-mm) thick ceiling of the heat chamber. Consequently, a more accurate heated length may be taken as 13.5 in. (343 mm) considering an additional 1.0 in. (25.4 mm) of heated length through the top hole and 0.5 in. (13 mm) through the bottom hole, with a resulting additional strain of 254 $\mu\varepsilon$.

Finally, it should be noted that when the temperature inside the chamber was 400 °F (204 °C), the maximum record temperature at the exterior top surface of the heat chamber was 129 °F (54 °C) and the highest recorded temperature at the bottom of the top anchorage device was 87.5 °F (31 °C) . Therefore, it can be safely concluded that the anchorage devices were protected from heat and did not participate in the recorded loss of the load due to temperature increase.

Figure 4.2-14 and Figure 4.2-15 show the testing and failure of test specimens in Phase III. Test results of are also presented in Table 4.2-2. The uniaxial tensile test of the four test specimens at ambient temperature in Phase III revealed an average breaking load of 70.5 kip (314 kN), which is approximately equal to the breaking load of non-heated test specimen. Besides, the average elastic modulus calculated based on uniaxial tensile test at ambient temperature of the four heated test specimens was approximately 23,101 ksi (159 GPa), which is slightly higher than the elastic modulus of non-heated specimen. No noticeable physical difference was observed between the first specimen (non-heated) and the rest of the specimens.

Table 4.2-1 Summary of observed load loss due to increase in temperature in Phase I

Start Temp.	End Temp.	TH-S1	TH-S2	TH-S3	TH-S4	TH-S5
°F (°C)	°F (°C)	kip (kN)	kip (kN)	kip (kN)	kip (kN)	kip (kN)
76 (24)	150 (65)	-	0.33 (1.5)	0.36 (1.6)	0.32 (1.4)	0.39 (1.7)
150 (65)	235 (112)	-	-	0.78 (3.5)	0.75 (3.3)	0.73 (3.2)
235 (112)	316 (158)	-	-	-	0.3 (1.3)	0.33 (1.5)
316 (158)	400 (204)	-	-	-	-	0.18 (0.8)

Table 4.2-2 Results of tensile testing of CFCC specimens

Specimen	Max. Temp.	Failure Load	Elastic Modulus
	°F (°C)	(kN)	ksi (GPa)
TH-S1	76 (24)	71.0 (316)	22,245 (153)
TH-S2	150 (65)	71.2 (317)	22,947 (158)
TH-S3	235 (112)	66.0 (294)	22,967 (158)
TH-S4	316 (158)	70.6 (314)	23,051 (159)
TH-S5	400 (204)	74.1 (330)	23,440 (162)

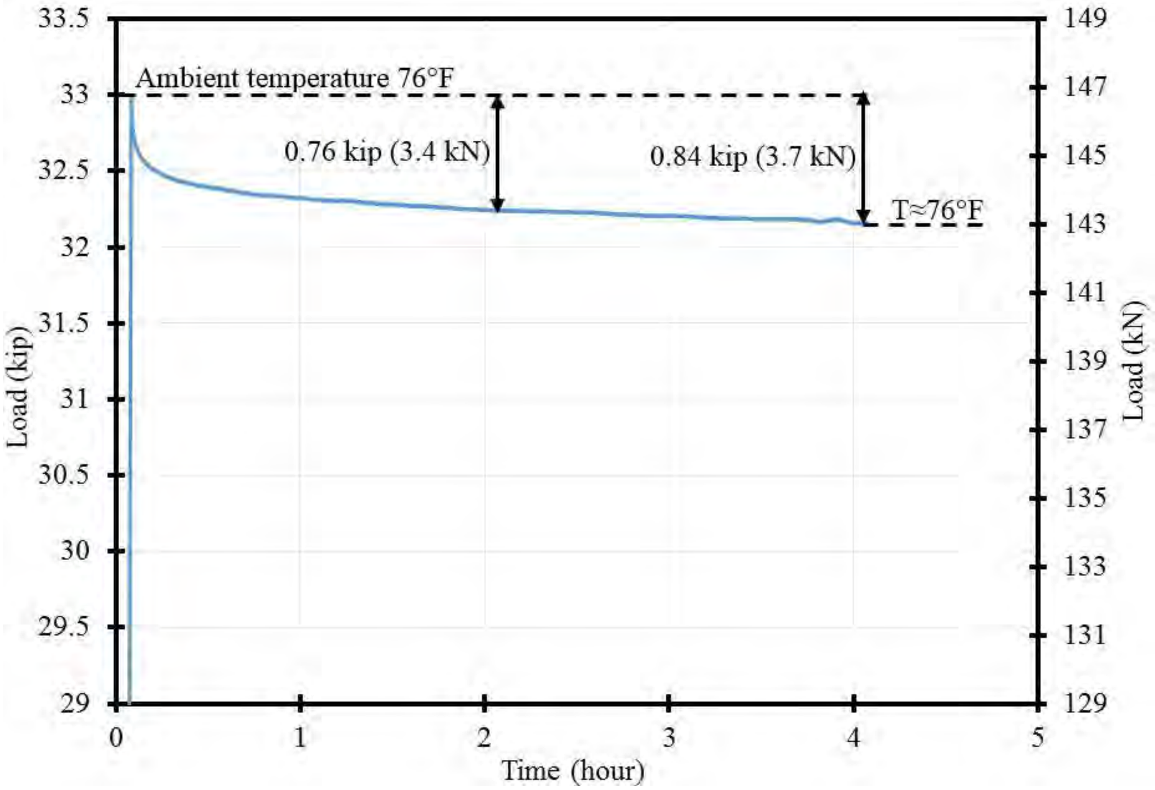

Figure 4.2-5 Load vs. time for TH-S1 in Phase I of thermal testing

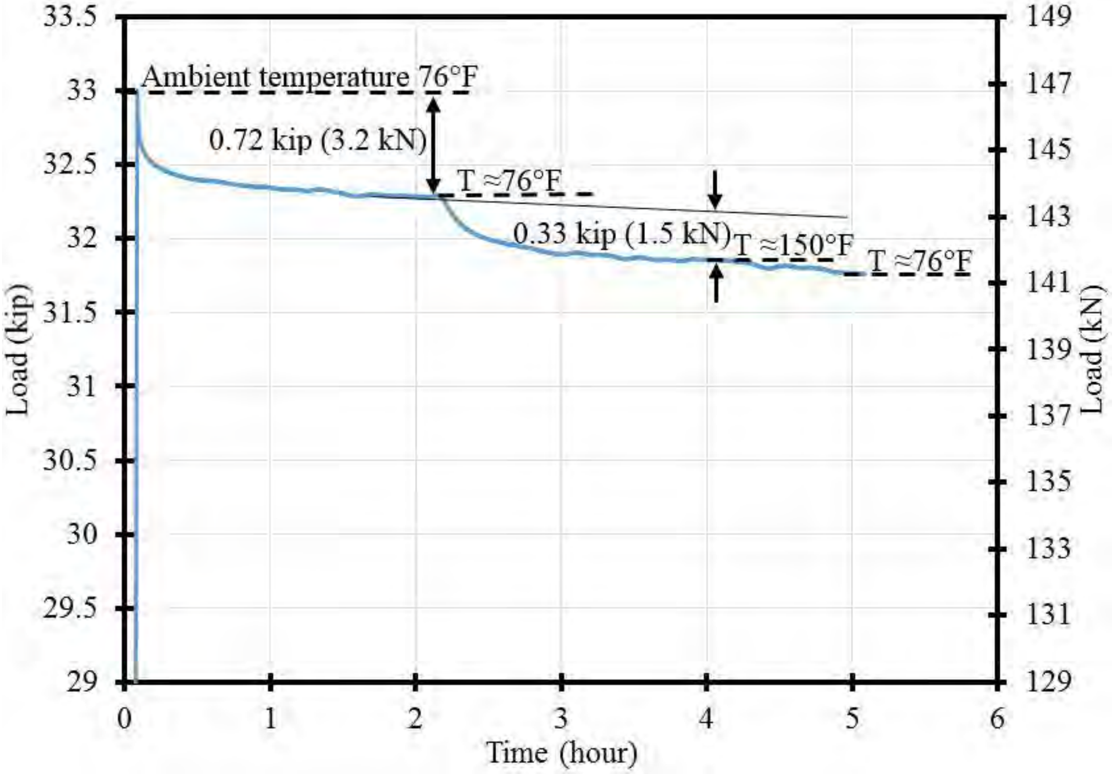

Figure 4.2-6 Load vs. time for TH-S2 in Phase I of thermal testing

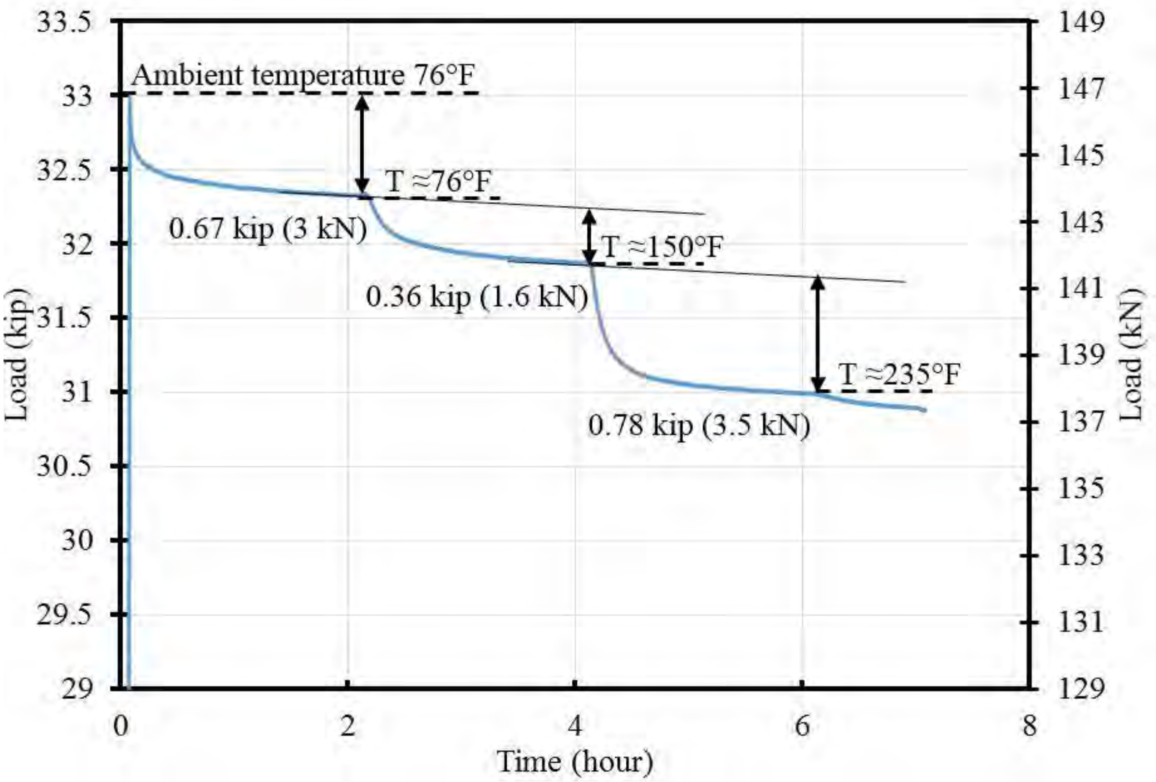

Figure 4.2-7 Load vs. time for TH-S3 in Phase I of thermal testing

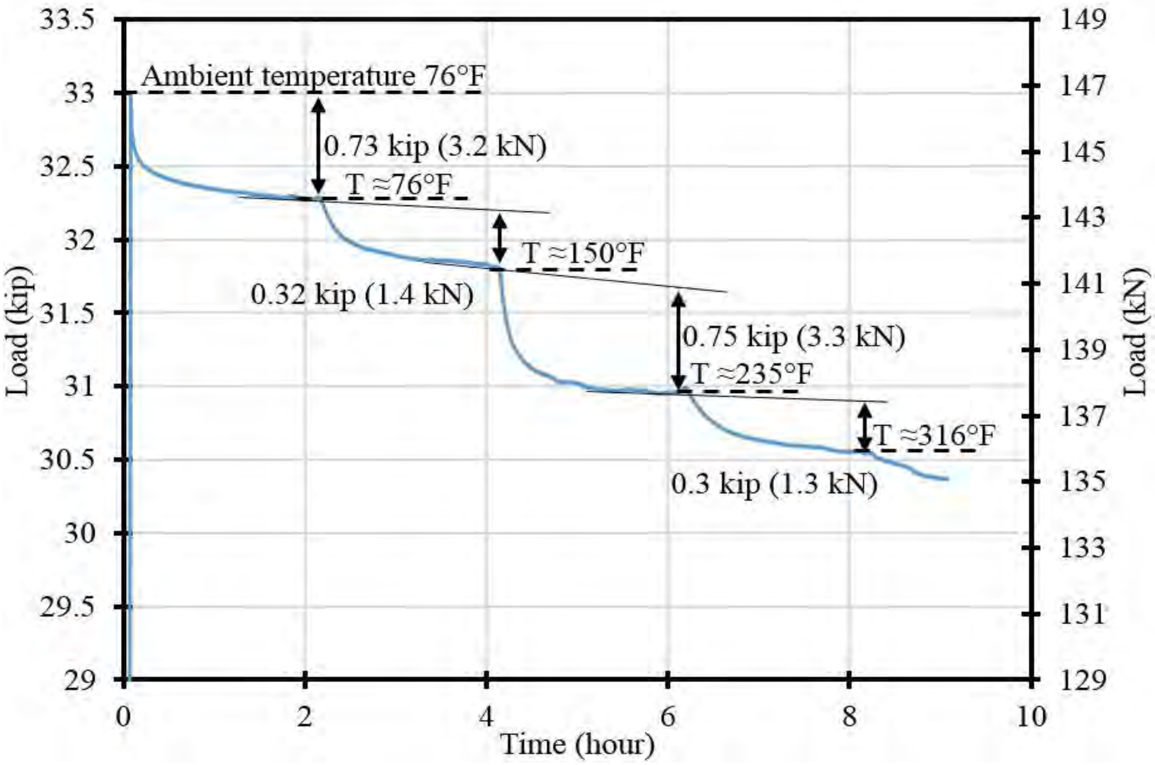

Figure 4.2-8 Load vs. time for TH-S4 in Phase I of thermal testing

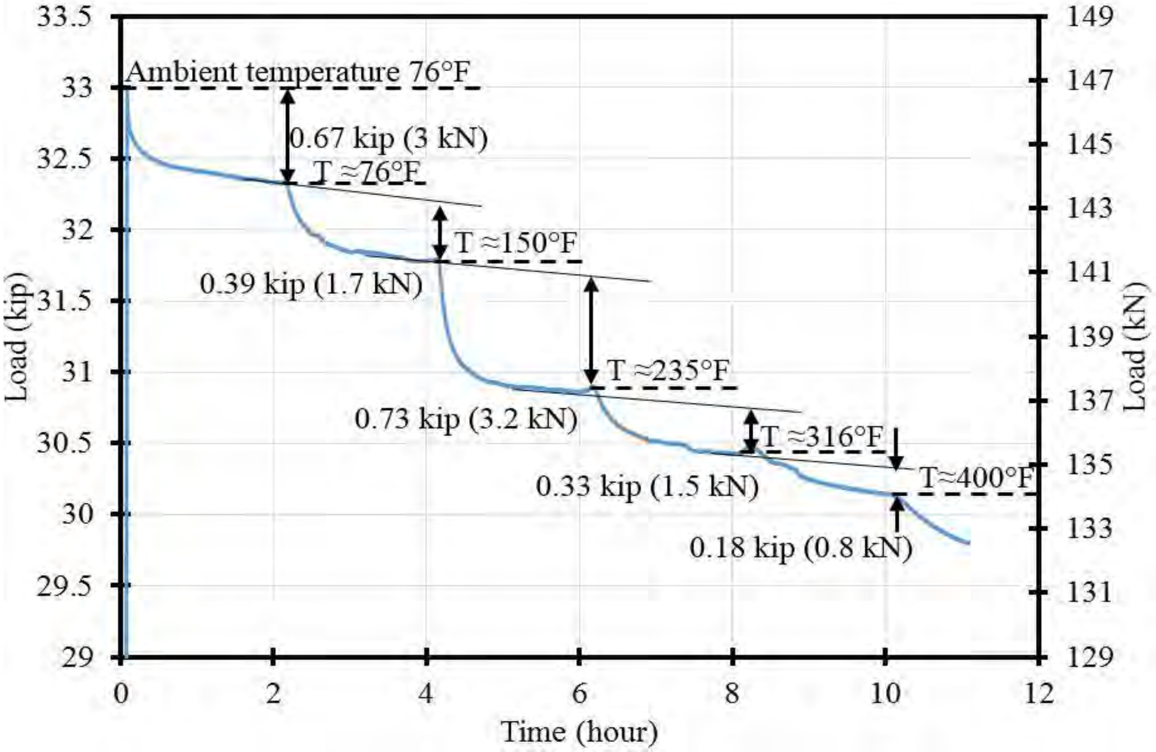

Figure 4.2-9 Load vs. time for TH-S5 in Phase I of thermal testing

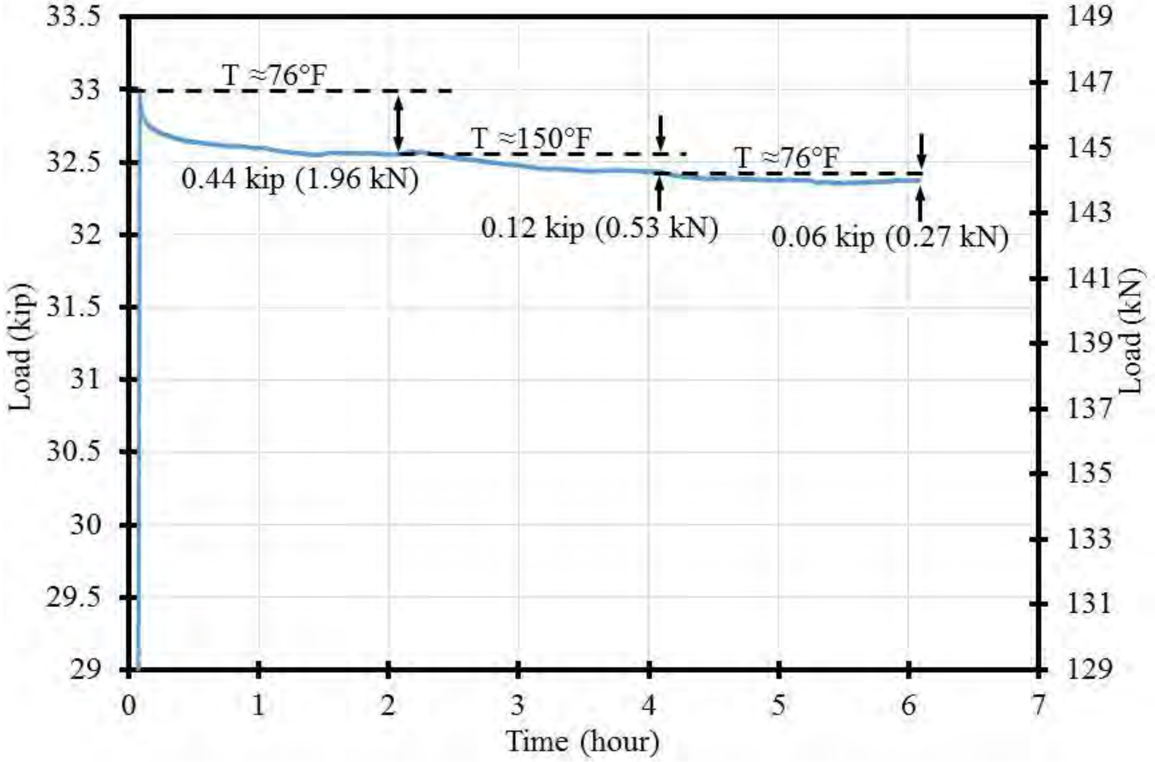

Figure 4.2-10 Load vs. time for TH-S2 in Phase II of thermal testing

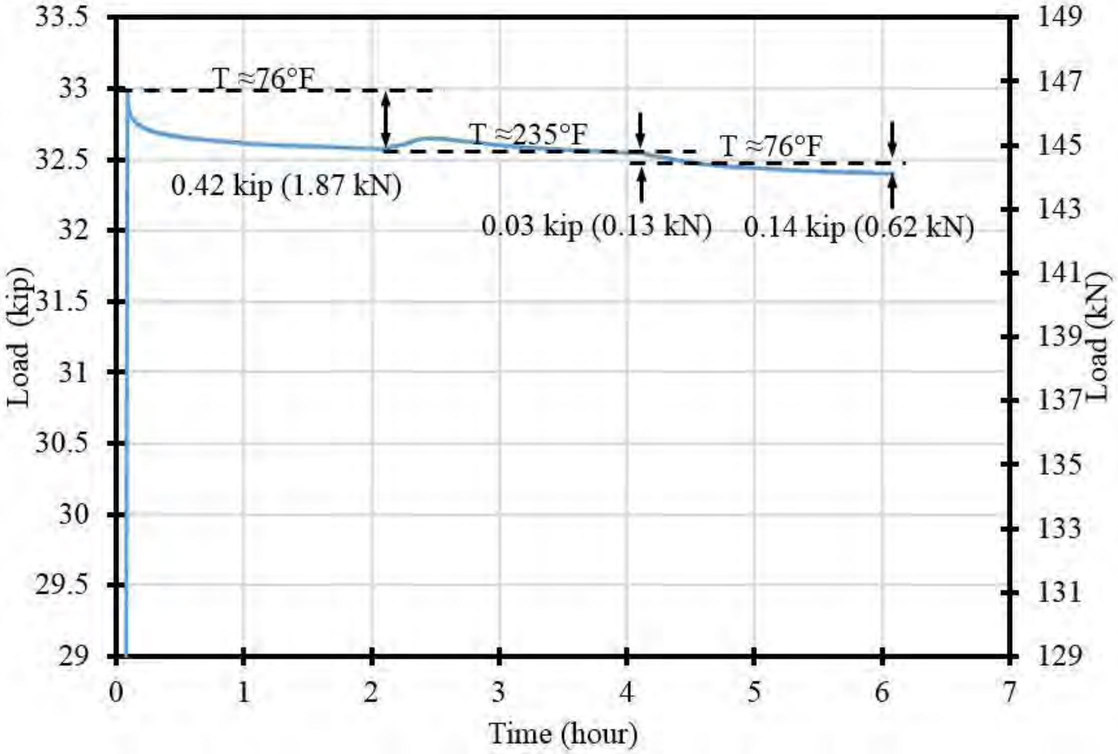

Figure 4.2-11 Load vs. time for TH-S3 in Phase II of thermal testing

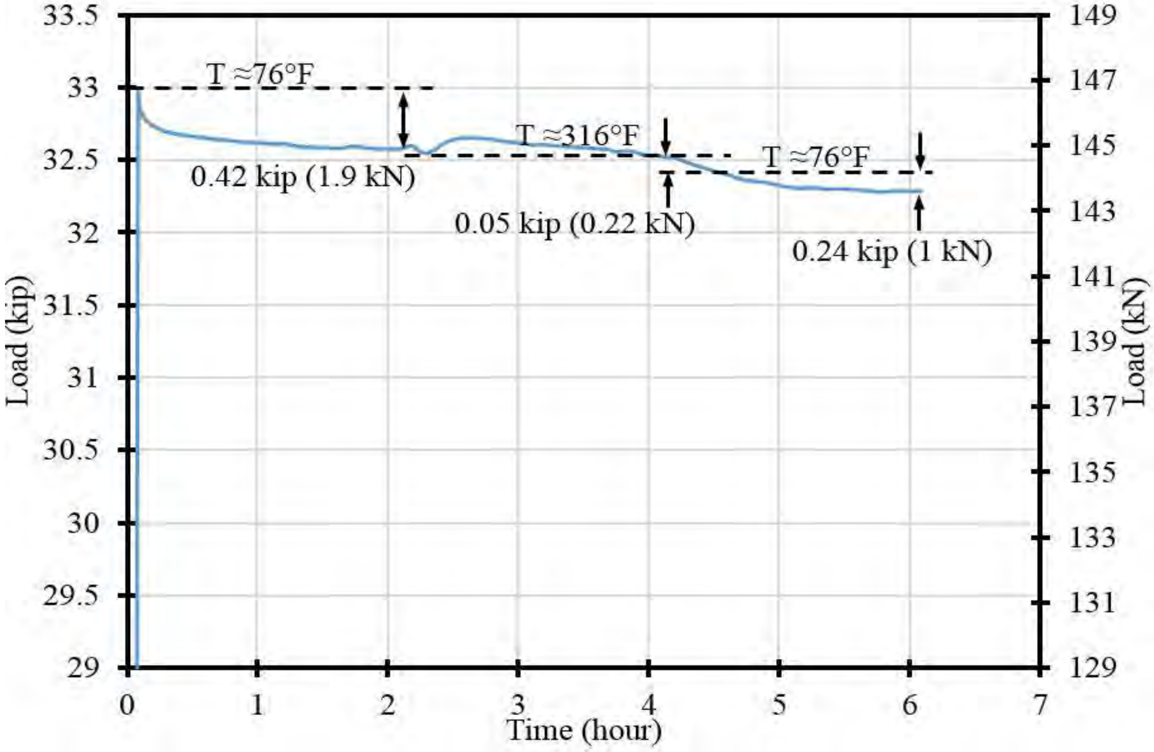

Figure 4.2-12 Load vs. time for TH-S4 in Phase II of thermal testing

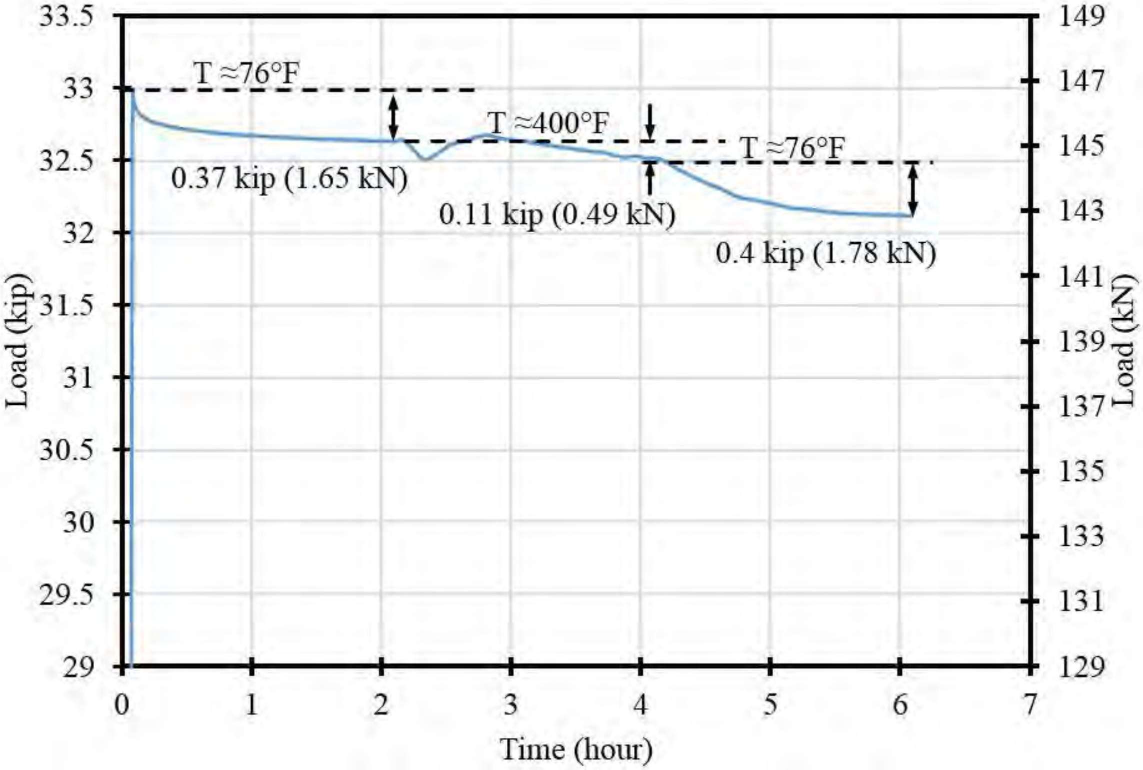

Figure 4.2-13 Load vs. time for TH-S5 in Phase II of thermal testing

Figure 4.2-14 Uniaxial testing of CFCC specimens in Phase III

Figure 4.2-15 Failure of CFCC specimens in Phase III

4.3 CFRP Prestressed Decked Bulb T Beams

4.3.1 Construction of test specimens

The coefficient of thermal expansion for concrete is approximately 6×10^{-6} /°F (12×10^{-6} /°C), while CFRP has a coefficient of thermal expansion less than 0.5×10^{-6} /°F (1×10^{-6} /°C). Therefore, concrete beams prestressed with CFRP strands experience a certain loss or gain in the level of prestressing force with the seasonal change in temperature. This experimental study was executed to verify the loss/gain in prestressing level due to thermal changes.

A total of six identical precast prestressed decked bulb T beams were constructed and tested under a flexural loading at different temperatures. The beams had a length of 16 ft (4.87 m), a top flange width of 18 in. (457 mm), and a depth of 16 in. (406 mm). Each beam was prestressed with CFCC strands with a diameter of 0.6 in. (15.2 mm). In addition, each beam was provided with five top non-prestressed CFCC strands in the top flange (Figure 4.3-1). In the transverse direction, the beams were reinforced with No. 3 (10 mm) steel stirrups spaced 4 in. (102 mm) on center.

The decked bulb T beams were constructed at the Structural Testing Lab. (STL), which hosts a prestressing bed that can accommodate beams with a length of 50 ft (15.24 m) and a width of 48 in. (1.22 m). Therefore, there was enough space to accommodate the simultaneous construction of the six beams. The formwork for the beams included a wood platform decking and sides. The decking platform was constructed of plywood and dimension lumber. The sides of the formwork were constructed from layers of plywood and polystyrene (Styrofoam) to form the required bulb T shape and accommodate the end blocks. These layers of polystyrene were pre-cut to shape using a table saw and attached to the plywood using adhesive and wood screws.

The reinforcement cages were assembled from the steel stirrups and the top non-prestressed CFCC strands. The steel stirrups were made of two pieces welded together with tack welds. End blocks were provided with rectangular stirrups every 2.0 in. (51 mm) to resist the bursting force at prestess release. After reinforcement cages were completed, they were moved to the platform decking, where prestressing strands were passed through the cages. Figure 4.3-2 through Figure 4.3-5 show different stages of construction.

To facilitate the prestressing and avoid damaging the CFCC strands, a special coupler system was used to connect the prestressing CFCC strands with conventional 7-wire 0.6 in. (15.2 mm) low relaxation steel strands as shown in Figure 4.3-5. The couplers were provided on both the live and dead ends. Therefore, conventional steel anchorage was used at both bulkheads and the prestressing was executed by tensioning the steel strands. After completing the installation of the coupler system, the steel strands were tensioned from the live end while a set of in-line load cells was attached to the prestressing strands at the dead end. The prestressing was executed using a hydraulic pump and a jacking system, shown in Figure 4.3-6 and Figure 4.3-7. The strands were prestressed in a predetermined sequence to avoid generating a significant eccentricity in the bulkhead. The initial prestressing force was set to 33 kip (147 kN)/strand. The force in each prestressing strand was verified through the readings form the load cells, the readings from hydraulic pump and the measured elongation of the strands. A seating loss of approximately1.5 kip (6.7 kN) per strand was observed immediately after releasing the pump.

All the beams were cast using a ready-mix concrete with a concrete mix as shown in Table 4.3-1. The concrete mix was designed to achieve a 28-day compressive strength of 7 ksi (48 MPa). The maximum aggregate size was limited to 0.75 in. (19 mm) and a slump of 10 in. (254 mm) was verified before pouring concrete. This concrete mix is a typical concrete mix used in highway bridge beams. After concrete casting, the beams were covered with wet burlap and plastic sheets to prevent moisture escape and allow for proper curing. In addition, concrete cylinders with a diameter of 6 in. (152 mm) and a length of 12 in. (305 mm) were also cast from the same batch of concrete. The cylinders were allowed to cure under the same conditions of the concrete beams and were tested under uni-axial compressive stress according to ASTM C39/C39M-12a (2012): "Standard Test Method for Compressive Strength of Cylindrical Concrete Specimens." to determine the compressive strength of concrete after 28 days. Figure 4.3-8 through Figure 4.3-12 document the process of casting the concrete.

Transfer of prestressing forces into concrete beams took place 10 days after casting of concrete and after verifying that the concrete had achieved more than 80 % of its 28-day compressive strength. The prestress release was executed by slowly heating the steel strands using an acetylene/oxygen torch. The camber of the beams was measured at the mid-span of the beam at prestress release. After prestress release, the beams were removed from the formwork and sent to the testing facility. Figure 4.3-13 and Figure 4.3-14 show the change of the prestressing force from the time of prestressing to the time of prestress release.

Table 4.3-1 Concrete mix per cubic yard

Material	Units	Design Quantity per yrd^3
Limestone Coarse Aggregate (LIA-OTT),	lb (kg)	1762 (801)
Fine Aggregate (2NS-AAR),	lb (kg)	1265 (575)
Type 1 Cement (CMT1-LAA),	lb (kg)	534 (243)
Slag Cement (CMGS-LA),	lb (kg)	288 (131)
Water (WAT1),	gal (m^3)	31.8 (0.12)
Water/Cement ratio		0.37
Retarding Admixture (0STAB-PR),	oz (kg)	25 (0.7)
High Range Water Reducer (0HRWR-PR),	oz (kg)	53 (1.5)

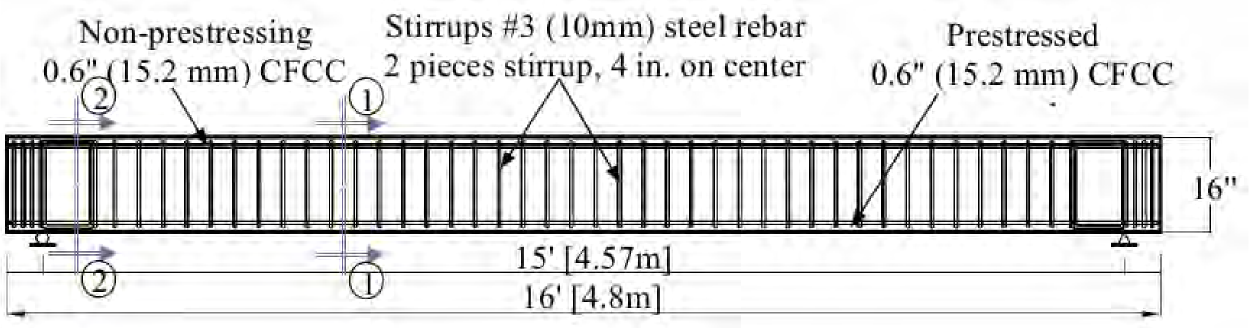

Figure 4.3-1 Cross section and internal reinforcement details of decked bulb T-beams

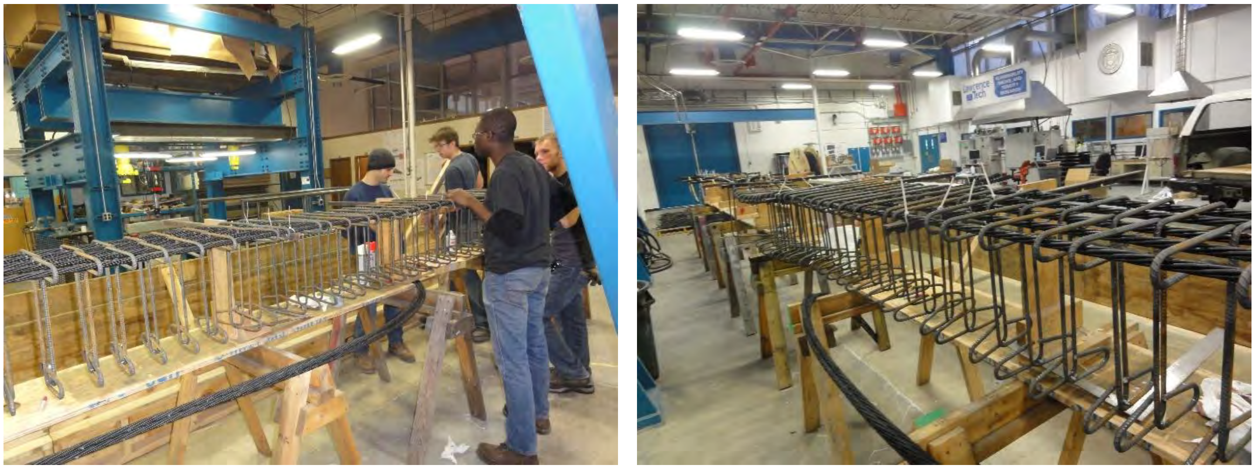

Figure 4.3-2 Assembling the reinforcement cages for decked bulb T beams

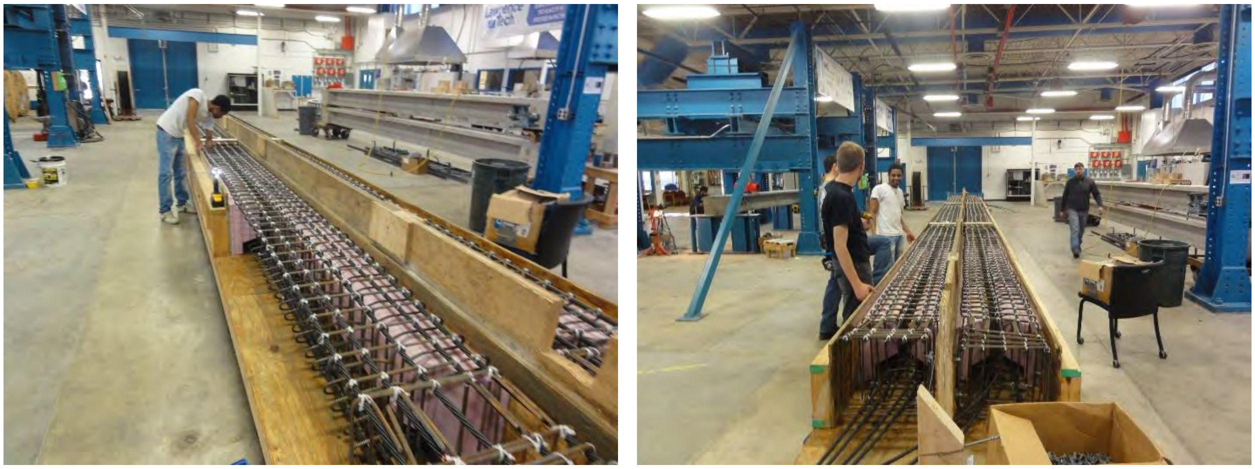

Figure 4.3-3 Placing completed reinforcement cages in formwork

Figure 4.3-4 Completing the formwork and adding separators between beams

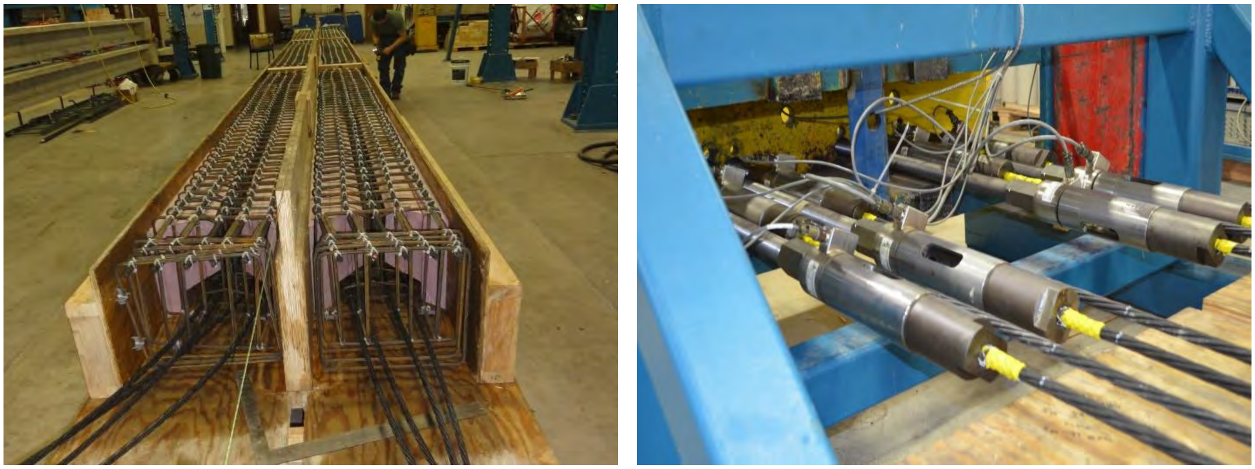

Figure 4.3-5 Passing prestressing CFCC strands through the reinforcement cages and connecting load cells and end couplers

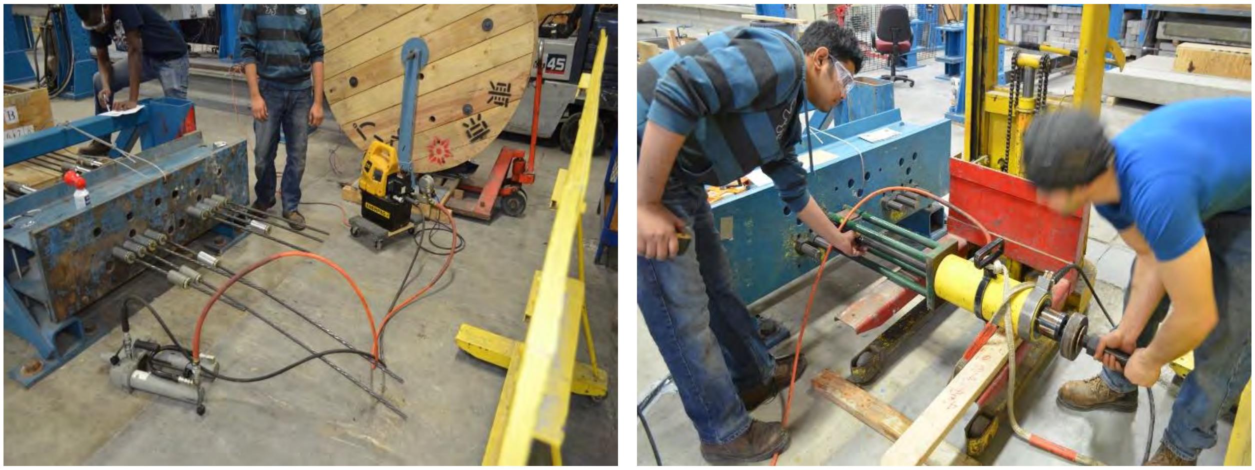

Figure 4.3-6 Attaching steel anchorage and applying prestressing force with a hydraulic jack

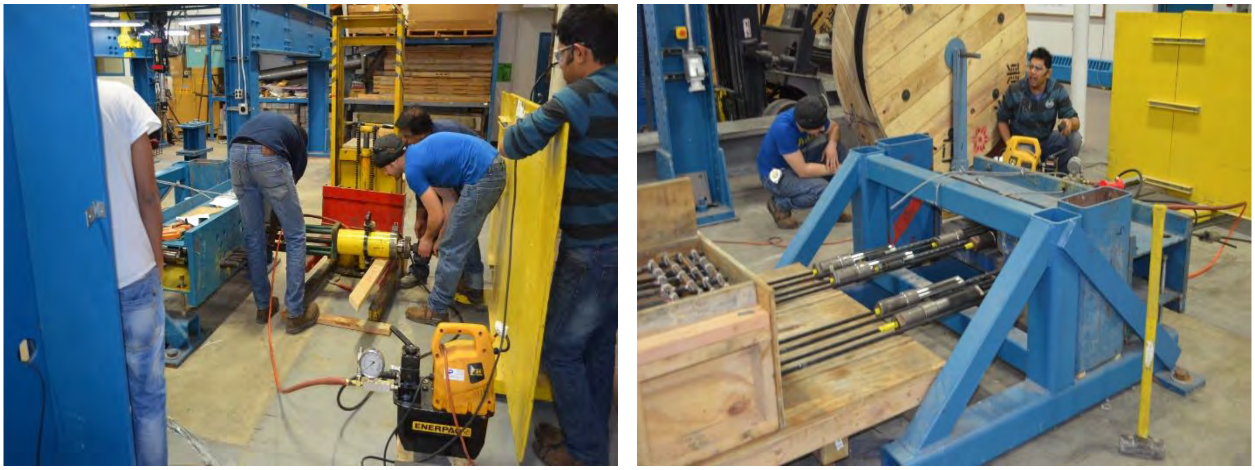

Figure 4.3-7 Applying prestressing force using a hydraulic pump

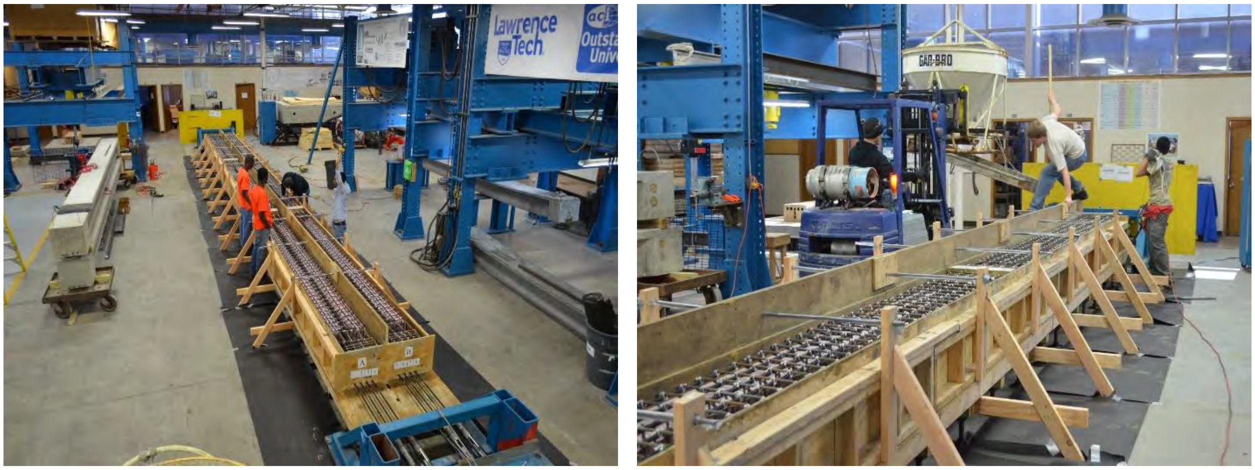

Figure 4.3-8 Placing concrete in the formwork

Figure 4.3-9 Slump test measuring 10 in. (254 mm)

Figure 4.3-10 Preparing concrete cylinders for uni-axial compressive strength test

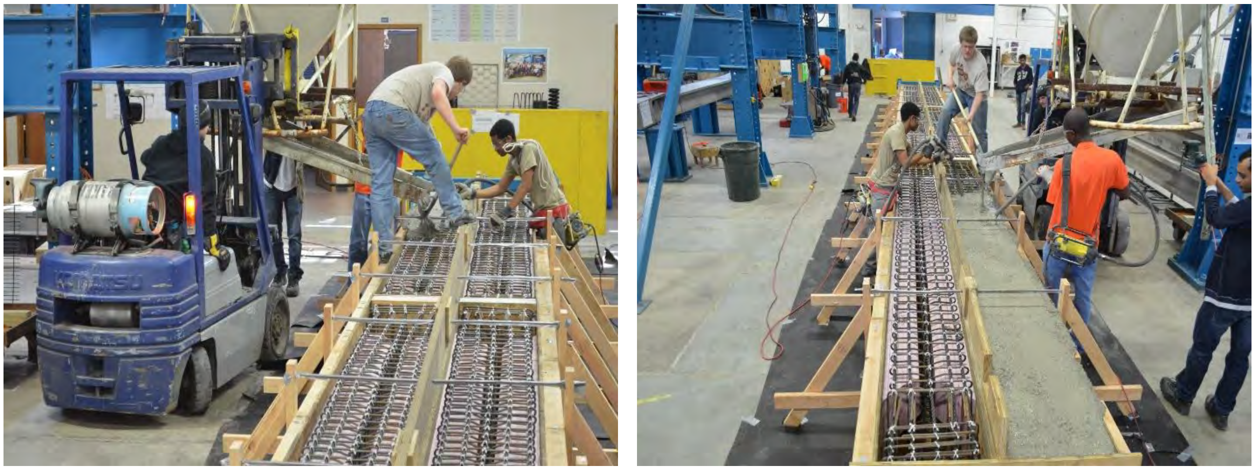

Figure 4.3-11 Compacting the concrete with electric vibrators

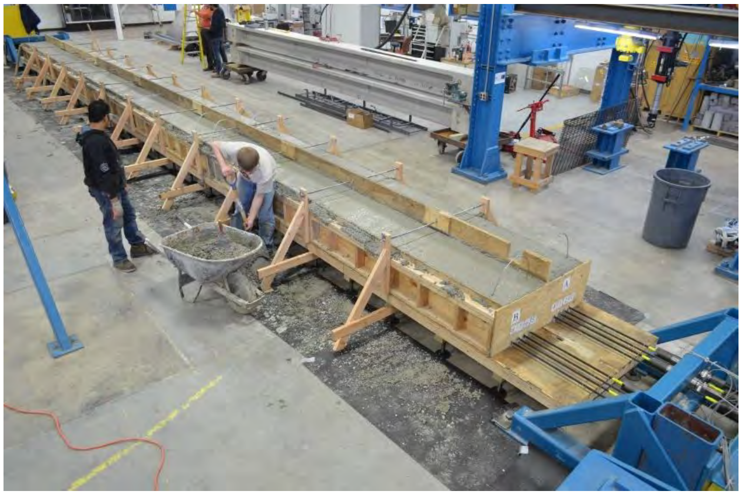

Figure 4.3-12 Completed decked bulb T beams ready for curing

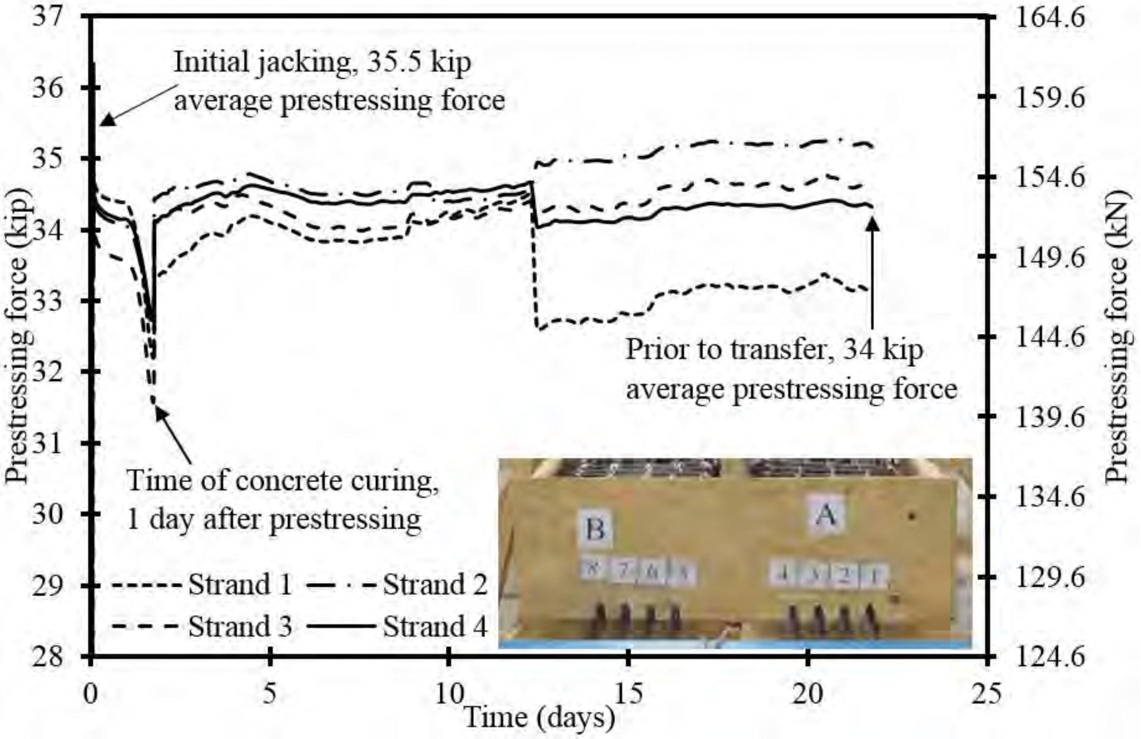

Figure 4.3-13 Prestress loss prior to transfer (Strand 1-4)

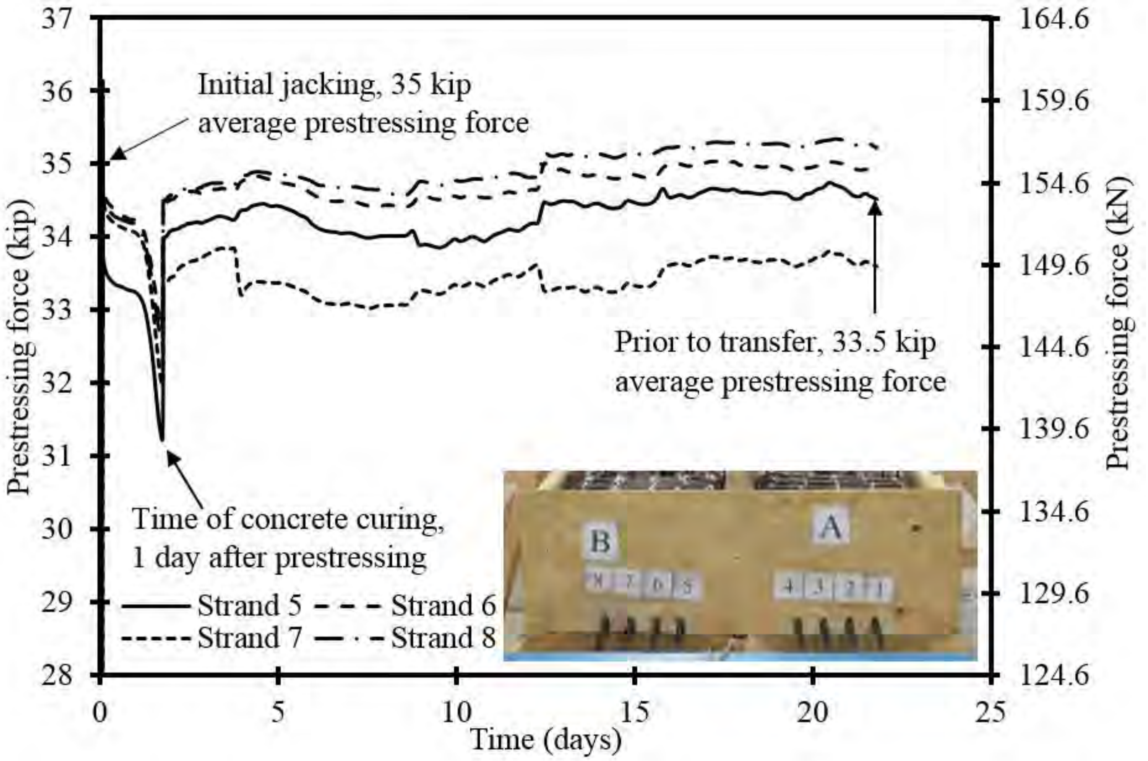

Figure 4.3-14 Prestress loss prior to transfer (Strand 5-8)

4.3.2 Test setup

The beams were loaded under three-point loading over an effective span of 15 ft (Figure 4.3-15). Strain gages, load cells, linear variable differential transducers (LVDTs), and linear motion transducers (LMTs) were used to capture the strain, applied load, and deformation of the beams during testing. To monitor the concrete strain, each beam was provided with two strain gages on the top surface at the mid-span section. In addition, two strain gages were provided at the bottom surface of the concrete to capture the onset and development of cracks. LVDTs were used to evaluate the strain at different depths at the mid-span section (Figure 4.3-16 and Figure 4.3-17).

The main objective of the test was to evaluate the prestressing force in the test beams and evaluate the change of that prestressing force due to the change in temperature. However, there is no feasible way of directly measuring the prestressing force in pretensioned beams. Nevertheless, the effective prestressing force can be evaluated indirectly by observing the cracking and decompression loads while loading the beam in flexure. The cracking load can be used to back calculate the effective prestressing force using the stress equation at the soffit of the beam.

However, the cracking load is dependent on the modulus of rupture of concrete and can only be spotted once. In other words, once the beam is cracked, there is no way of verifying the obtained cracking load. The decompression load provides a good alternative for calculating the effective prestressing force once the beam is cracked.

After cracking, the decompression load marks the stage where the flexural cracks start to open under the applied loads. The decompression load is the load required to counteract the effect of prestressing force and cause the stresses in the soffit of the beam to reach zero. The decompression load can be identified by attaching a strain gage next to the flexural crack and capture the reading of the strain in the soffit of the beam while loading. The strain will gradually increase with applying the load. But as the flexural crack starts to open, the strain peaks and then starts to decrease. The load at the peak of the strain is approximately equal to the decompression load.

Another method of calculating the decompression load is by observing the load-deflection curves while loading the beam. Before the load reaches the decompression load, the beam acts as an un-cracked beam and the gross section area resists the load. After the load exceeds the decompression load, the cracks start to open and the section acts as a cracked section with a reduced moment of inertia. This can be clearly observed from the slope of load-deflection curve. Before the decompression load, the curve is represented by a straight line with a steep slope, while after the decompression, the curve is also represented by a straight line but with a much flatter slope. The decompression load therefore can be precisely calculated from the load-deflection curve by estimating the load at which the curve starts to deviate from its linear un-cracked segment.

Out of six beams, two beams were tested under three-point loading setup at ambient temperature (68 °F or 20 °C) as shown in Figure 4.3-15. The test included loading the beam in cycles of loading and unloading to a load level of 60 kip (267 kN). Since the theoretical loading capacity of the beam was approximately 90 kip (400 kN), the beams were not expected to sustain any permanent damage other than the flexural cracks. Two of the remaining four beams were also tested under the same loading setup but at a temperature of 176 °F (80 °C). After concluding the load cycles at high temperature. The beams were allowed to cool down and the load cycles were repeated at ambient temperature (68 °F or 20 °C). The remaining two beams were tested under the same loading setup but at a temperature of -40 °F (-40 °C). After concluding the load cycles at this low temperature, the beams were allowed to warm back to ambient temperature, then the load cycles were repeated. In addition, the testing scenario (load at 176 °F (80 °C) then ambient or load at -40 °F (-40 °C) then ambient) was repeated for two beams to verify the results. Consequently, it was feasible to precisely relate the change of the decompression load in each individual beam to the change in temperature.

Figure 4.3-15 A decked bulb T beam under three-point loading in the environmental chamber

Figure 4.3-16 LMTs, LVDTs, and strain gages on the soffit of the beam at mid-span

Figure 4.3-17 Strain gages on the top surface of the decked bulb T beam

4.3.3 Test results

The following discussion provides the main finding and observations from the test. Four beams were tested and labeled as F1, F2, H1, H2. Beams F1 and F2 were first tested at -40 °F (-40 °C) then at 68 °F (20 °C), while Beams H1 and H2 were first tested at 176 °F (80 °C) then at 68 °F (20 °C). In addition, two more sets of test results F2-R and H2-R are obtained by repeating the testing scenario on test Beams F2 and H2, respectively. All beams were kept at the assigned temperature for at least 24 hours before conducting the flexural test. The core temperature of each beam was measured using embedded thermocouples and was verified against the air temperature. The flexural test was executed only after the beams reached the steady state with the core temperature matching the surrounding air temperature.

4.3.3.1 Beam F1

The first phase of testing included loading Beam F1 under three-point loading at a freezing temperature of -40 °F (-40 °C). As shown in Figure 4.3-18, the load was applied in cycles of loading and unloading with a load cycle increment of 5 kip (22 kN). The beam was checked for flexural cracks during and after each load cycle. The flexural cracks were observed at the end of the 40-kip (178-kN) load cycle, which suggested a cracking load between 35 (156 kN) and 40 kip (178 kN). The load cycles stopped at a load level of 60 kip (267 kN).

The second phase of testing included loading the beam in load cycles to 60 kip (267 kN) at ambient temperature as shown in Figure 4.3-19. Since the beam was cracked in the previous phase, no cracking load was observed. However, the decompression load was observed in each load cycle of both phases. The load-deflection curves from both test phases for each post-crack load cycle were overlapped as shown in Figure 4.3-20 for the 60-kip (267-kN) load cycle. As shown in the figure, there is a slight difference in the decompression load, but this difference is not visually estimated easily. To precisely estimate the decompression load for each case, the slope of the un-cracked segment was estimated as shown in Figure 4.3-21. Then, using the estimated slope, a straight line was drawn to overlap the un-cracked segment and extended as a linear function between the load and deflection. Finally, the deviation of the actual load-deflection curve from this straight line was calculated by subtracting the theoretical linear deflection from the measured experimental deflection.

The difference in the deflection from the theoretical linear un-cracked load-deflection curve was plotted against the load as shown in Figure 4.3-22 and the close-up view in Figure 4.3-23. As shown on the figures, when this difference is small, the experimental curve follows the linear un-cracked function, or in other words, the section acts as an un-cracked section. Nevertheless, when this difference increases, the experimental curve starts to significantly deviate from the linear un-cracked function, or in other words, the cracks start to open and the section begins to act as a cracked section. Therefore, the decompression load can be easily determined when the difference in deflection increases. As shown in Figure 4.3-24, the decompression load recorded at ambient temperature was higher than that recorded at freezing temperature, the difference tends to be constant and is estimated as 2.5 kip (11 kN).

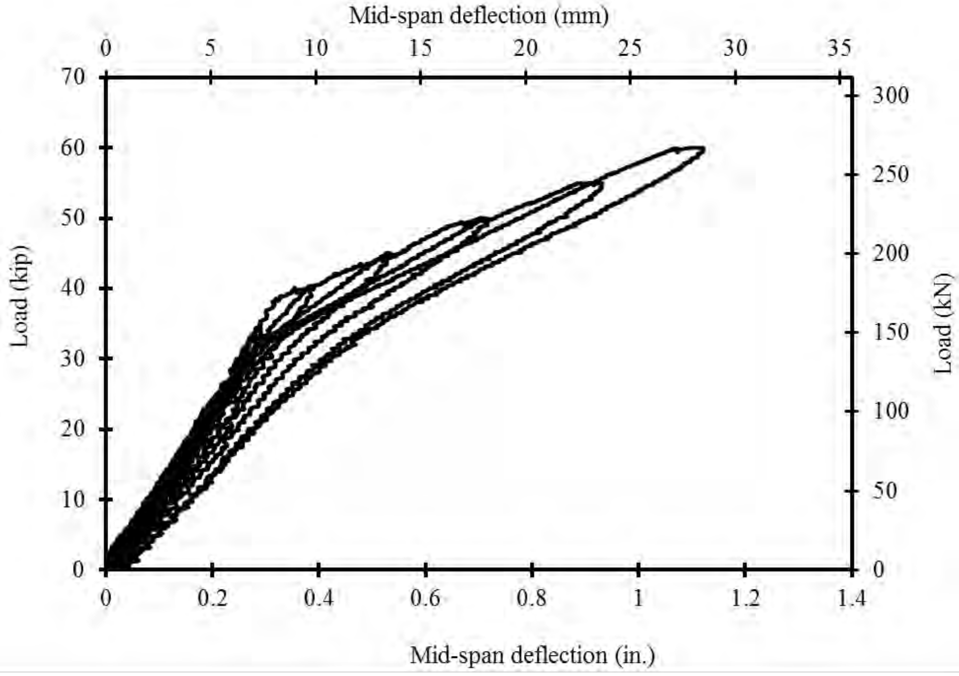

Figure 4.3-18 Load-deflection curves of Beam F1 due to loading at -40 °F (-40 °C)

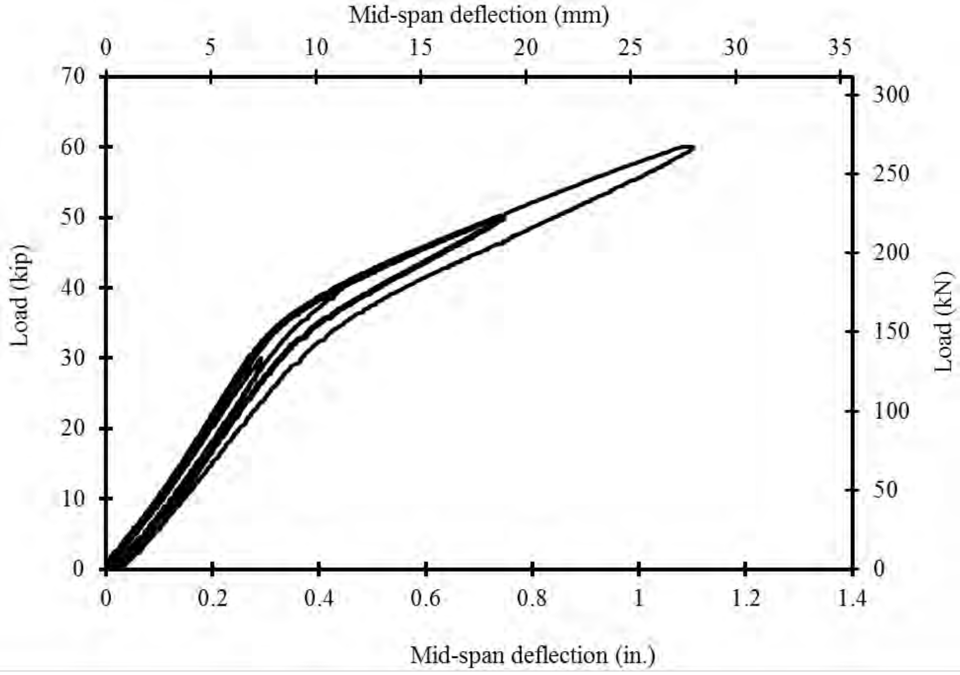

Figure 4.3-19 Load-deflection curves of Beam F1 due to re-loading at ambient temperature

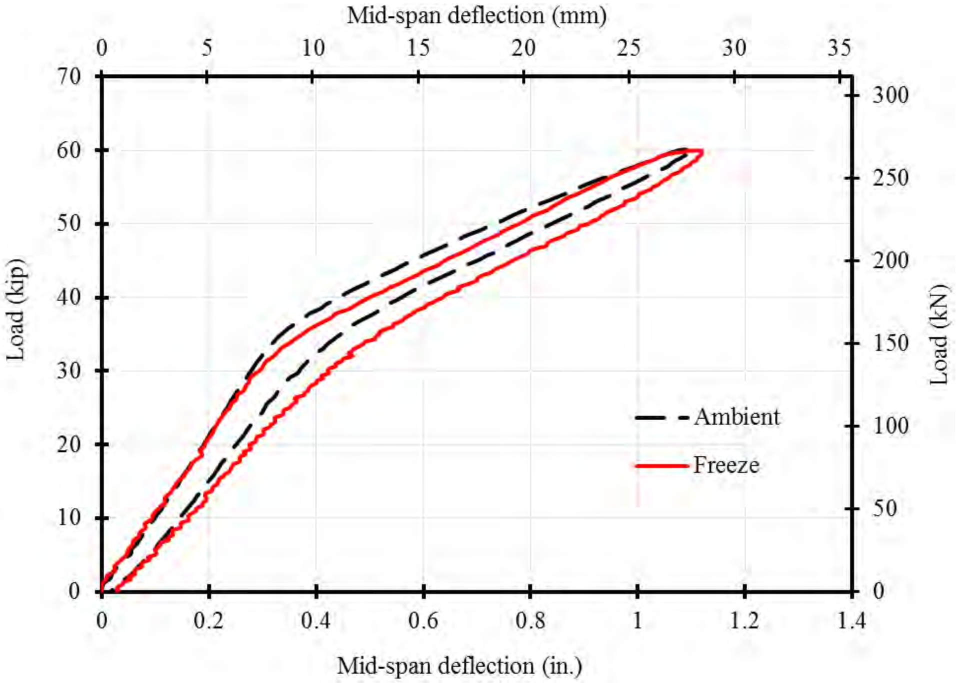

Figure 4.3-20 Load-deflection curves of Beam F1 during 60-kip (267-kN) load cycle

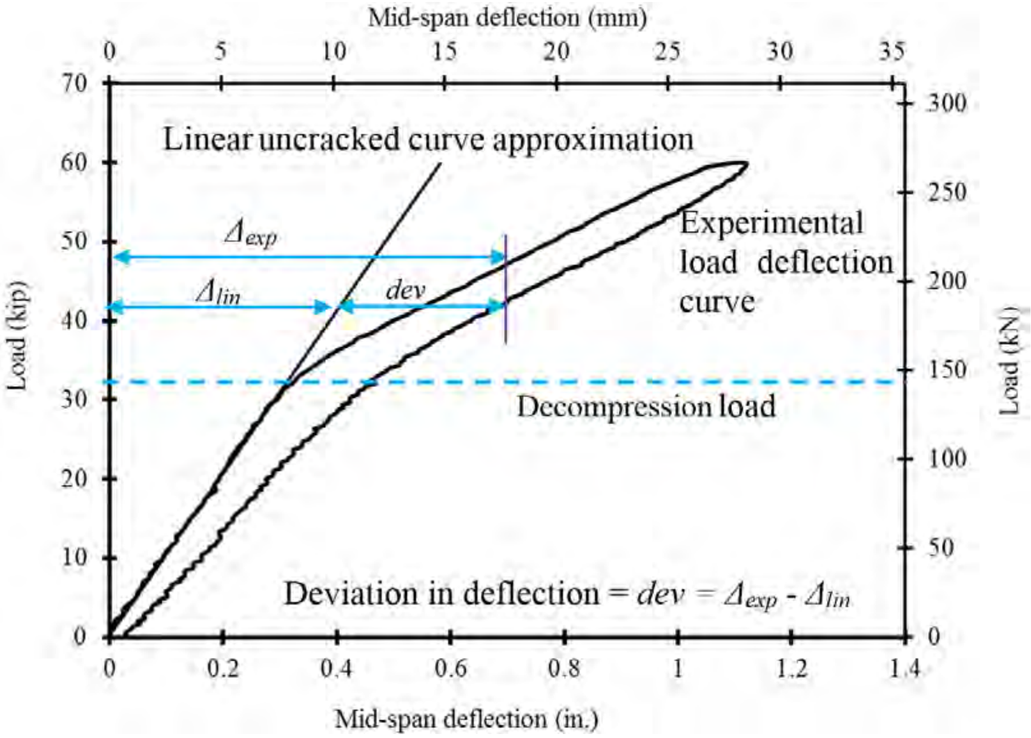

Figure 4.3-21 Calculation of the decompression load by evaluating the deviation of the load-deflection curve from the linear un-cracked curve

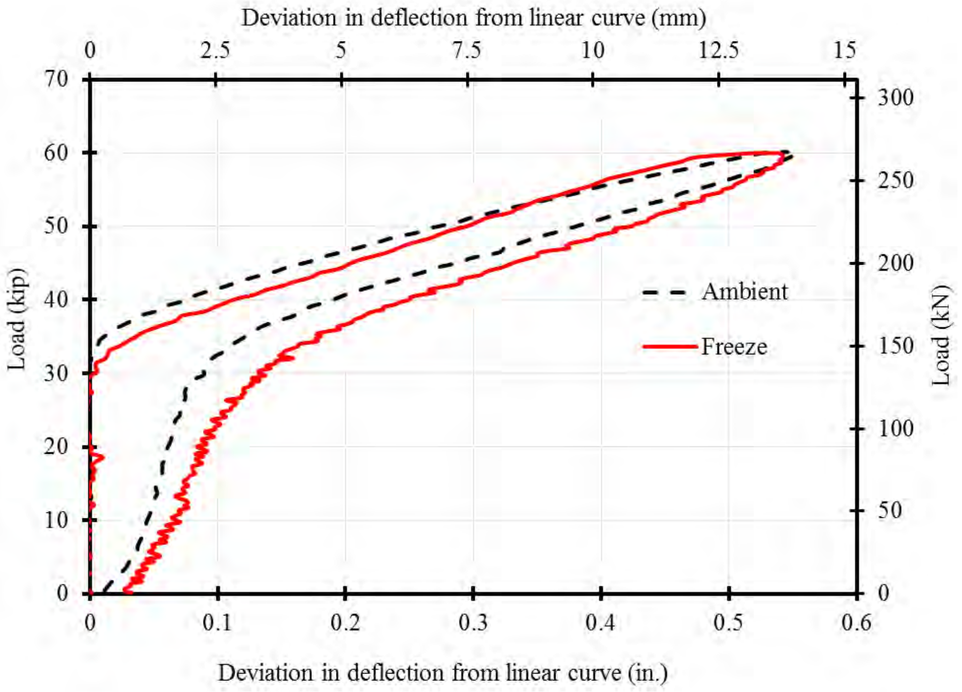

Figure 4.3-22 Deviation of load-deflection curves from the linear un-cracked curve in Beam F1 indicating the decompression loads at ambient and -40 °F (-40 °C)

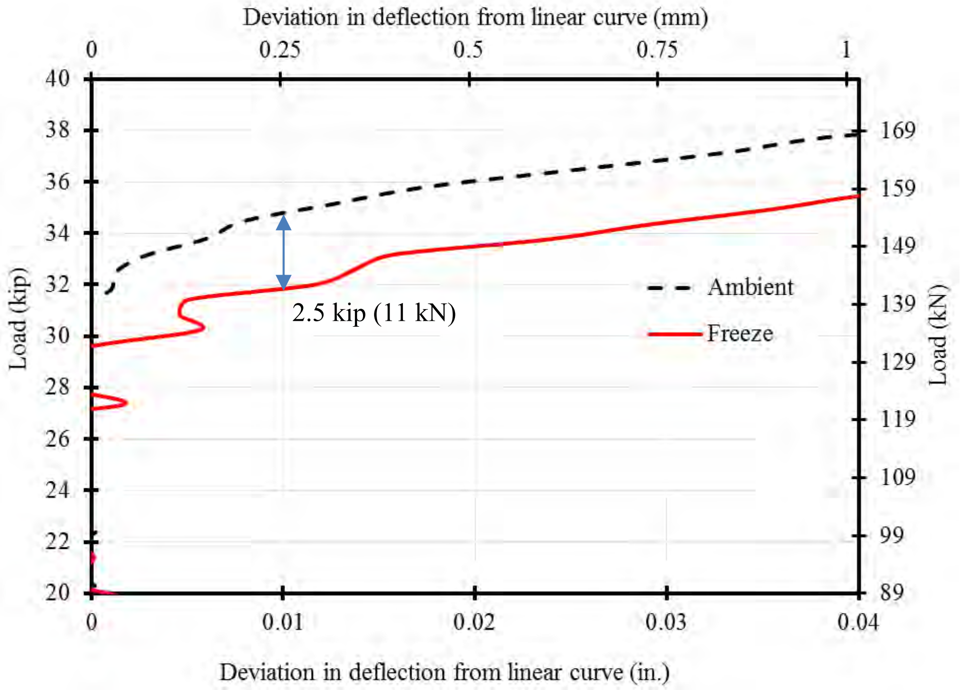

Figure 4.3-23 Close-up view showing the deviation of load-deflection curves from the linear un-cracked curves in Beam F1 and indicating the decompression loads at ambient & -40 °F (-40 °C)

4.3.3.2 Beam F2

Beam F2 was identical in testing conditions to Beam F1. The test was repeated to verify the results through two test specimens. This beam was first saturated at a freezing temperature of -40 °F (-40 °C) and then tested under loading and unloading cycles to determine the cracking and decompression loads. After the freezing phase ended, the beam was loaded again at ambient temperature to evaluate the decompression load and calculate the change in prestressing due to temperature change. The load-deflection curves for all load cycles at freezing at ambient conditions are presented in Figure 4.3-24 and Figure 4.3-25, respectively, while Figure 4.3-26 shows the load-deflection curves for the 60-kip (267-kN) load cycles at both freezing and ambient temperatures. As shown in the figure, there is a slight change in the decompression load. To estimate this change with good accuracy, the deviation of the experimental deflection curve from the linear un-cracked curve was calculated for both curves as shown in Figure 4.3-27 with the close-up view shown in Figure 4.3-28. The decompression load at ambient temperature was higher than that at freezing temperature with a difference of approximately 2.3 kip (10 kN).

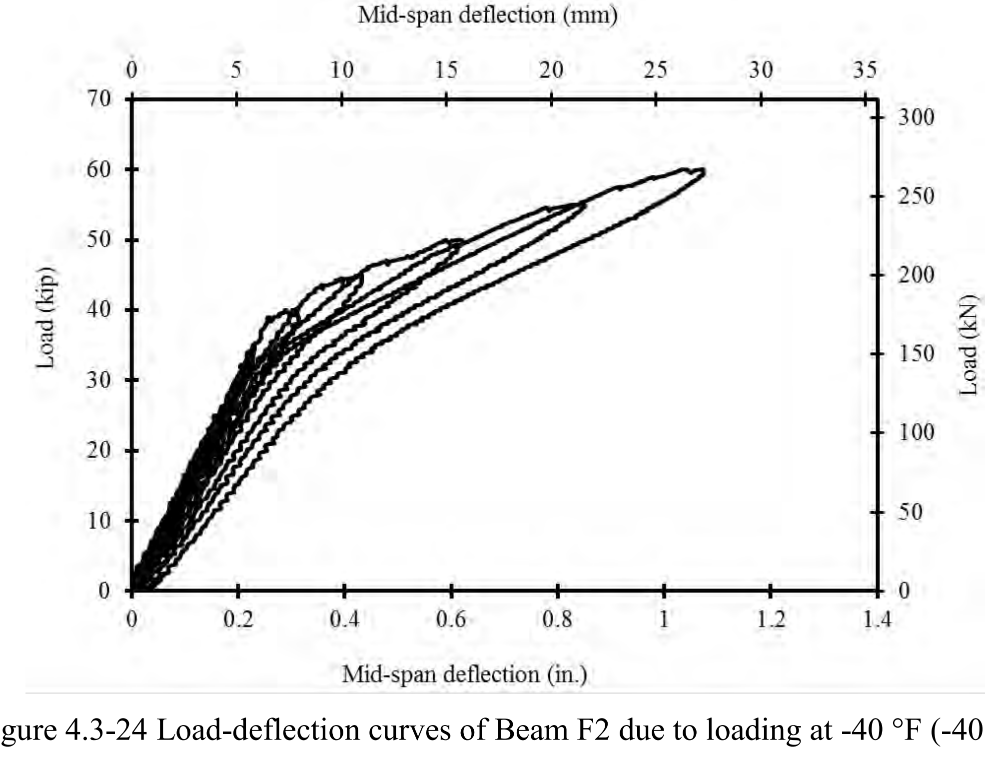

Figure 4.3-24 Load-deflection curves of Beam F2 due to loading at -40 °F (-40 °C)

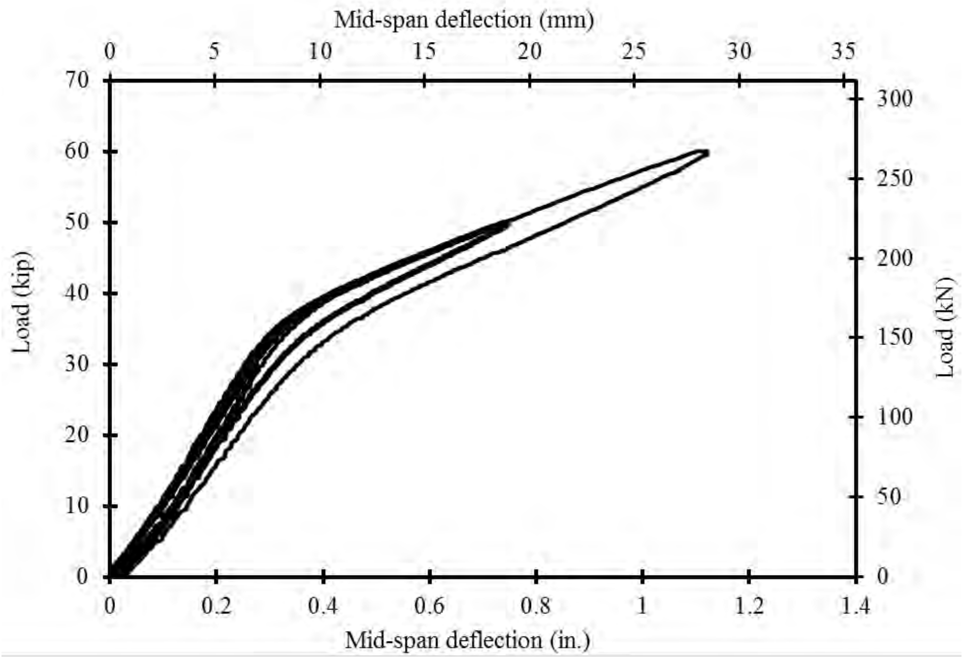

Figure 4.3-25 Load-deflection curves of Beam F2 due to loading at ambient temperature

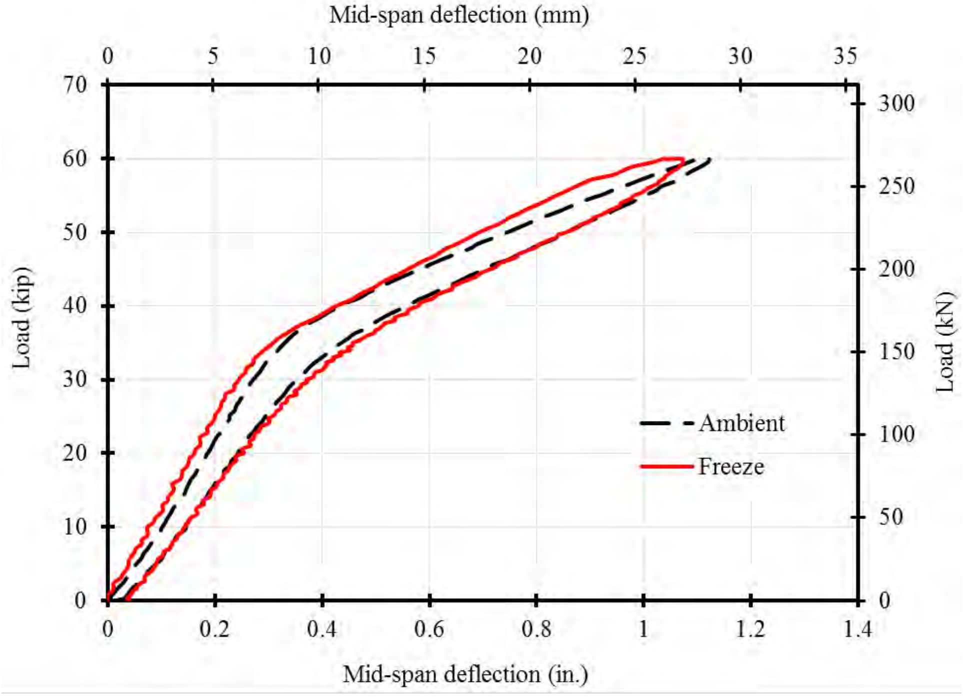

Figure 4.3-26 Load-deflection curves of Beam F2 during 60-kip (267-kN) load cycle at ambient & -40 °F (-40 °C)

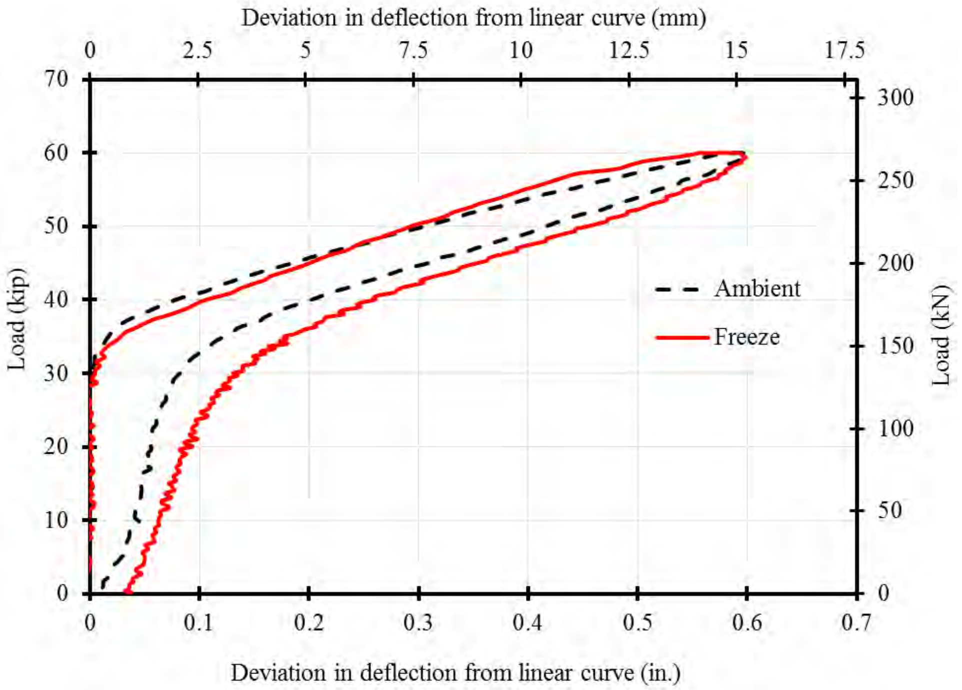

Figure 4.3-27 Deviation of load-deflection curves from the linear un-cracked curve in Beam F2 indicating the decompression loads at ambient and -40 °F (-40 °C)

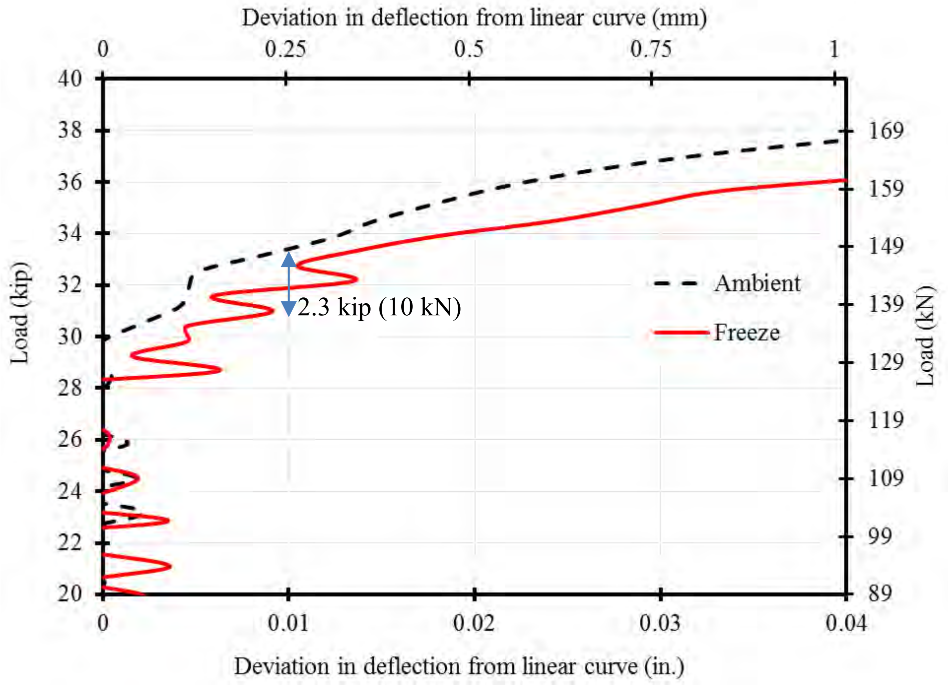

Figure 4.3-28 Close-up view showing the deviation of load-deflection curves from the linear un-cracked curves in Beam F2 and indicating the decompression loads at ambient & -40 °F (-40 °C)

4.3.3.3 Beam H1

Beam H1 was tested in a similar manner to previous beams but at an elevated temperature of 176 °F (80 °C). The beam was allowed to saturate at this high temperature until the core temperature matched the surrounding air temperature. Thereafter, the beam was loaded under three-point loading in loading and unloading cycles to a maximum load of 60 kip (267 kN). The cracking load was observed from the load-deflection curves and was estimated between 35 and 40 kip (156 and 178 kN) as shown in Figure 4.3-29. After completing the load cycles, the beam was allowed to cool down until it reached the ambient temperature and the load cycles were performed again as shown in Figure 4.3-30. The load-deflection curves from the first set of load cycles were compared to those from the second set as shown in Figure 4.3-31 for the 60-kip (267-kN) load cycle. Similar to Beams F1 and F2, the difference in the decompression load between the heating and ambient load cycles was estimated by calculating the deviation of the load-deflection curve from the linear un-cracked curve as shown in Figure 4.3-32 and the close-up view in Figure 4.3-33. As shown in the figure, the decompression load observed while heating the beam was higher than that observed at ambient temperature with a difference of approximately 2.9 kip (13 kN). In other words, the increase in temperature results in an increase in the effective prestressing force.

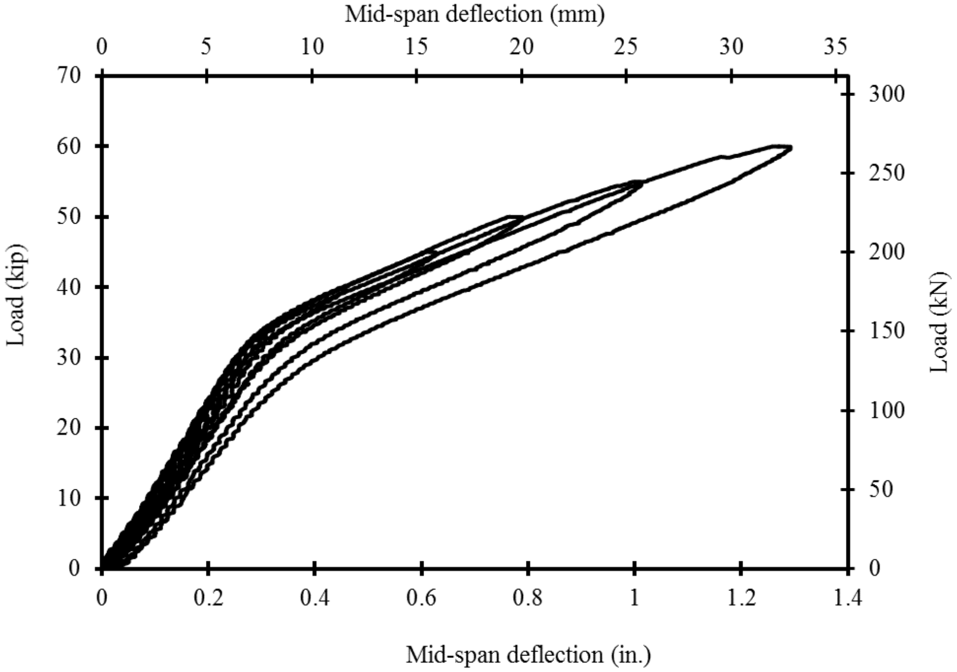

Figure 4.3-29 Load-deflection curves of Beam H1 due to loading at 176 °F (80 °C)

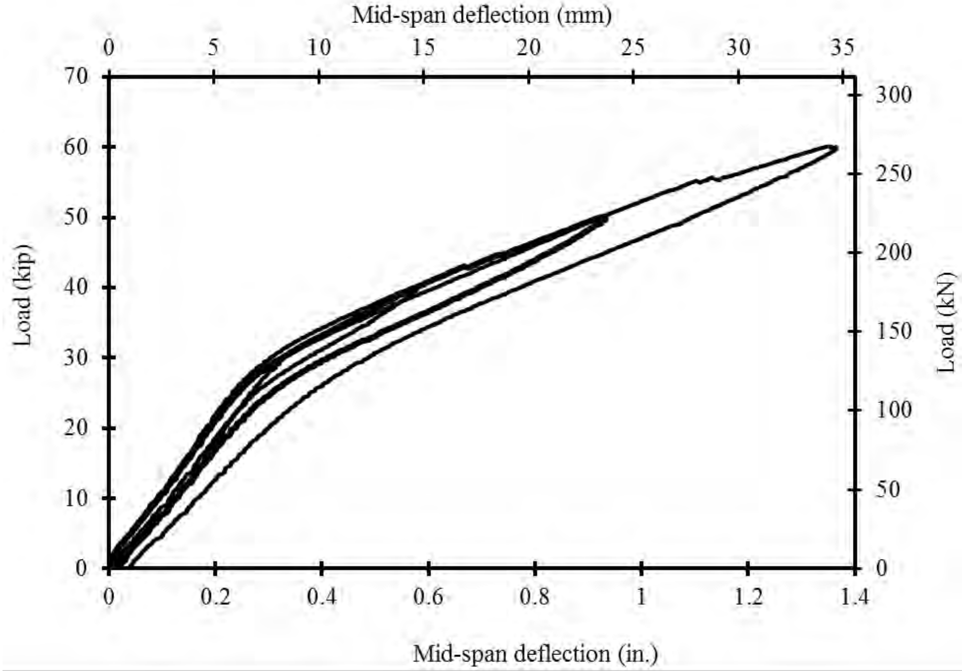

Figure 4.3-30 Load-deflection curves of Beam H1 due to loading at ambient temperature

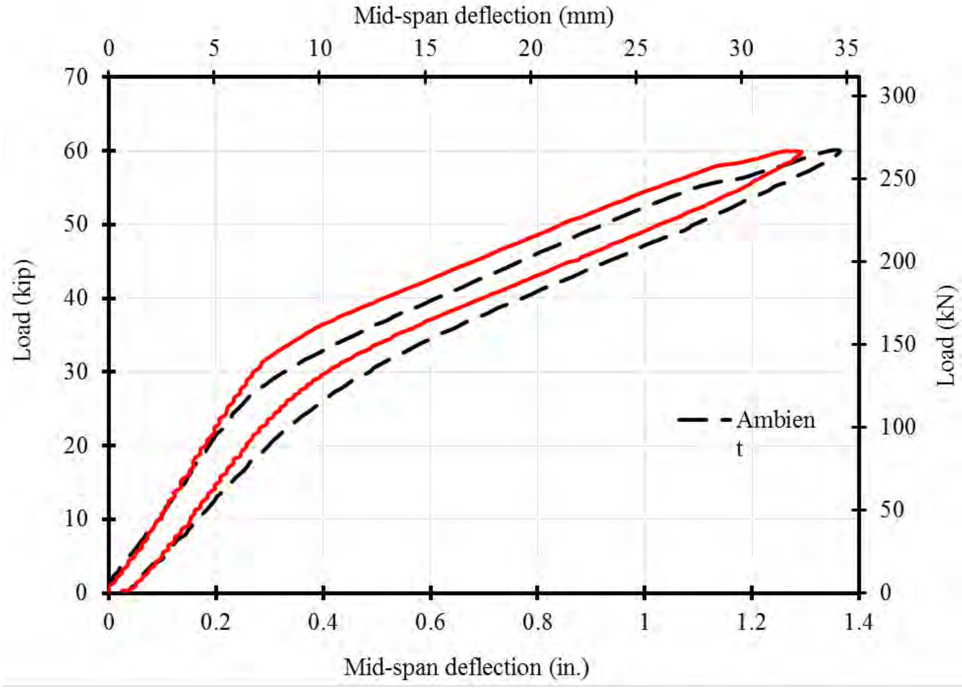

Figure 4.3-31 Load-deflection curves of Beam H1 during 60-kip (267-kN) load cycle at ambient and 176 °F (80 °C)

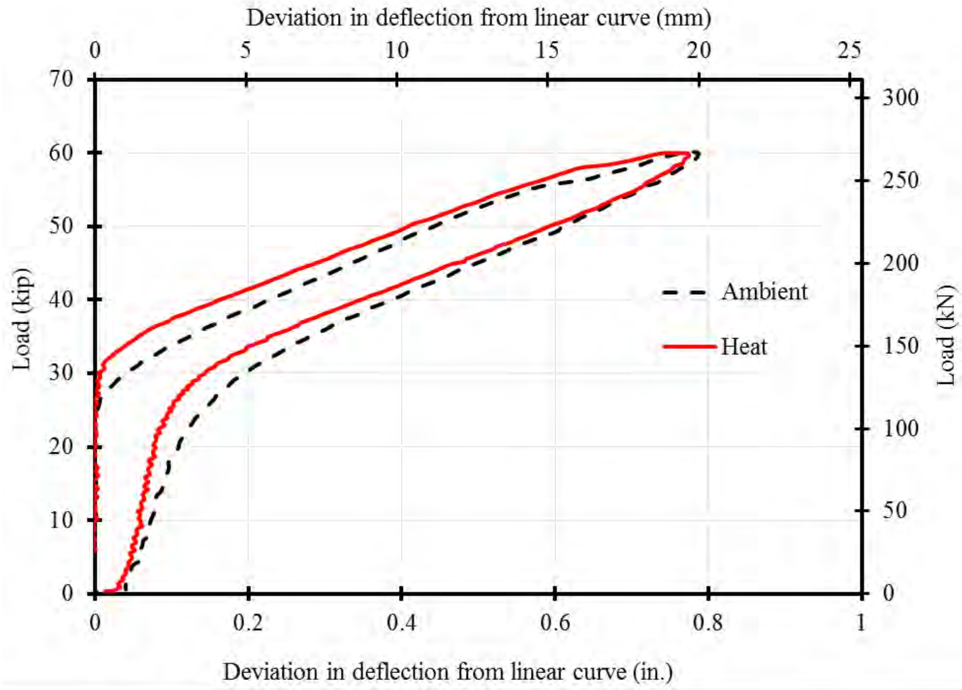

Figure 4.3-32 Deviation of load-deflection curves from the linear un-cracked curve in Beam H1 indicating the decompression loads at ambient and 176 °F

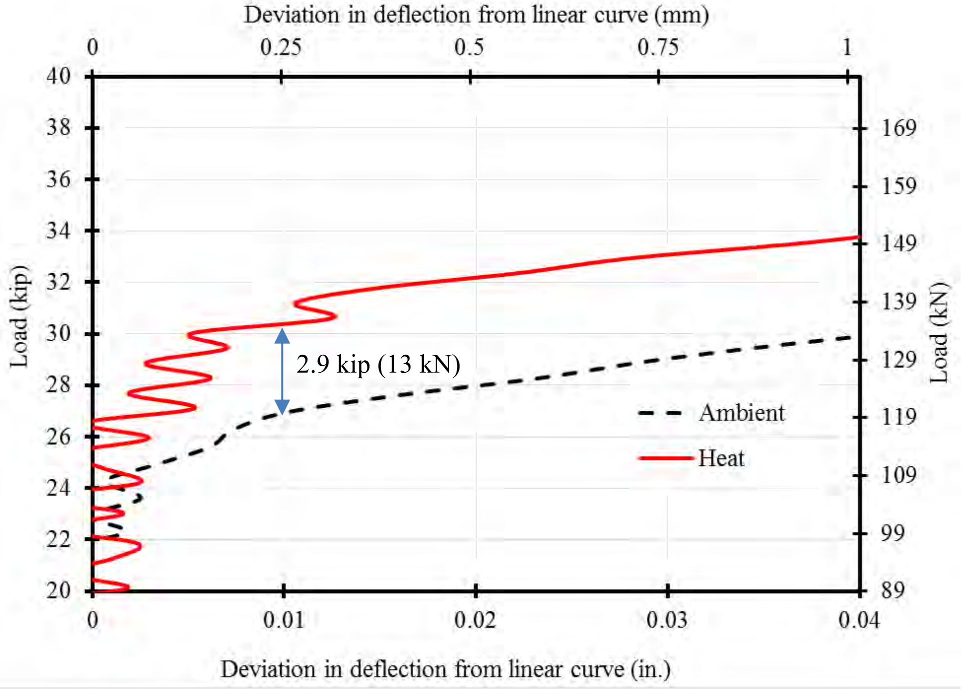

Figure 4.3-33 Close-up view showing the deviation of load-deflection curves from the linear un-cracked curves in Beam H1 and indicating the decompression loads at ambient & 176 °F (80 °C)

4.3.3.4 Beam H2

Beam H2 was similar to Beam H1 in loading scenario and the load cycles at elevated and ambient temperatures are shown in Figure 4.3-34 and Figure 4.3-35, while the analysis for the decompression loads at both elevated and ambient temperatures are shown in Figure 4.3-36 through Figure 4.3-38. The figures confirm the findings from Beam H1 and showed a decompression load at elevated temperature approximately 3.9 kip (17 kN) higher than that at ambient temperature.

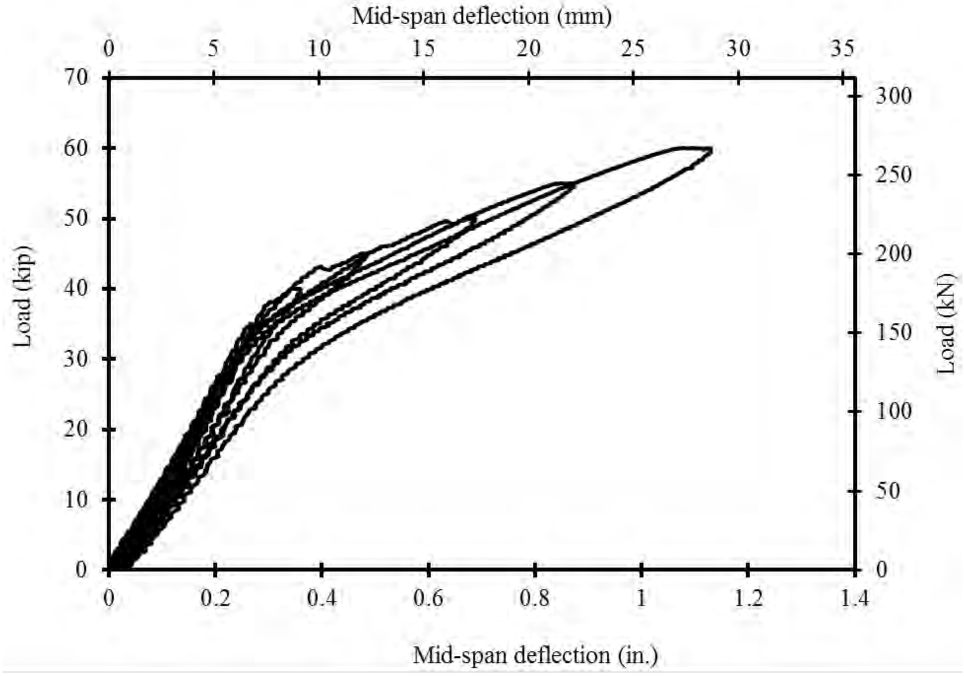

Figure 4.3-34 Load-deflection curves of Beam H2 due to loading at 176 °F (80 °C)

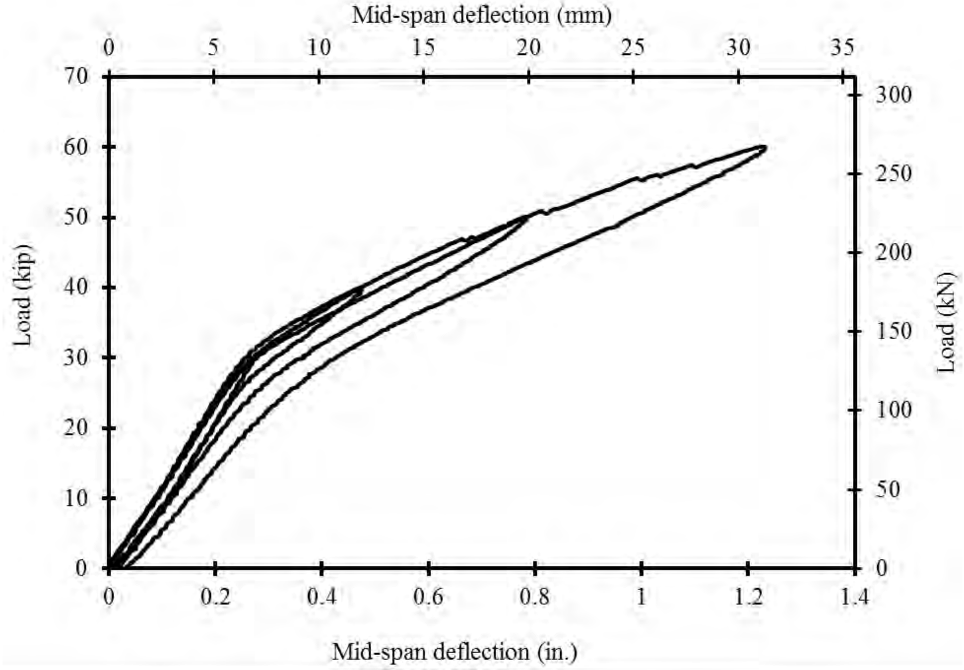

Figure 4.3-35 Load-deflection curves of Beam H2 due to loading at ambient temperature

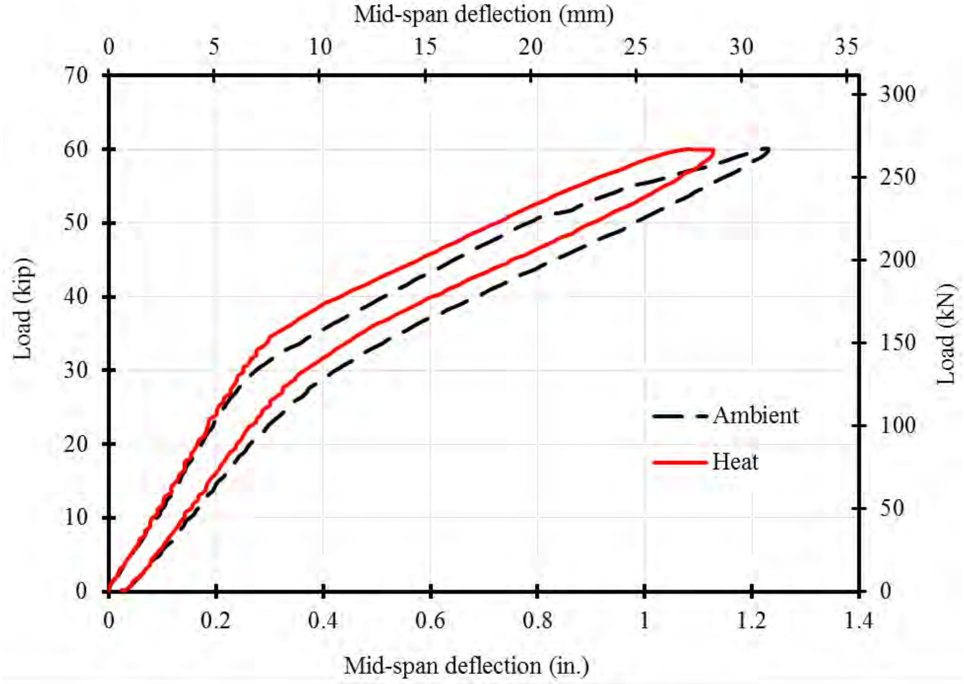

Figure 4.3-36 Load-deflection curves of Beam H2 during 60-kip (267-kN) load cycle at ambient and 176 °F (80 °C)

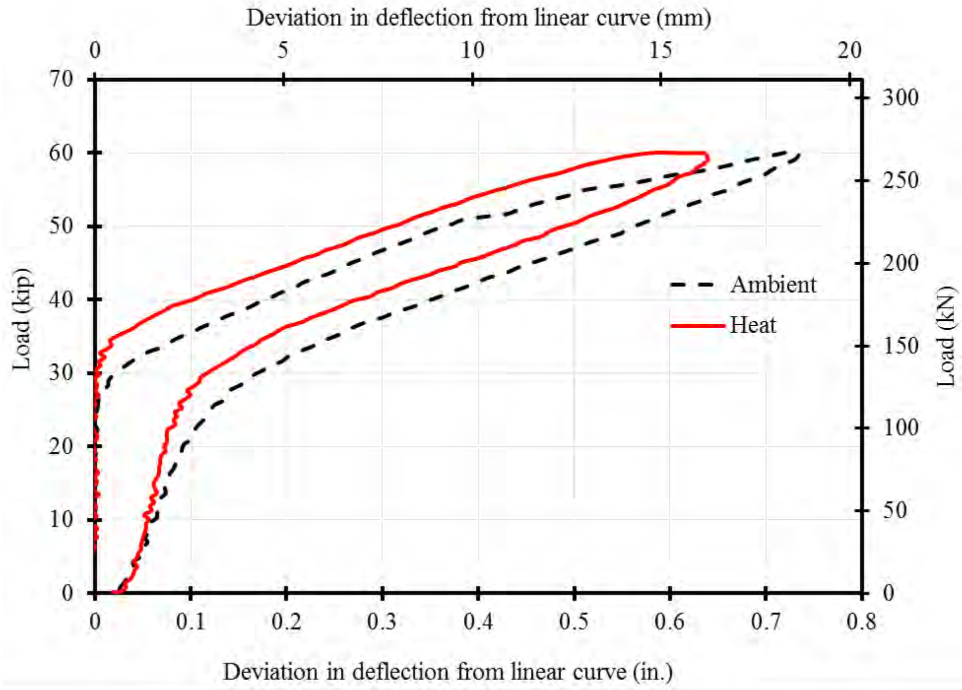

Figure 4.3-37 Deviation of load-deflection curves from the linear un-cracked curve in Beam H2 indicating the decompression loads at ambient and 176 °F (80 °C)

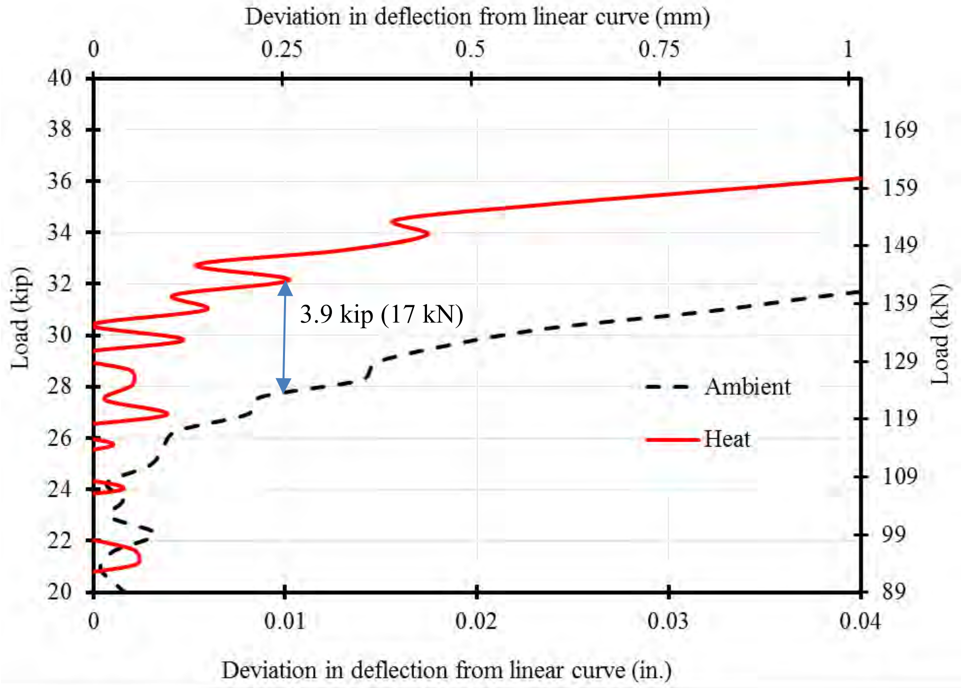

Figure 4.3-38 Close-up view showing the deviation of load-deflection curves from the linear un-cracked curves in Beam H2 and indicating the decompression loads at ambient & 176 °F (80 °C)

4.3.3.5 Beam F2-R

The first phase of testing included loading Beam F2 in load cycles at ambient temperature. In second phase the beam was first saturated at a freezing temperature of -40 °F (-40 °C) and then tested under the same loading and unloading pattern. Figure 4.3-39 shows the load-deflection curves for the 60-kip load cycles at both freezing and ambient temperatures. To estimate the difference in decompression load, the deviation of the experimental deflection curve from the linear un-cracked curve was calculated for both curves as shown in Figure 4.3-40 with the close-up view shown in Figure 4.3-41. Similar to beam F2, the decompression load at ambient temperature was higher than that at freezing temperature with a difference of approximately 2.1 kip (9 kN).

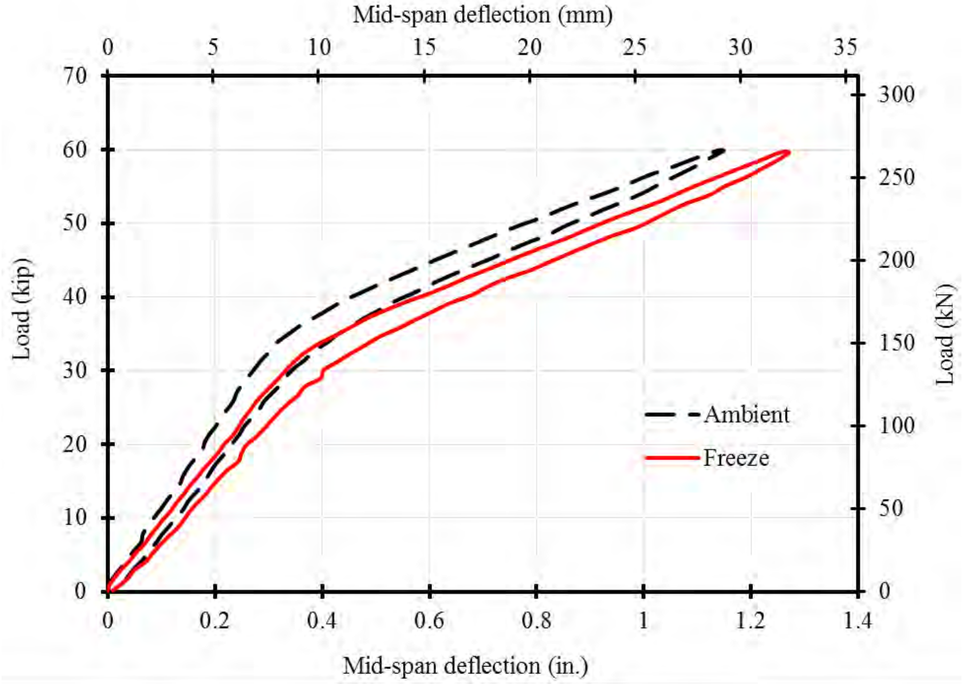

Figure 4.3-39 Load-deflection curves of Beam F2-R during 60-kip (267-kN) load cycle at ambient and -40 °F (-40 °C)

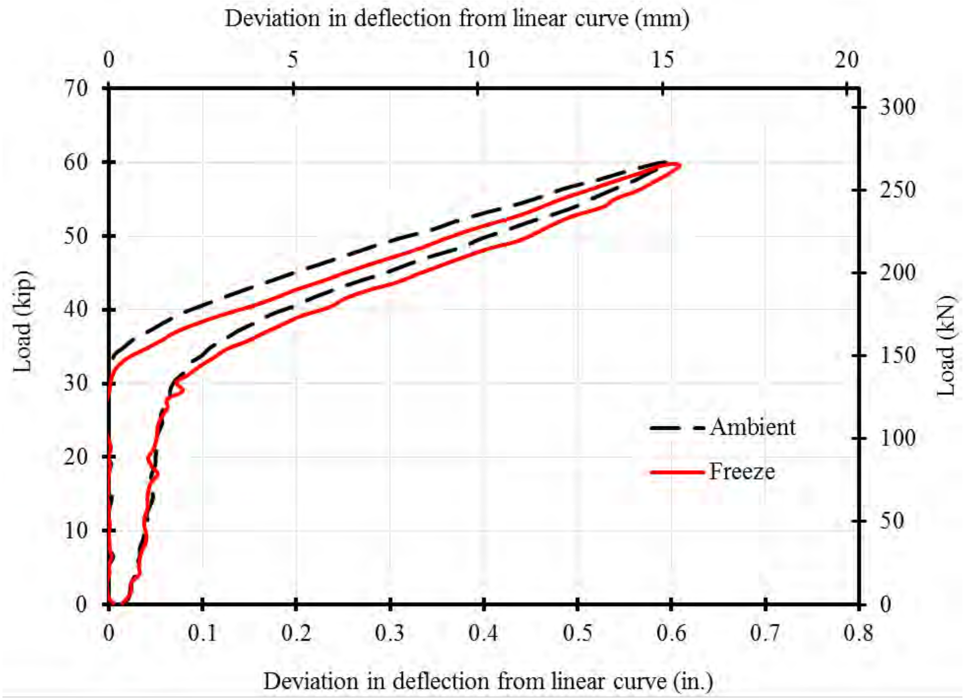

Figure 4.3-40 Deviation of load-deflection curves from the linear un-cracked curve in Beam F2-R indicating the decompression loads at ambient and -40 °F (-40 °C)

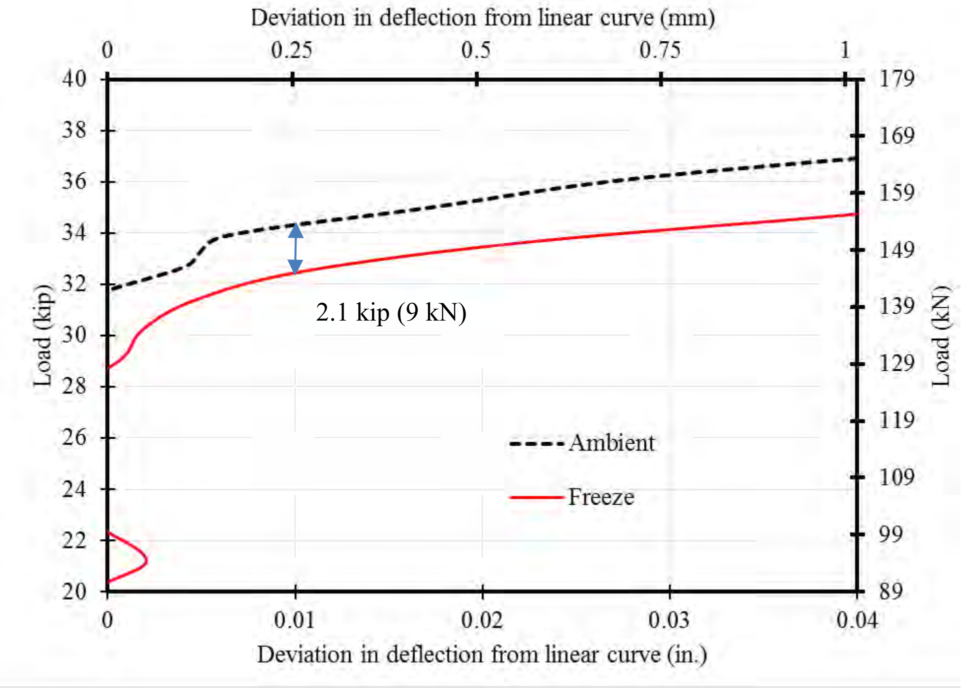

Figure 4.3-41 Close-up view showing the deviation of load-deflection curves from the linear un-cracked curves in Beam F2-R indicating the decompression loads at ambient & -40 °F (-40 °C)

4.3.3.6 Beam H2-R

Beam H2-R was tested in the similar manner to beam F2-R but at an elevated temperature of 176 °F (80 °C). The first phase of testing was performed at ambient temperature followed by second phase of testing at an elevated temperature of 176 °F (80 °C). The analysis for decompression loads at both elevated and ambient temperatures are shown in Figure 4.3-42 through Figure 4.3-44 . The decompression load at elevated temperature was found to be approximately 2.3 kip (10 kN) higher than that at ambient temperature.

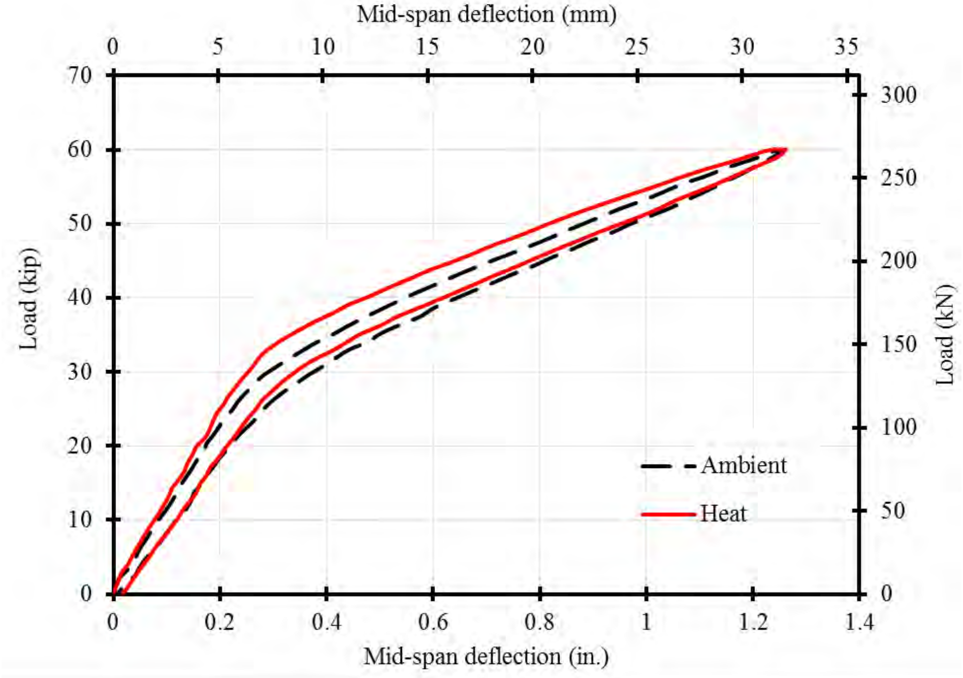

Figure 4.3-42 Load-deflection curves of Beam H2-R during 60-kip (267-kN) load cycle at ambient and 176 °F (80 °C)

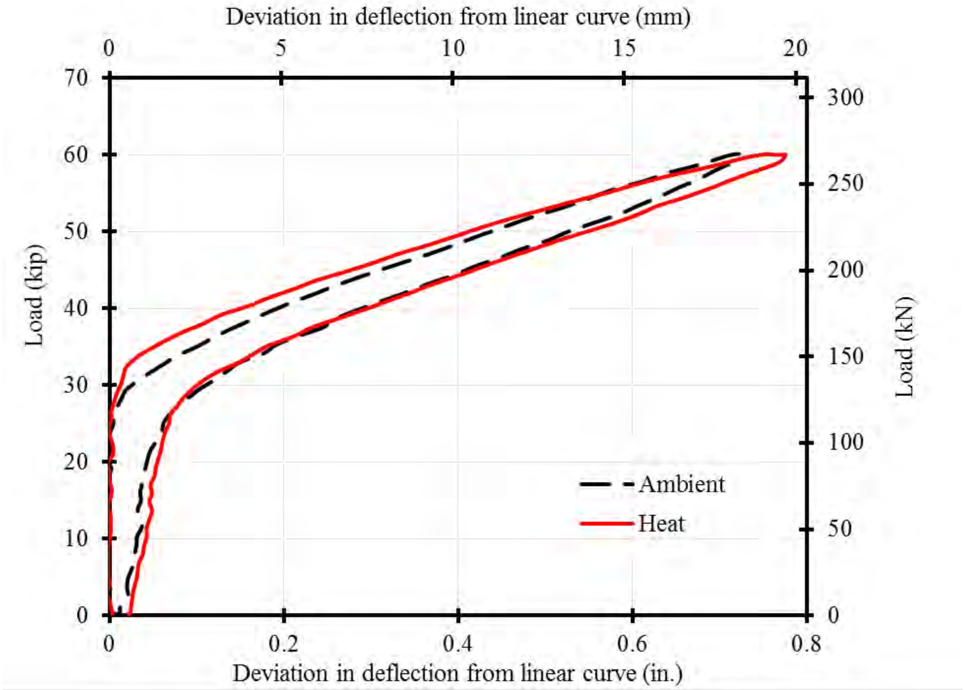

Figure 4.3-43 Deviation of load-deflection curves from the linear un-cracked curve in Beam H2-R indicating the decompression loads at ambient and 176 °F (80 °C)

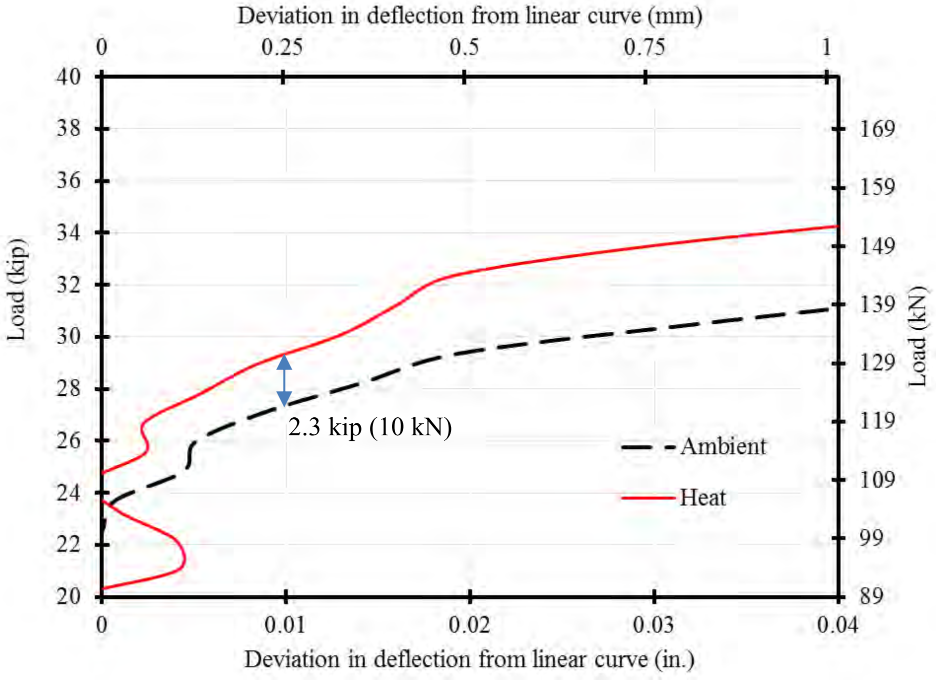

Figure 4.3-44 Close-up view showing the deviation of load-deflection curves from the linear un-cracked curves in Beam H2-R indicating the decompression loads at ambient & 176 °F (80 °C)

4.3.3.7 Discussion

At the stage of decompression, the stress at the soffit of the beam at mid-span section (σ_{bot}) is equal to zero. Therefore, the stress equation at the beam soffit can be written as:

$$\sigma_{bot} = -\frac{P_e}{A} - \frac{P_e.e}{S_{bot}} + \frac{M_{DL}}{S_{bot}} + \frac{M_{decomp}}{S_{bot}} = 0\ ksi\ or\ MPa \qquad (4.3\text{-}1)$$

where:

P_e = Effective prestressing force (kip or kN)

M_{DL} = Moment due to dead load = 44.35 kip.in. (5.0 kN.m)

M_{decomp} = Moment due to the decompression load = $\frac{P_{decomp}.L}{4}$ (kip.in. or kN.m)

P_{decomp} = Decompression load (kip or kN))

L = Effective span of the beam = 15 ft (4.57 m)

A = Cross sectional area of the beam = 126.5 in.^{2} (81,612 mm^2)

S_{bot} = Section modulus = 468.8 in.^{3} (7,682,255 mm^3)

e = Eccentricity of prestressing, = 7.04 in. (179 mm)

By substituting the aforementioned values, the equation of the stress can be rearranged to represent a direct relationship between the effective prestressing force and the decompression load as follows:

$$0 = -P_e\left(\frac{1}{A} + \frac{e}{S_{bot}}\right) + \frac{M_{DL}}{S_{bot}} + \frac{P_{decomp}.L/4}{S_{bot}} \qquad (4.3\text{-}2)$$

$$P_e = \frac{\frac{M_{DL}}{S_{bot}} + \frac{P_{decomp}.L/4}{S_{bot}}}{\left(\frac{1}{A} + \frac{e}{S_{bot}}\right)} = \frac{44.35 + 45\ P_{decomp}}{11.11} = 4 + 4.05\ P_{decomp} \qquad (4.3\text{-}3)$$

The change in the effective prestressing force ($\Delta\ P_e$) can also be directly related to the change in decompression load (ΔP_{decomp}) as:

$$\Delta P_e = 4.05\,\Delta P_{decomp} \tag{4.3-4}$$

With the increase or decrease in temperature, it is expected that the effective prestressing force will increase or decrease accordingly due to the difference in thermal expansion between concrete and CFCC. For instance, assuming the difference in coefficient of thermal expansion between concrete and CFCC is 6×10^{-6} /°F (12×10^{-6} /°C), the increase in temperature from 68 to 176 °F (20 to 80 °C) or the decrease in temperature from 68 to -40 °F (20 to -40 °C) (that is an increase or decrease of 108 °F or 60 °C), would yield a strain increase or decrease of 0.000648. As the total area of prestressing (a_{frp}) is 0.719 in.^{2} (463 mm^2) and approximate elastic modulus of CFCC (E_{frp}) is 22,480 ksi (155 GPa), this increase or decrease in strain shall yield an increase or decrease in the effective prestressing force of approximately 10.43 kip (46 kN)/beam, or an increase/decrease in the decompression load by approximately 2.57 kip (11 kN).

By comparing this theoretical value with the experimentally obtained differences in the decompression loads in Beams F1, F2, H1, H2, F2-R and H2-R it can be concluded that there is reasonable agreement between the experimental and theoretical values and the gain or loss in the prestressing force due to seasonal temperature change can be accurately predicted by estimating the normal temperature range and calculating the prestressing gain/loss due to the temperature change.

4.4 Discussion of Test Results

Temperature change seems to be a key element in the design of beams prestressed with CFRP strands. CFCC strands showed a slight decrease in the elastic modulus that was corresponding to a decrease in the prestressing force with the increase in temperature. The second-time heating did not result in any significant loss of the prestressing force or the elastic modulus. Besides, after CFCC strands were allowed to cool down and tested to failure at ambient temperature, their attained average tensile strength and average elastic modulus were matching, or even slightly exceeding, those of unheated specimens. Therefore, it can be concluded that the increase in temperature to 400 °F (204 °C) did not cause any permanent damage in the CFCC strands.

Based on the results from the experimental investigation of decked bulb T beams exposed to temperature change, it appears that beams prestressed with CFCC strands experience a loss in the prestressing force with the decrease in temperature. However, this loss in prestressing is recovered when the temperature increases back to the normal range. Similarly, beams prestressed with CFCC strands experience gain in the effective prestressing force when the temperature increases but this gain in prestressing is lost once the temperature drops down to the normal range. The gain or loss in effective prestressing force conforms with a reasonable degree of accuracy to the theoretical calculations. In addition, beams subjected to multiple cycles of heating and cooling tend to experience loss and gain in prestressing force without any signs of slippage or delamination of CFCC strands.